STUDIES OF RESPONSE TO EARTHQUAKE GROUND MOTION

Thesis by

Arthur Gerald Brady

In Partial Fulfillment of the Requirements

For the Degree of

Doctor of Philosophy

California Institute of Technology

Pasadena, California

1966

(Submitted January 7, 1966)

ACKNOWLEDGMENTS

The author wishes to thank Professor D. E. Hudson for his guidance and assistance throughout the investigation and in the preparation of this work.

The time devoted by Professors T. K. Caughey and W. D. Iwan and by Mr. R. Husid in obtaining the electric analog computer results is gratefully appreciated.

The author is grateful for the teaching and research assistantships and tuition scholarships granted by the California Institute of Technology during the course of this work.

ABSTRACT

A study is made of the accuracy of electronic digital computer calculations of ground displacement and response spectra from strong-motion earthquake accelerograms. This involves an investigation of methods of the preparatory reduction of accelerograms into a form useful for the digital computations and of the accuracy of subsequent digital calculations. Various checks are made for both the ground displacement and response spectra results, and it is concluded that the main errors are those involved in digitizing the original record. Differences resulting from various investigators digitizing the same experimental record may become as large as 100% of the maximum computed ground displacements. The spread of the results of ground displacement calculations is greater than that of the response spectra calculations. Standardized methods of adjustment and calculation are recommended, to minimize such errors.

Studies are made of the spread of response spectral values about their mean. The distribution is investigated experimentally by Monte Carlo techniques using an electric analog system with white noise excitation, and histograms are presented indicating the dependence of the distribution on the damping and period of the structure. Approximate distributions are obtained analytically by confirming and extending existing results with accurate digital computer calculations. A comparison of the experimental and analytical approaches indicates

good agreement for low damping values where the approximations are valid. A family of distribution curves to be used in conjunction with existing average spectra is presented. The combination of analog and digital computations used with Monte Carlo techniques is a promising approach to the statistical problems of earthquake engineering.

Methods of analysis of very small earthquake ground motion records obtained simultaneously at different sites are discussed. The advantages of Fourier spectrum analysis for certain types of studies and methods of calculation of Fourier spectra are presented. The digitizing and analysis of several earthquake records is described and checks are made of the dependence of results on digitizing procedure, earthquake duration and integration step length. Possible dangers of a direct ratio comparison of Fourier spectra curves are pointed out and the necessity for some type of smoothing procedure before comparison is established. A standard method of analysis for the study of comparative ground motion at different sites is recommended.

TABLE OF CONTENTS

INTRODUCTION

The response of structures to earthquake excitation has been the subject of a great deal of investigation by the earthquake engineering profession. Analysis by normal mode techniques has allowed studies to be made of complicated structures in a simplified way through the use of a small number of equivalent one degree-of-freedom elements. This approach has led to detailed investigations of the response of such simple oscillators to many types of excitation of a much simpler nature than that due to earthquakes. The ultimate goal for design purposes of course is the expected response to real earthquake excitation. Natural extensions to these studies have led to the use of nonlinear elements in the simple structure and to investigations of the response resulting from various excitations increasing in complexity to actual earthquake excitation.

In structural dynamics, the most suitable method of specifying earthquake motion at any point is with a record of three rectangular components of ground acceleration as a function of time. This results from the fact that the response of an oscillator to a base acceleration $a(t)$ is the same as that of a fixed-base oscillator of mass m excited by a force $-ma(t)$. Calculation of the response, or suitable properties of it, to earthquake motion thus requires the ground acceleration $a(t)$. The accelerograms of eighteen strong-motion earthquakes may be found in reference 1.

In some engineering investigations an estimate of the ground displacements during strong earthquakes is useful. For example,

long period ground motion, often evident in displacement curves, can cause sloshing of water in reservoirs under special conditions of matching periods. In tunnels, ground displacements in the axial direction are able to damage pipes and other longitudinal attachments unless specially designed against direct straining. Using a digital computer and the digitized accelerograms of the four strongest recorded ground motions, Berg and Housner[2] have obtained integrated curves of velocity and displacement. The first chapter of the present study includes the results of work carried out at the California Institute of Technology for the Earthquake Engineering Research Institute committee investigation on the accuracy of computed displacements.

The ground motion of an earthquake, as regards its effect on structures, is characterized by the relative velocity response spectrum, defined as the maximum value of the relative velocity of a single degree-of-freedom oscillator in response to the earthquake base acceleration and depending, therefore, on the natural period and damping of the oscillator. A number of authors have described the usefulness of the response spectra characterization of earthquakes and have reported on calculations and comparisons of different computing procedures[1, 3, 4, 5]. The first chapter concludes with a description of checks on the accuracy of response spectra calculations.

The relative velocity response spectra of the larger strong-motion earthquakes have similar appearances. Although there are not many of these spectra available, an average spectrum, useful

in studies of expected structural response, has been calculated by Housner[4]. The number of recorded strong-motion earthquakes is too small for an estimate of the spread of the spectral values about their mean to be made. Many investigators have used model earthquake accelerograms based on that of Housner[6] in preparing the way for the analytical determinations of the spectra's statistical properties[7,3,8]. In particular, Rosenblueth and Bustamante[9] have used Housner's model in obtaining theoretical curves for the probability distribution of maximum responses. The second chapter describes a technique of experimental mathematics which produces distribution curves directly, and these are compared with curves obtained from Rosenblueth and Bustamante's results.

The undamped relative velocity response spectrum is closely related to the Fourier amplitude spectrum of the earthquake record in question[5]. The response spectrum in general is of more interest to the civil engineer because it combines the properties of earthquake and structure in useful form. However, if only the frequency components in a record are desired, the Fourier spectrum is sufficient and it has the advantage that it is simpler to determine. Matthiesen et al.[10], and Herrera et al.[11], basing their work on Japanese and Mexican investigators, respectively, have studied frequency components of ground motion in bedrock and softer deposits, in attempts to determine by how much some components are amplified on passage through these softer deposits. The California Division of Water Resources is interested in the same amplification studies and the

third chapter describes the analysis made at the California Institute of Technology of some simultaneous records from the U. S. Coast and Geodetic Survey's instrumentation for the project.

Primarily, this thesis as a whole is concerned with the accuracy of digital calculations of corrected accelerations, displacements, response spectra and Fourier spectra, using data obtained from typical earthquake engineering records. It has been found that occasionally considerably more care should be taken with high-speed modern digital computers than has previously always been the case. By using the digital computer in conjunction with the analog computer, each being employed where best suited, further problems connected with the statistical nature of earthquakes and which are not amenable to theoretical analysis, appear solvable.

I. ANALYSIS OF EARTHQUAKE STRONG-MOTION ACCELEROGRAMS

A. Introduction

This chapter is concerned with the accuracy of electronic digital computer calculations of ground velocity and displacement, and of the relative velocity response spectra, from the accelerograms of strong-motion earthquakes. The basic information is in the form of an acceleration-time record because of the fundamental importance of the acceleration in earthquake engineering. This importance is due to several factors. Firstly, the inertia forces acting on vibrating buildings during ground motion are proportional to the ground acceleration at the base. Secondly, response spectra are derived from formulas which specifically include ground acceleration. Lastly, velocities and displacements can be calculated from the ground acceleration by integration procedures which are basically more accurate than the reverse process, that is, calculating velocities and accelerations from displacement records by differentiating. It is thus apparent that the most complete data possible are contained in the acceleration records.

From the curves of ground acceleration, velocity and displacement it is possible to obtain a visual indication of the various frequency components present in the ground motion. The integration processes tend to smooth out the rapid oscillations of the acceleration and allow the lower frequencies to become predominant. Other

reasons for calculating ground velocity and displacement have been mentioned in the preliminary Introduction, and have led to numerical and graphical methods of integration of the ground acceleration[12,13]. More recently the digital computer has been put to good use improving the accuracy of the arithmetic calculations and making it possible to employ more elaborate adjustments to the original accelerations than were previously feasible[2].

Calculations of response spectra, particularly of maximum relative velocity response spectra, have been much more common. Comparisons have been made between different digital calculations on the same data, between digital and analog calculations on the same data, and between the different results arising from using the same calculations on independently reduced input data[5].

A committee set up by the Earthquake Engineering Research Institute in 1962 pursued the question of the accuracy of digital calculations and of the preparatory reduction of the original accelerogram into a form useful for the digital computer. Four members of the committee, at institutions having different computing facilities, were given identical copies of the N 21° E component of the 1952 Taft earthquake and independently digitized it, each forwarding copies of the resulting deck to the other three members for computational checks. The present account describes the work done at the California Institute of Technology as a contribution to this study.

The first part of this chapter, starting in section B, is concerned with the digitizing and adjusting of the original acceleration-

time record and the computation of velocity and displacement. Various corrections and methods of maintaining accuracy are described and a standard method of computation is recommended.

The second part, starting in section F, deals with the calculations of response spectra using the accelerations as adjusted earlier. The important points investigated are dependence on the integration step length, comparison of the velocity spectra with the pseudo-velocity spectra, and dependence on the record length. There follows a comparison of the four spectra calculated from different digitizing of copies of the same record, and recommendations for a standard method of velocity spectra calculation.

The symbols are defined where they first appear and are consistent throughout the three chapters. The nomenclature for Chapter I follows.

NOMENCLATURE

$A = v_i - a_i t_i + \frac{1}{2} t_i^2 \Delta a_i / \Delta t_i$

$a(t) = \ddot{y}(t)$, unadjusted ground acceleration

$a_i = a(t_i)$

$\Delta a_i = a_{i+1} - a_i$

$a^*(t)$, adjusted ground acceleration

$B = a_i - t_i \Delta a_i / \Delta t_i$

$C = \frac{1}{2} \Delta a_i / \Delta t_i$

(C), column vector (c_o, c_1, c_2)

(C'), a first approximation to (C)

$(\delta C) = (C) - (C')$

c_o, c_1, c_2, constants

g, acceleration of gravity

$I_1 = \int_0^s tv(t)\, dt$

$I_2 = \int_0^s t^2 v(t)\, dt$

$I_3 = \int_0^s t^3 v(t)\, dt$

$PS_v = \omega_o S_d$, pseudo-velocity spectrum

(R), column vector (I_1, I_2, I_3)

[S], 3×3 matrix of coefficients

$S_a = S_a(n, \omega_o, s)$, maximum absolute acceleration response spectrum

$S_d = S_d(n, \omega_o, s)$, maximum relative displacement response spectrum

$S_v = S_v(n, \omega_o, s)$, maximum relative velocity response spectrum

s, length of record

T, natural period

t, time

t_i, a discrete time value

$\Delta t_i = t_{i+1} - t_i$

$v(t) = \dot{y}(t)$, unadjusted ground velocity

$v_i = v(t_i)$

$v^*(t)$, adjusted ground velocity

$w = x\omega_o^2/g$, dimensionless parameter

x, relative displacement of oscillator

$y(t)$, unadjusted ground displacement

$y_i = y(t_i)$

$y^*(t)$, adjusted ground displacement

$\tau = \omega_o t$, dimensionless parameter

$\Delta\tau$, numerical integration step length

ω_o, natural frequency

B. Digitizing Technique

The digitizing procedure consisted of first photographically enlarging the record by a factor of two. Three enlargements covering the whole record length were made and fastened together, possibly introducing a small alignment error at the points where the records were connected. The numerical values were obtained by placing a piece of tracing paper over the enlargement and pricking through the points of change of slope with a sharp point. A base line was estimated visually and the points were read off with an engineer's scale, using units of seconds and g/10. These were punched in pairs on IBM cards. There were 1786 pieces of data defining 893 points, obtained for 72.58 seconds of the record. This density, of just over ten points per second, was similar to that of the decks received from the other universities, namely:

The University of California at Berkeley,

The University of Michigan,

The University of Illinois.

The investigators at Illinois carried out some preliminary integrations for the unadjusted velocity and visually chose a velocity base line from the results for each of the four decks. It was noticed that a small break in the slope of this velocity base line for the C.I.T. deck occurred at twelve seconds--this point did not coincide with either of the two points at which the record was connected. This minor anomaly did not introduce a measurable discrepancy in any successive calculations and hence has been considered negligible.

C. Computation Techniques

The record was adjusted by application of a parabolic base line correction to the acceleration diagram with minimization of the mean square value of the resulting velocity. The need for a correction and a description of correction techniques are discussed in the Appendix. Numerical calculations of the adjusted velocity and displacement were then carried through. The computational procedure will now be described and a discussion of the accuracy of the various calculations is included in the next section.

The unadjusted acceleration $a(t)$ is assumed to be linear between data points. The velocity $v(t)$ resulting from one integration is thus a succession of parabolic arcs and the displacement $y(t)$ resulting from a further integration is a succession of cubic arcs. A typical enlarged portion of a section of $a(t)$ and the results of these integrations are shown in Fig. 1.1. Assuming that the initial conditions on $v(t)$ and $y(t)$ are zero, it is possible to use the recursion formulae of Berg and Housner[2] to calculate $v(t)$ and $y(t)$ from $a(t)$:

$$v(t_{i+1}) = v_{i+1} = v_i + \tfrac{1}{2}\Delta t_i(a_i + a_{i+1}) \qquad (1.1)$$

$$y(t_{i+1}) = y_{i+1} = y_i + v_i\Delta t_i + \frac{1}{6}(\Delta t_i)^2(2a_i + a_{i+1}) \qquad (1.2)$$

where the t_i's are those discrete values of time read from the record, and $\Delta t_i = t_{i+1} - t_i$.

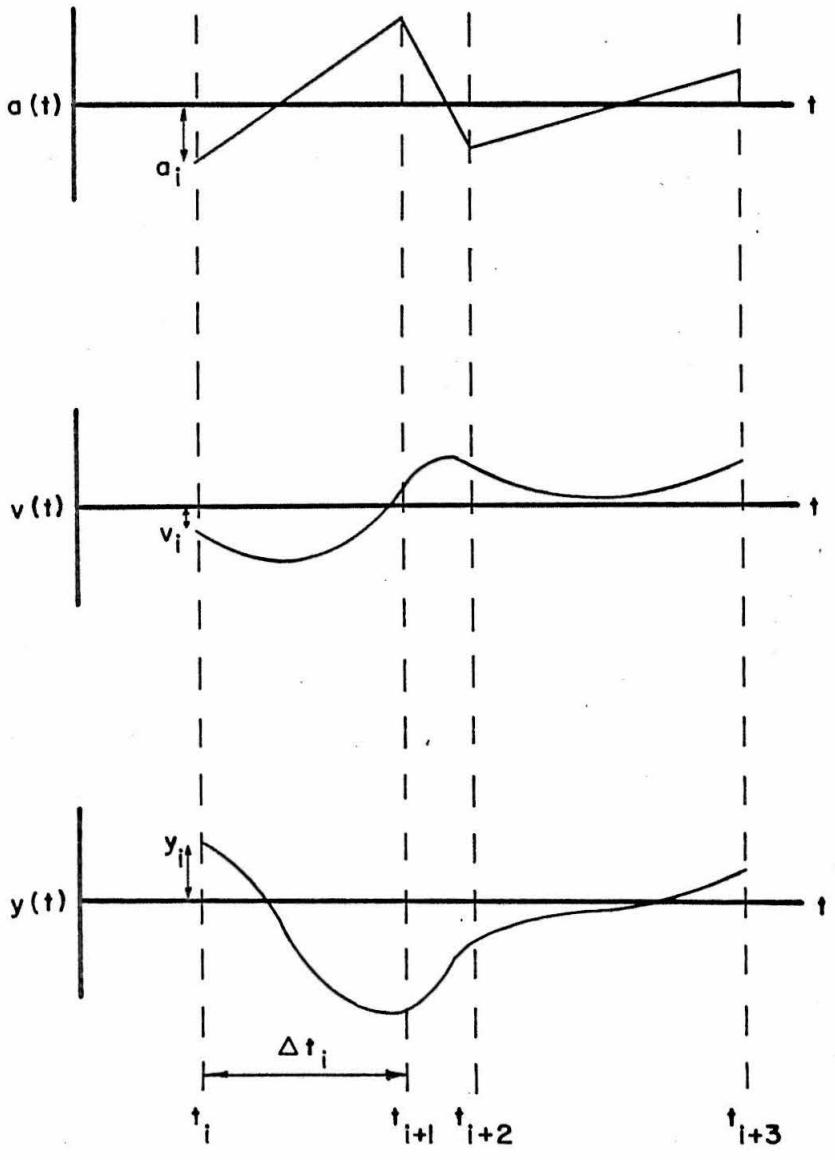

FIG. 1.1 TYPICAL ENLARGED PORTION OF a(t), v(t) and y(t).

A parabolic adjustment to the acceleration base line gives the following form to the adjusted acceleration $a^*(t)$:

$$a^*(t) = a(t) - c_o - c_1 t - c_2 t^2 \tag{1.3}$$

where c_o, c_1, and c_2 are constants. The corresponding adjusted velocity and displacement have the form:

$$v^*(t) = v(t) - c_o t - \tfrac{1}{2} c_1 t^2 - \tfrac{1}{3} c_2 t^3 \tag{1.4}$$

$$y^*(t) = y(t) - \tfrac{1}{2} c_o t^2 - \tfrac{1}{6} c_1 t^3 - \tfrac{1}{12} c_2 t^4 \tag{1.5}$$

Both $v^*(t)$ and $y^*(t)$ are zero at $t = 0$.

In order that the velocity $v^*(t)$ has a minimum mean square value, the following three equations must hold:

$$\frac{\partial}{\partial c_i} \int_0^s [\, v^*(t)\,]^2 \, dt = 0 \quad , \qquad (i = 0,1,2) \tag{1.6}$$

where s is the total length of the record used. Substituting for $v^*(t)$ from Eq. 1.4 and evaluating immediately where possible yields:

$$\begin{aligned}
\tfrac{1}{3} c_o s^3 + \tfrac{1}{8} c_1 s^4 + \tfrac{1}{15} c_2 s^5 &= \int_0^s tv(t)\, dt \\
\tfrac{1}{4} c_o s^4 + \tfrac{1}{10} c_1 s^5 + \tfrac{1}{18} c_2 s^6 &= \int_0^s t^2 v(t)\, dt \\
\tfrac{1}{5} c_o s^5 + \tfrac{1}{12} c_1 s^6 + \tfrac{1}{21} c_2 s^7 &= \int_0^s t^3 v(t)\, dt
\end{aligned} \tag{1.7}$$

These equations can be written in matrix form:

$$[S](C) = (R) \tag{1.8}$$

where (C) is the column vector (c_o, c_1, c_2), [S] is a 3×3 matrix of the coefficients and duration s, and (R) is the column vector of the three integrals appearing on the right-hand side.

Referring again to Fig. 1.1, it is possible to derive an expression for v(t) within the interval $t_i < t < t_{i+1}$ so that the integrals in (R) can be calculated:

$$a(t) = a_i + \frac{t - t_i}{\Delta t_i} \Delta a_i \,, \qquad t_i < t < t_{i+1}$$

$$= \left(a_i - t_i \frac{\Delta a_i}{\Delta t_i}\right) + \frac{\Delta a_i}{\Delta t_i} t \tag{1.9}$$

$$v(t) = v_i + \left(a_i - t_i \frac{\Delta a_i}{\Delta t_i}\right)(t - t_i) + \frac{\Delta a_i}{\Delta t_i} \cdot \frac{t^2 - t_i^2}{2}$$

$$= \left(v_i - a_i t_i + \tfrac{1}{2} t_i^2 \frac{\Delta a_i}{\Delta t_i}\right) + \left(a_i - t_i \frac{\Delta a_i}{\Delta t_i}\right) t + \tfrac{1}{2} \frac{\Delta a_i}{\Delta t_i} t^2 \,,$$

$$t_i < t < t_{i+1} \tag{1.10}$$

Defining the constant term and the coefficients of t and t^2 as A, B and C respectively this expression for v(t) becomes

$$v(t) = A + Bt + Ct^2 \tag{1.11}$$

Substituting this into the integrals of Eqs. 1.7 enables them to be written:

$$I_1 = \int_0^s tv(t)\,dt = \sum_{i=0}^{N-1} \left(A\,\frac{t_{i+1}^2 - t_i^2}{2} + B\,\frac{t_{i+1}^3 - t_i^3}{3} + C\,\frac{t_{i+1}^4 - t_i^4}{4} \right)$$

$$I_2 = \int_0^s t^2 v(t)\,dt = \sum_{i=0}^{N-1} \left(A\,\frac{t_{i+1}^3 - t_i^3}{3} + B\,\frac{t_{i+1}^4 - t_i^4}{4} + C\,\frac{t_{i+1}^5 - t_i^5}{5} \right)$$

$$I_3 = \int_0^s t^3 v(t)\,dt = \sum_{i=0}^{N-1} \left(A\,\frac{t_{i+1}^4 - t_i^4}{4} + B\,\frac{t_{i+1}^5 - t_i^5}{5} + C\,\frac{t_{i+1}^6 - t_i^6}{6} \right)$$

(1.12)

An alternative approach to the calculation of these integrals can be made. Substituting for A, B and C, expanding, and re-factoring, leads to the following different algebraic form of the expressions for these integrals:

$$I_1 = \sum_{i=0}^{N-1} \left\{ \tfrac{1}{2} v_i \Delta t_i (t_i + t_{i+1}) + \frac{1}{24} (\Delta t_i)^2 \left[a_i (3t_i + 5t_{i+1}) + a_{i+1} (t_i + 3t_{i+1}) \right] \right\}$$

$$I_2 = \sum_{i=0}^{N-1} \left\{ \frac{1}{3} v_i \Delta t_i (t_i^2 + t_i t_{i+1} + t_{i+1}^2) + \frac{1}{60} (\Delta t_i)^2 \left[a_i (4t_i^2 + 7t_i t_{i+1} + 9t_{i+1}^2) \right.\right.$$
$$\left.\left. + a_{i+1} (t_i^2 + 3t_i t_{i+1} + 6t_{i+1}^2) \right] \right\}$$

$$I_3 = \sum_{i=0}^{N-1} \left\{ \tfrac{1}{4} v_i \Delta t_i (t_i^3 + t_i^2 t_{i+1} + t_i t_{i+1}^2 + t_{i+1}^3) + \frac{1}{120} (\Delta t_i)^2 \right.$$
$$\times \left[a_i (5t_i^3 + 9t_i^2 t_{i+1} + 12 t_i t_{i+1}^2 + 14 t_{i+1}^3) \right.$$
$$\left.\left. + a_{i+1} (t_i^3 + 3t_i^2 t_{i+1} + 6 t_i t_{i+1}^2 + 10 t_{i+1}^3) \right] \right\}$$

(1.13)

It is evident that there are three methods for calculating the integrals of Eqs. 1.7. The first involves the direct use of Simpson's rule obtaining the velocity from Eq. 1.10 where $v(t)$ is given within each interval in terms of known data and the time t. By taking sufficiently small increments of time within each interval any reasonable desired accuracy can be attained. The other two methods use Eqs. 1.12 and Eqs. 1.13 which yield the integrals directly. All three methods require the calculation of v_i for the beginning of each interval; this is obtained from Eq. 1.1.

Once the integrals are calculated and the matrix $[S]$ inverted, the constants (C) are given from Eq. 1.8 by

$$(C) = [S^{-1}](R) \tag{1.14}$$

Substitution into Eqs. 1.3, 1.4 and 1.5 yields the adjusted values of $a^*(t)$, $v^*(t)$ and $y^*(t)$.

D. Checks on Accuracy

The original time and acceleration data used in the expressions for the integrals I_1, I_2 and I_3 were read to an accuracy of ± 2 in the fourth significant figure. This value is based on successive readings by the same individual. As will be shown later a rather larger range must be expected for different individuals. This accuracy corresponds to reading the time in seconds to two decimal places and the acceleration in $g/10$ to three decimals. In the following discussions adjusted accelerations will always be considered with the above accuracy in mind since their accuracy is necessarily limited by that of the basic original data.

As will be shown later in this section, errors in acceleration of this size can cause errors in the calculated displacement of up to 20%. Some minor alterations which also can cause errors of this magnitude, together with less significant ones, are now described.

(i) Although the calculation of the integrals I_1, I_2 and I_3 might seem to be a routine problem, some important questions of accuracy arise. Eqs. 1.13 are more accurate than Eqs. 1.12 for computer calculations. The difference between the relatively large, slightly different quantities t_{i+1}^r and t_i^r, where r may range from two to six, causes appreciable loss of accuracy, as suspected by Professor Veletsos at Illinois. The integrals evaluated by the two methods agree to four significant figures for I_1 and only three figures for I_2 and I_3. These errors in the integrals cause errors in the adjusted accelerations of up to 0.0002 g and in the resulting

displacements of up to two inches in a maximum displacement of nine inches. This is illustrated in Fig. 1.2 which clearly demonstrates the effect of different computing techniques on the same input data. Using Simpson's rule with a time increment of 0.01 seconds gives results agreeing to six significant figures with those using Eqs. 1.13.

(ii) The matrix [S] is nearly singular, that is, its determinant is two or three orders of magnitude smaller than its individual elements. Calculation of det [S] showed that three significant figures were lost using a desk calculator. It could be expected, therefore, that calculation of (C) by any method involving inversion of [S] would lead to a loss of three significant figures. This was verified by the following procedure.

Suppose (C') is the result of computing $[S^{-1}](R)$ with an inaccurate $[S^{-1}]$, and that the true (C) is given by (C' + δC). Resubstituting (C') into the left-hand side of Eq. 1.8 yields (R'), differing slightly from (R). The correction (δC) to (C) is then given by

$$(\delta C) = (C) - (C') = [S^{-1}](R) - [S^{-1}](R') = [S^{-1}](R - R') \qquad (1.15)$$

When this correction was compared with the value of (C) calculated on the first run, it was found that of the eight figures the computer uses, between two and four had been lost. By applying this correction once, the eight figure accuracy with which the computer deals was recovered.

FIG. 1.2 DISPLACEMENTS FROM TWO DIFFERENT COMPUTING TECHNIQUES ON THE SAME DATA.
TAFT, 1952, N21°E.

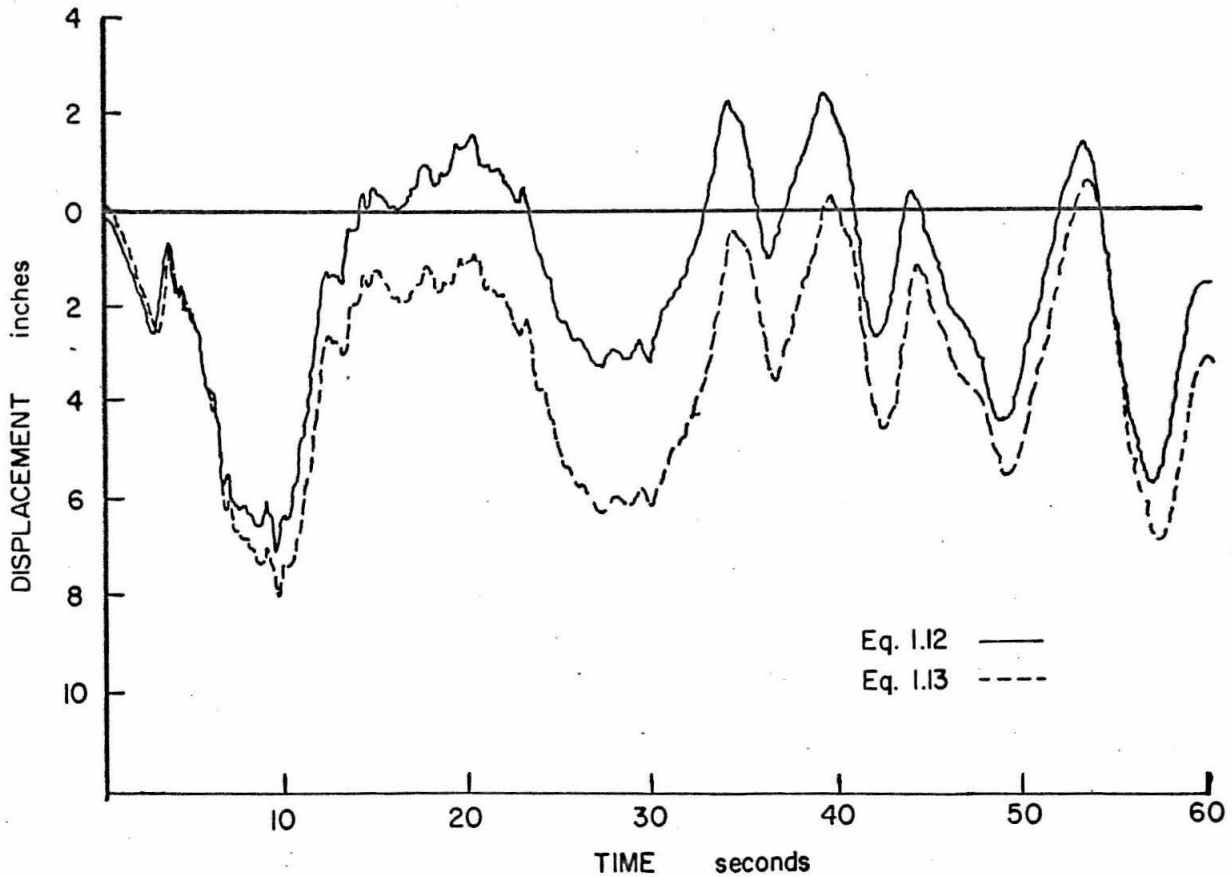

(iii) The inverse of the matrix [S] was very sensitive to the value of the record duration, s, chosen in the adjustment procedure. The four participating schools are listed below together with the length of record initially digitized and the first discrete time coordinate at or higher than 60.00 sec.

C.I.T.	72.58 sec.	60.01 sec.
Michigan	73.05 "	60.07 "
Berkeley	60.00 "	60.00 "
Illinois	60.65 "	60.10 "

Using the full 72.58 sec. of the C.I.T. record resulted in the constants (C) differing in the second significant figure from the values when the 60.01 sec. duration was used. The discrepancies in the resulting acceleration and displacement were similar to those in (i) above, with displacements differing by up to 20%. However, using the Illinois data, first with an interpolated duration of 60.00 sec. and secondly with the 60.10 sec. duration of the second column, the displacements differed by no more than 0.1 inches. Thus it was not considered necessary to interpolate between the two data points surrounding s = 60.00 sec. for an exact record length of 60.00 sec.

(iv) During the adjustment calculations the adjusted acceleration exists in the computer with eight significant figures, although the punched card output is rounded off to four figures, the same accuracy as the original data. This is the form in which the adjusted acceleration is to be used in later analyses. Reprocessing this adjusted acceleration deck and comparing the resulting displacements

with the first adjusted ones gave an indication of the effect of rounding off to four figures. The difference in the displacement was up to 0.05 in., or ±5 in the third significant figure which is of a much smaller order than the previous three described. As would be expected this iterative adjustment converged very rapidly so that only one step was found necessary.

(v) Although the original data assume straight lines joining adjacent acceleration-time points, the parabolic base line correction in effect replaces these straight lines by parabolic arcs as well as altering the acceleration ordinates. In subsequent computation these adjusted accelerations are also assumed to be joined by straight lines. A check of this assumption showed that there was a difference of up to two in the fourth significant figure of the displacement and the assumption can thus be taken as valid.

E. Standardizing the Calculation Procedure

A reasonable method of standardizing the adjustment of the acceleration records and of calculating the velocity and displacement would be the following:

(i) Use a record of some convenient specified length.

(ii) Have a standard digitized representation of each earthquake produced and supplied on the same basis as copies of official accelerograph records.

(iii) Use Eqs. 1.13 or a Simpson's rule calculation with a 0.01 sec. time increment for the integrals I_1, I_2 and I_3.

(iv) Correct the constants (C) by the procedure outlined in D(ii).

(v) Calculate the adjusted acceleration at the discrete times of the original reduced data by Eq. 1.3 and punch it out on cards to the same accuracy as this original data.

(vi) For velocity and displacement calculations assume the adjusted acceleration is linear between the discrete points, using Eqs. 1.1 and 1.2.

The results of the above recommended procedure on the four decks used in this study are shown in Fig. 1.3. The calculated displacements of the independently digitized accelerograms show a wide scatter. The scatter is even broader than that expected from the discussion in section D on the accuracy of the digitizing procedure and indicates that the range of values chosen by several observers reading the same record is wider than that for one observer. Fig. 1.3 indicates in a qualitative way the discrepancies that can

FIG. 1.3 DISPLACEMENTS FROM FOUR INDEPENDENT READINGS OF ACCELEROGRAM. TAFT, 1952, N21°E.

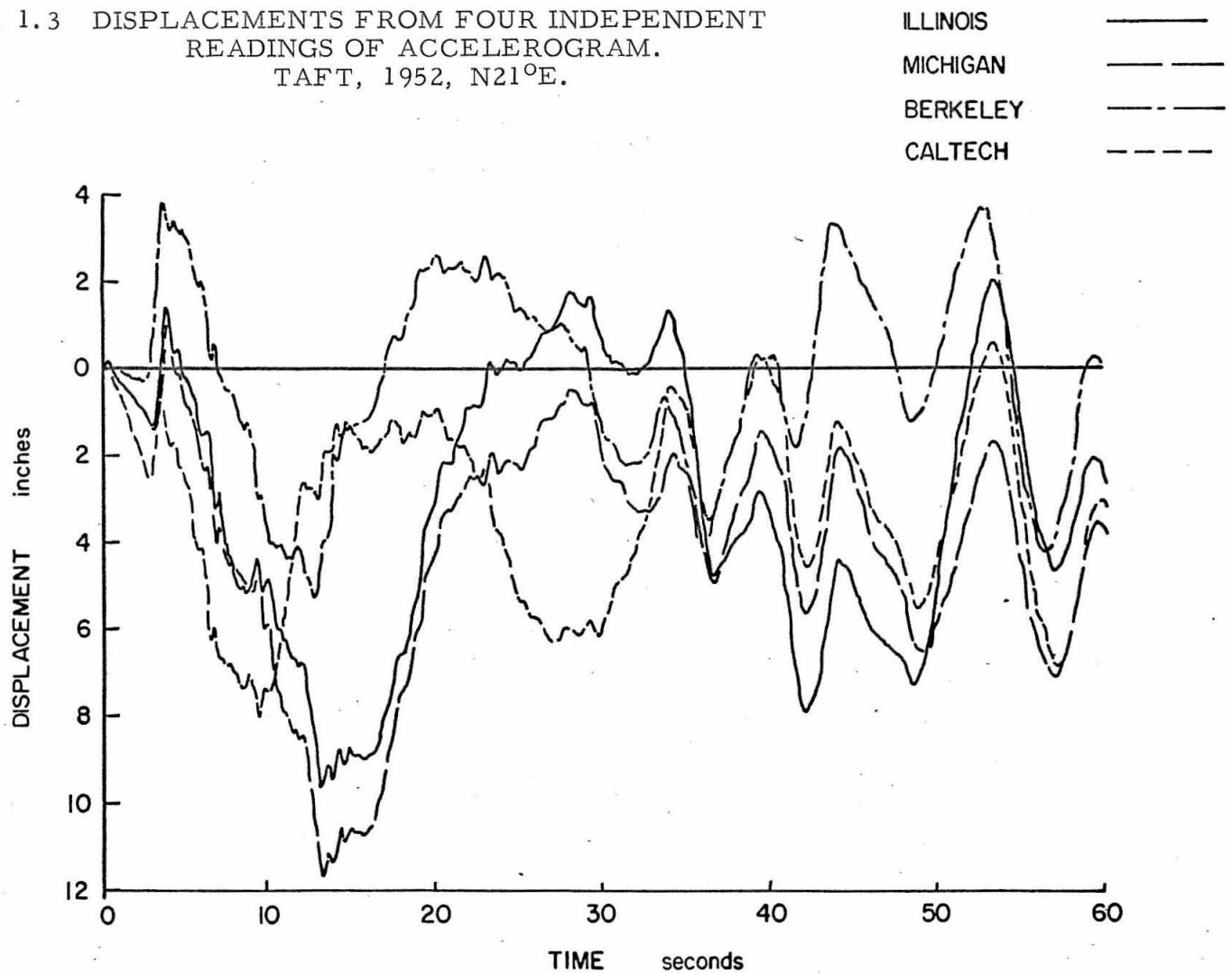

arise in calculated displacements when different individuals reduce acceleration records to digital form. If displacements during strong-motion earthquakes are to be obtained from the accelerograms with less scatter than this more accurate ways of getting the original input data are required.

F. Computational Techniques for Response Spectra

The velocity spectrum, S_v, is the maximum absolute value of the relative velocity $\dot{x}$ of a single degree of freedom damped linear oscillator whose base is excited by the adjusted earthquake acceleration $a^*(t)$ of the preceding sections. The spectrum value is a function of the natural frequency, ω_o, the fraction, n, of critical damping of the oscillator, and of the duration, s, of the earthquake acceleration. The following equations determine the velocity spectrum value:

$$\ddot{x} + 2n\omega_o\dot{x} + \omega_o^2 x = -a^*(t) \tag{1.16}$$

$$S_v = S_v(n,\omega_o,s) = |\dot{x}|_{max} \tag{1.17}$$

where the arguments of $S_v(n,\omega_o,s)$ indicate the parameters on which S_v depends. A convenient method for calculating S_v is to integrate Eq. 1.16 numerically with zero initial conditions for x and $\dot{x}$, keeping track of the maximum value of $|\dot{x}|$. At the same time, the maximum values of $|x|$ and of $|2n\omega_o\dot{x} + \omega_o^2 x|$ can be obtained, thus yielding the relative displacement response spectrum, S_d:

$$S_d(n,\omega_o,s) = |x|_{max} \tag{1.18}$$

and the absolute acceleration response spectrum, S_a:

$$S_a(n,\omega_o,s) = |2n\omega_o\dot{x} + \omega_o^2 x|_{max} \tag{1.19}$$

For small damping it may be noted from Eq. 1.19 that S_a is given

approximately by $\omega_o^2 S_d$. There is no correspondingly simple relationship between S_v and S_d. Consequently it is useful to define a pseudo-velocity spectrum, PS_v, by

$$PS_v = \omega_o S_d \tag{1.20}$$

so that

$$S_a \doteq \omega_o PS_v = \omega_o^2 S_d \tag{1.21}$$

This definition has been used previously by Veletsos et al.[14] because it allowed suitable graphs to be drawn in their studies of maximum deformations. Another definition of the pseudo-velocity spectrum, used by Jenschke et al.[15] in their studies of response spectra, is

$$PS_v = \omega_o \sqrt{(1 - n^2)} \cdot S_d \tag{1.22}$$

For damping values up to 20%, these two definitions are within 2% of each other and for smaller typical damping values they are effectively identical.

Before integrating Eq. 1.16 it is first transformed by letting $\tau = \omega_o t$ and $w = x\omega_o^2/g$, becoming

$$w'' + 2nw' + w = -\frac{1}{g} a^*(\tau/\omega_o) \tag{1.23}$$

and the spectra become

$$\begin{aligned} S_v &= \frac{g}{\omega_o} |w'|_{max} \\ S_d &= \frac{g}{\omega_o^2} |w|_{max} \\ S_a &= g|2nw' + w|_{max} \end{aligned} \tag{1.24}$$

where primes indicate differentiation with respect to τ.

The numerical procedure used to integrate Eq. 1.23 was a third order Runge-Kutta method attributed to Heun and described in detail by Housner and Jennings[16]. Because the basic interval of the excitation was not a constant no attempt was made to divide each interval into an integral number of equal integration steps. The bounds on the length of the integration step, $\Delta\tau$, were chosen similarly to those in reference 16 and were, basically, 0.15 for the two highest frequency oscillators (T = 0.1 and 0.2 sec.) and 0.1 for the remainder. These figures strike a balance between the accuracy required in the results and the computer time required in the calculations. For forty-four natural periods ranging from 0.1 to 10.0 sec., and five values of damping (n = 0, 0.02, 0.05, 0.1, 0.2), the computer time was about twenty minutes. The graphs presented here indicate only three values of damping, n = 0, 0.05 and 0.2, to avoid confusion.

The response of an undamped oscillator tends to build up with time during excitation so that the spectrum values often occur towards the end of the record. For this reason the record was assumed to continue with zero acceleration after the last data point until such time as the relative velocity had changed sign three times. Frequently the response reached its maximum value during these last cycles for the undamped case, especially for the longer periods, for example with $T > 3$ sec. The spectral values in these instances are not true values but may be compared with those at adjacent

points and indicate convincingly that the response was building up towards the end of the record.

G. Preliminary Testing

Preliminary tests on the accuracy of response spectra and studies of the dependence on the parameters were made using the adjusted C.I.T. acceleration of 72.58 sec. duration. Later, comparisons of the spectra obtained from the four independent reductions used the standard record lengths close to 60 seconds tabulated in section D.

(i) Dependence of S_v on $\Delta\tau$, the integration step length.

The basic step length was $\Delta\tau = 0.15$ for $T < 0.25$ sec. and $\Delta\tau = 0.1$ for the remainder. Two different sets of values were also investigated, the first being twice as long as these with a tendency to be less accurate, and the second being half as long with a tendency to be more accurate. The results of these changes are shown in Fig. 1.4, where the spectra for the basic step length are depicted with solid lines and fluctuations greater than 0.2 in./sec. due to changes in $\Delta\tau$ are indicated with offset points. There was no change in the values of the spectra for non-zero damping while those of the undamped case were altered by up to 4% for periods less than two seconds. The longer step length tended to lower the spectral values while the shorter step length, with its accompanying extra accuracy tended to raise the spectral values, only to a much smaller extent. It was concluded that the basic step length chosen was suitable for future spectral calculations.

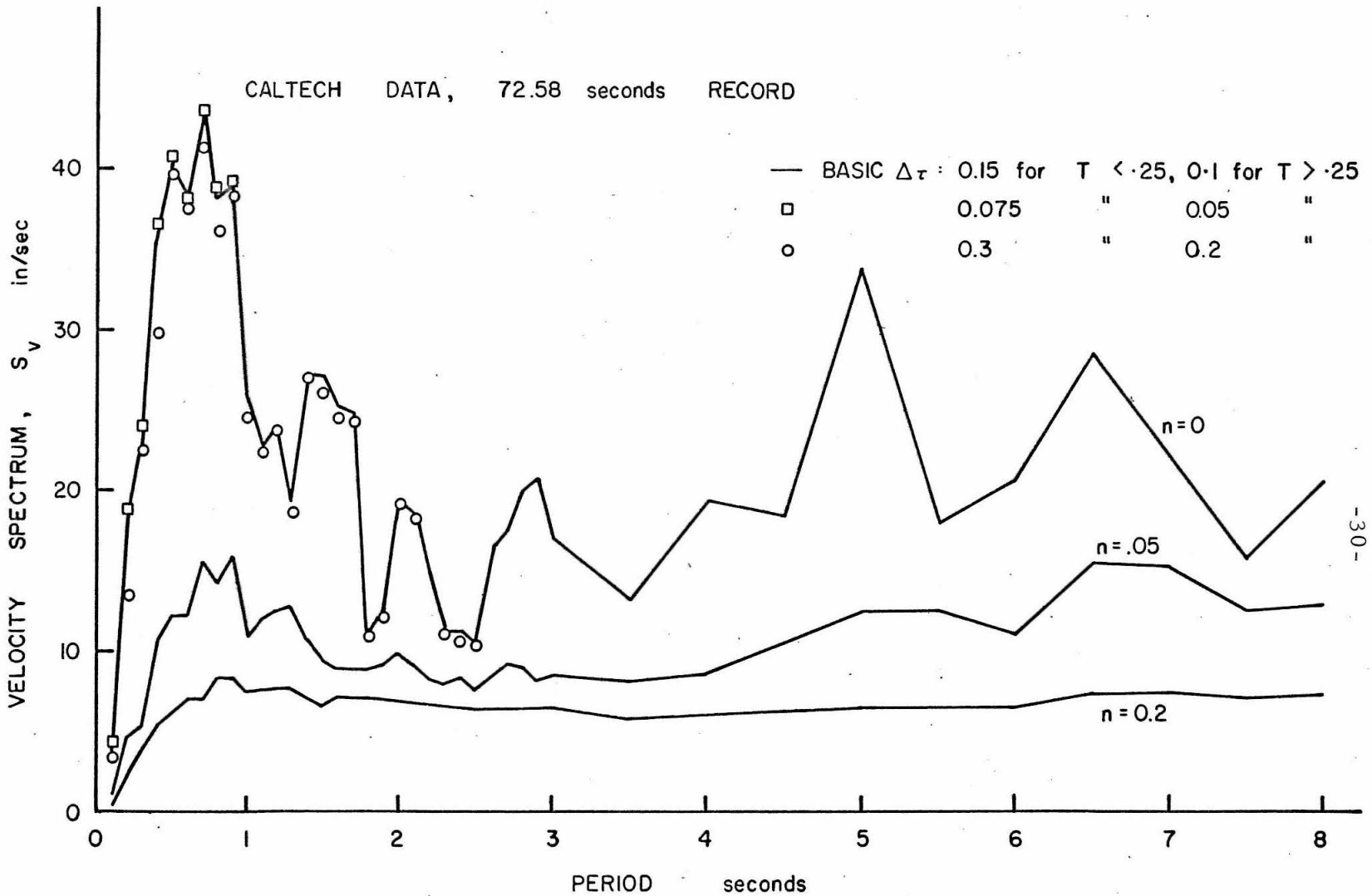

FIG. 1.4 DEPENDENCY OF VELOCITY SPECTRA ON INTEGRATION STEP LENGTH.

(ii) Comparison of the velocity spectra, S_v, with the pseudo-velocity spectra, PS_v, shown in Fig. 1.5.

(a) Undamped. The pseudo-velocity spectra followed S_v very closely throughout the whole range of periods, being 25% low for the high periods.

(b) Damped. The difference between the two spectra fluctuated throughout the range of periods. The pseudo-velocity remained below the corresponding value of S_v, sometimes dropping to 50% of S_v.

These results, when viewed overall in Fig. 1.5, indicate that while for the most part the discrepancies between the two spectra are within the range of acceptable engineering accuracy, there are certain regions where more consideration might be necessary.

(iii) Effect of the length of record.

The previous two tests used the adjusted C.I.T. record of 72.58 seconds duration. Whether or not the same behavior could be expected when a different record duration is used can be judged from Figs. 1.6 and 1.7 where the effect of using the first 60.01 seconds of the record is shown, for the undamped and damped cases, respectively. For those periods at which the spectrum value depends appreciably on the length of the record, the approximate time of occurrence of the maximum value is shown. For the shorter periods (less than 3-1/2 seconds in the undamped case and 5-1/2 seconds in the damped case) there is a negligible dependency

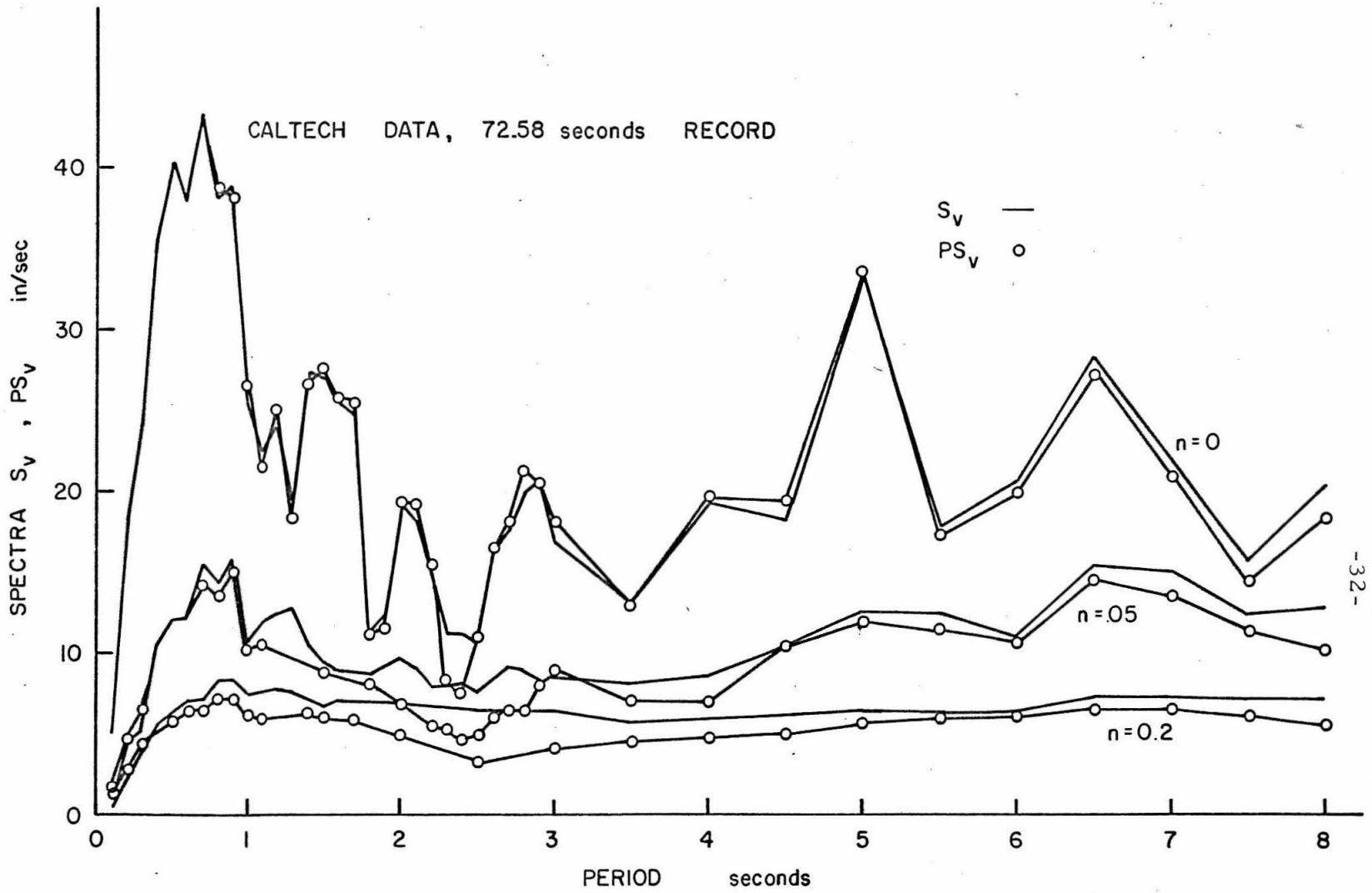

FIG. 1.5 COMPARISON OF VELOCITY SPECTRA WITH PSEUDO-VELOCITY SPECTRA.

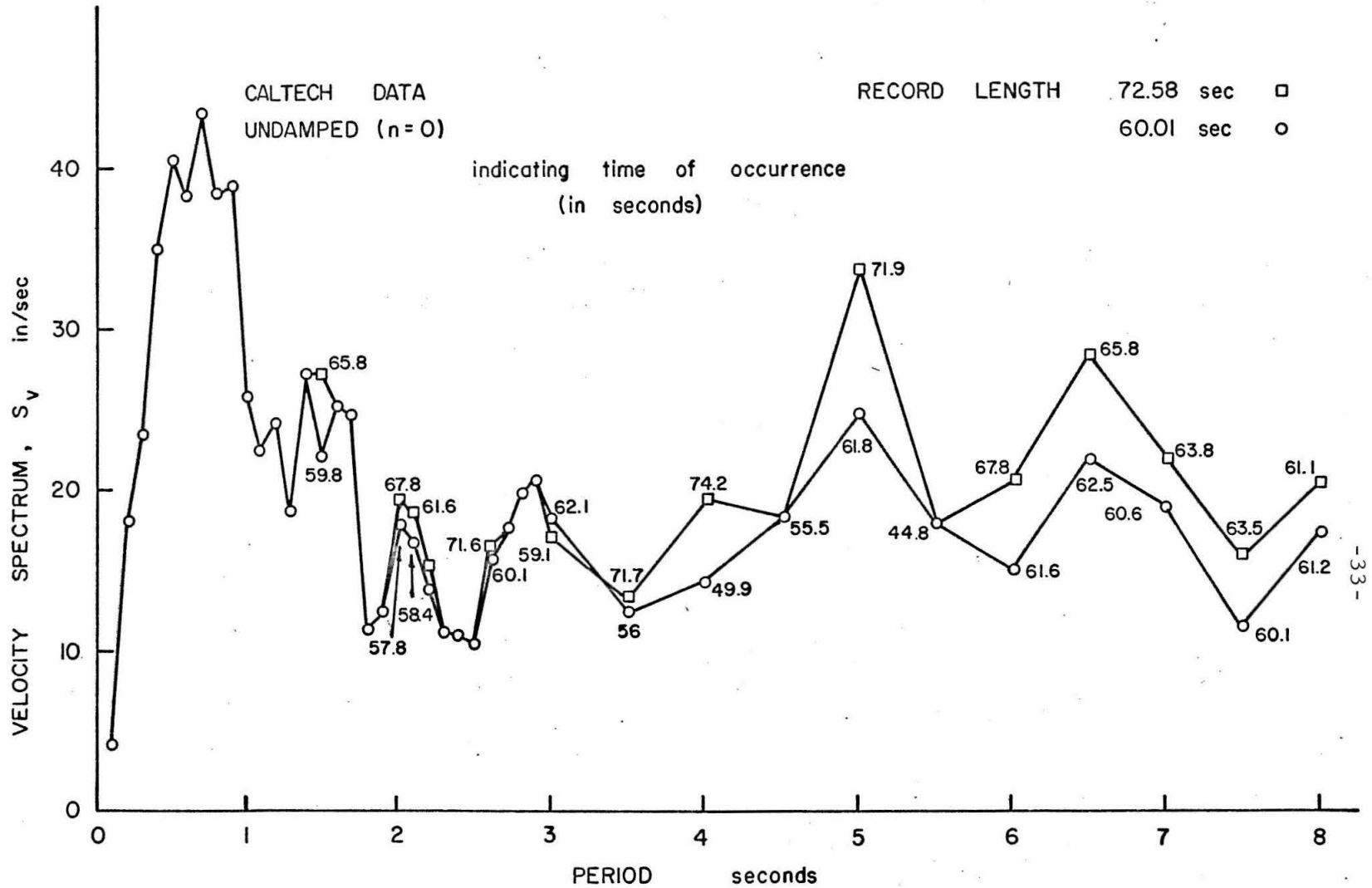

FIG. 1.6 EFFECT OF LENGTH OF RECORD ON UNDAMPED SPECTRA.

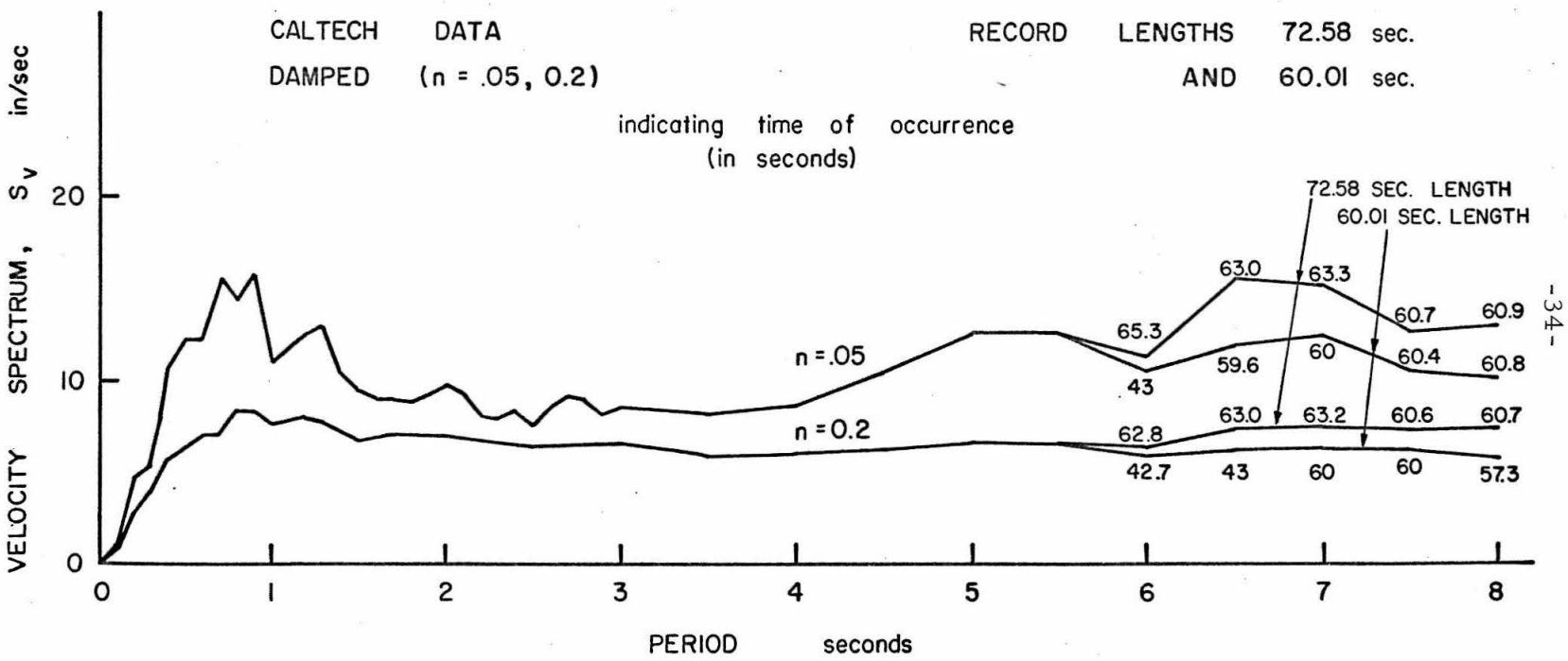

FIG. 1.7 EFFECT OF LENGTH OF RECORD ON DAMPED SPECTRA.

on the length of the record. In these regions, therefore, it is expected that Figs. 1.4 and 1.5 are reasonably indicative of the behavior of the spectra for any record length in the vicinity of sixty to seventy seconds. However, Fig. 1.6 indicates how in the undamped case the majority of the spectral values are attained towards the end of the record. Some occur after the excitation is over, during the last cycle of the response, when a zero exciting acceleration has been in effect. Particularly for the longer periods of the undamped case, then, the length of the record has a marked influence on the maximum response attained. The same is true to a lesser extent in the damped case shown in Fig. 1.7.

Some explanation for this unexpected behavior of the damped case of Fig. 1.7, where the longer period maximum values still have a tendency to occur around sixty seconds, can be seen from the displacements of Fig. 1.3, calculated from the record. Between thirty-four and forty-four seconds a strong five-second oscillation is apparent, and from forty-four seconds on another strong seven-second oscillation is building up. This long period ground movement, occurring as it does during the second half of the record, tends to increase the response for all the long period spectral values.

H. Comparison of Velocity Spectra and Standardization of Calculations

Using the four adjusted accelerations obtained from the earlier work on displacements, the velocity response spectra were calculated for comparison. The accelerations were adjusted using a record length varying from 60.00 sec. for the Berkeley data to 60.10 sec. for the Illinois data. This difference in duration was not considered critical in the response calculations. The four independent readings of identical reproductions of the same record gave rise to the spectra shown in Figs. 1.8 to 1.11, and the scatter found in the computed spectra is shown in Fig. 1.12.

The results check well with those of Professor Berg[17] at Michigan over the range of periods--0 to 3 sec.-- which he had selected for analysis. The few points at which small differences were noticed can be explained by the different treatment of the records beyond the sixty second duration. At Michigan the zero acceleration continuation, described in Section F, was not used.

The scatter can be seen to increase generally with increasing period, T, for the undamped case, being up to 25% from the mean value for T less than two seconds, and up to 40% for T greater than two seconds. The damped responses are less scattered, with a spread of 6% from the mean for T less than one second and 20% thereafter. Professor Berg has pointed out[17] that the spread displays an order of accuracy that one can ordinarily tolerate from an engineering viewpoint. By considering the earthquake record

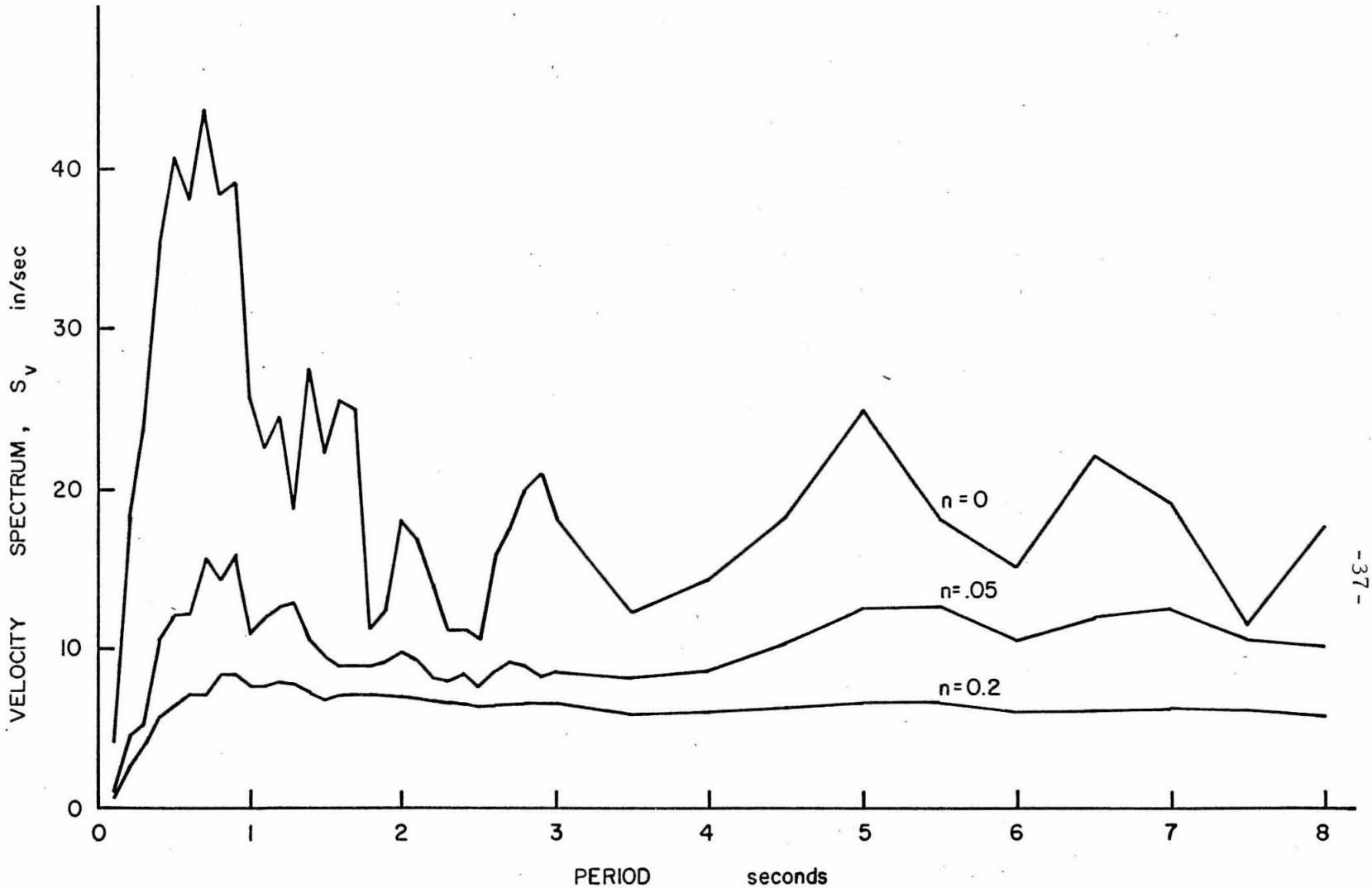

FIG. 1.8 VELOCITY SPECTRA OF C.I.T. DATA, 60.01 SEC.

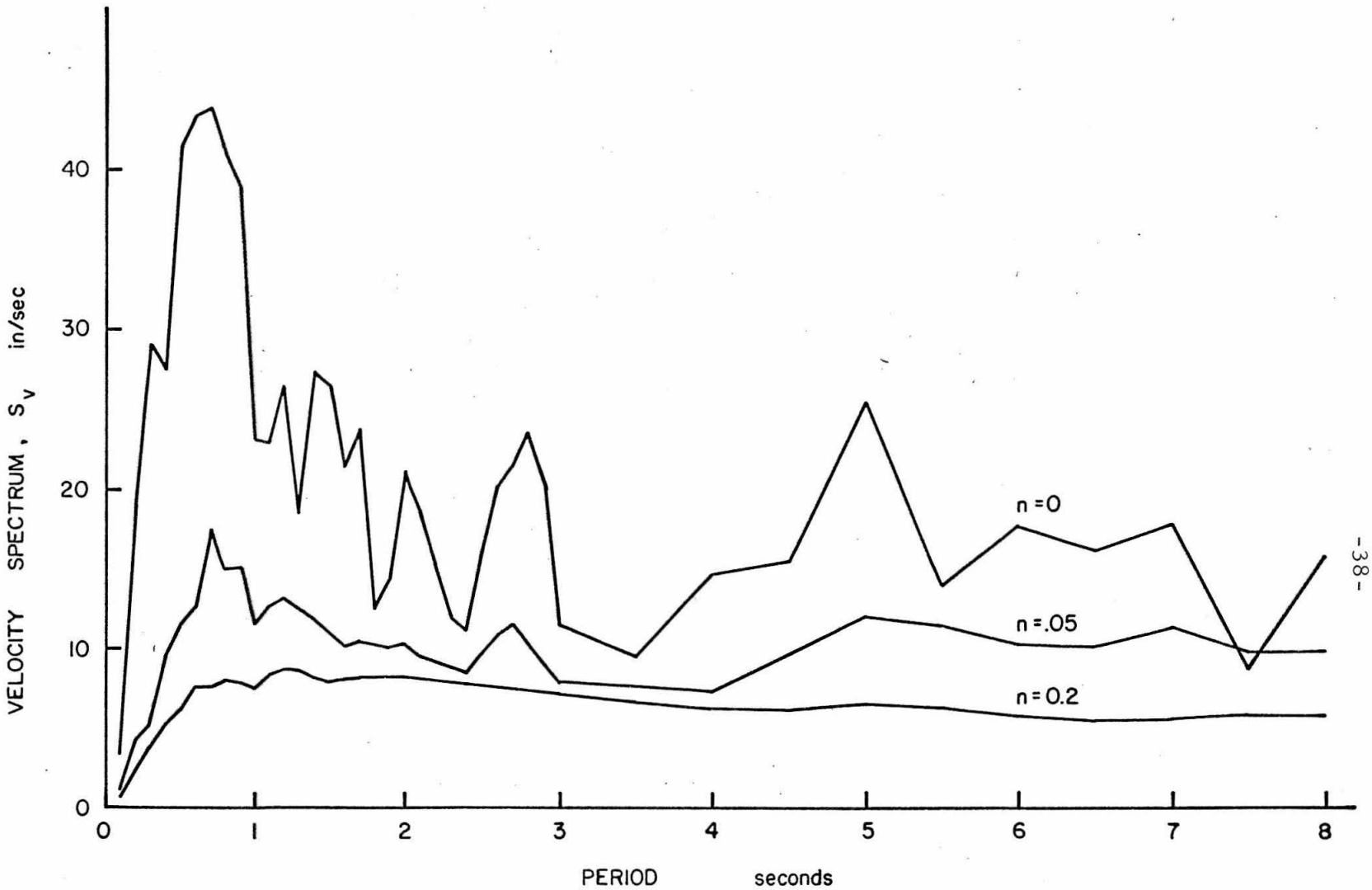

FIG. 1.9 VELOCITY SPECTRA OF MICHIGAN DATA, 60.07 SEC.

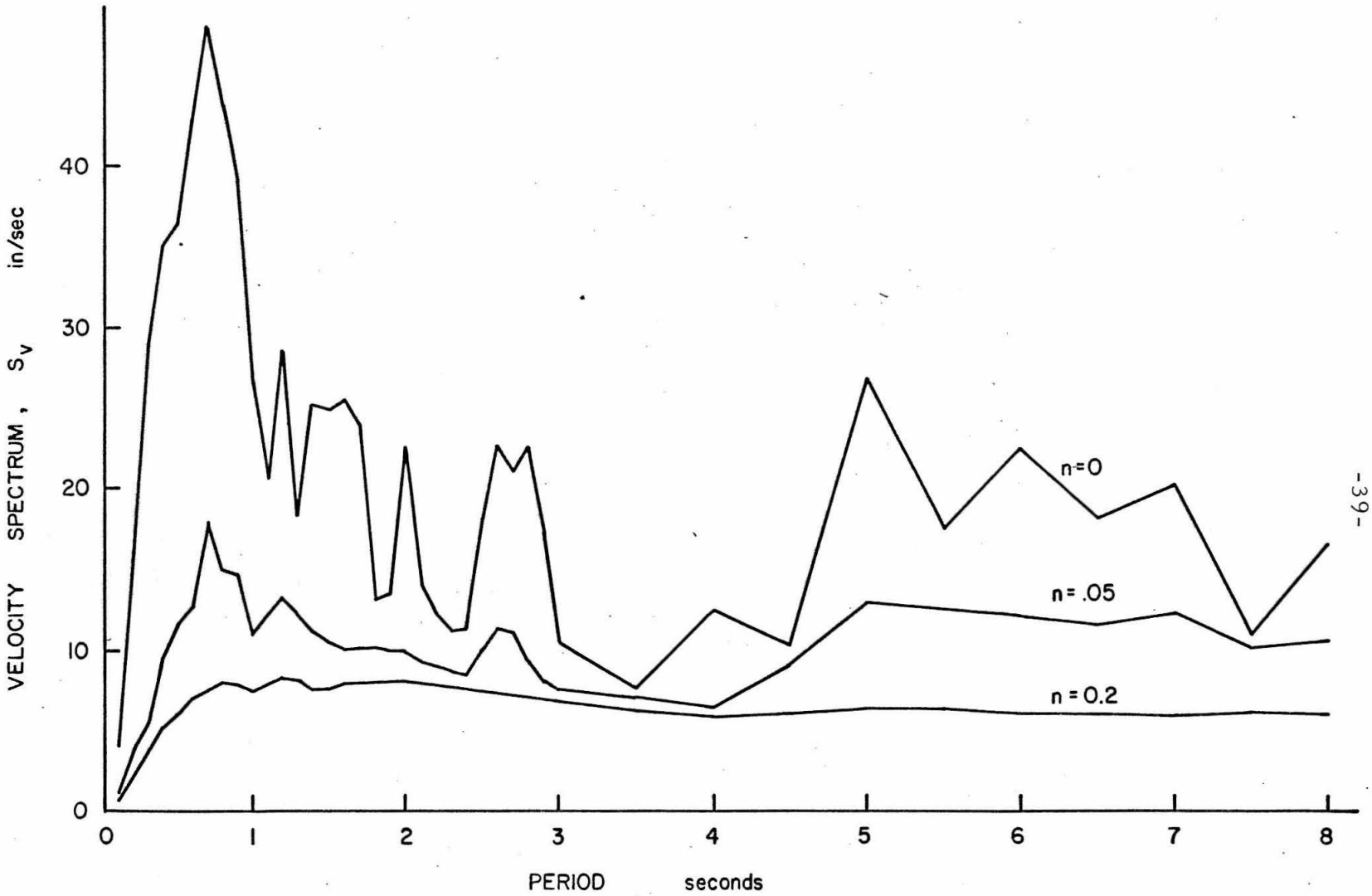

FIG. 1.10 VELOCITY SPECTRA OF ILLINOIS DATA, 60.10 SEC.

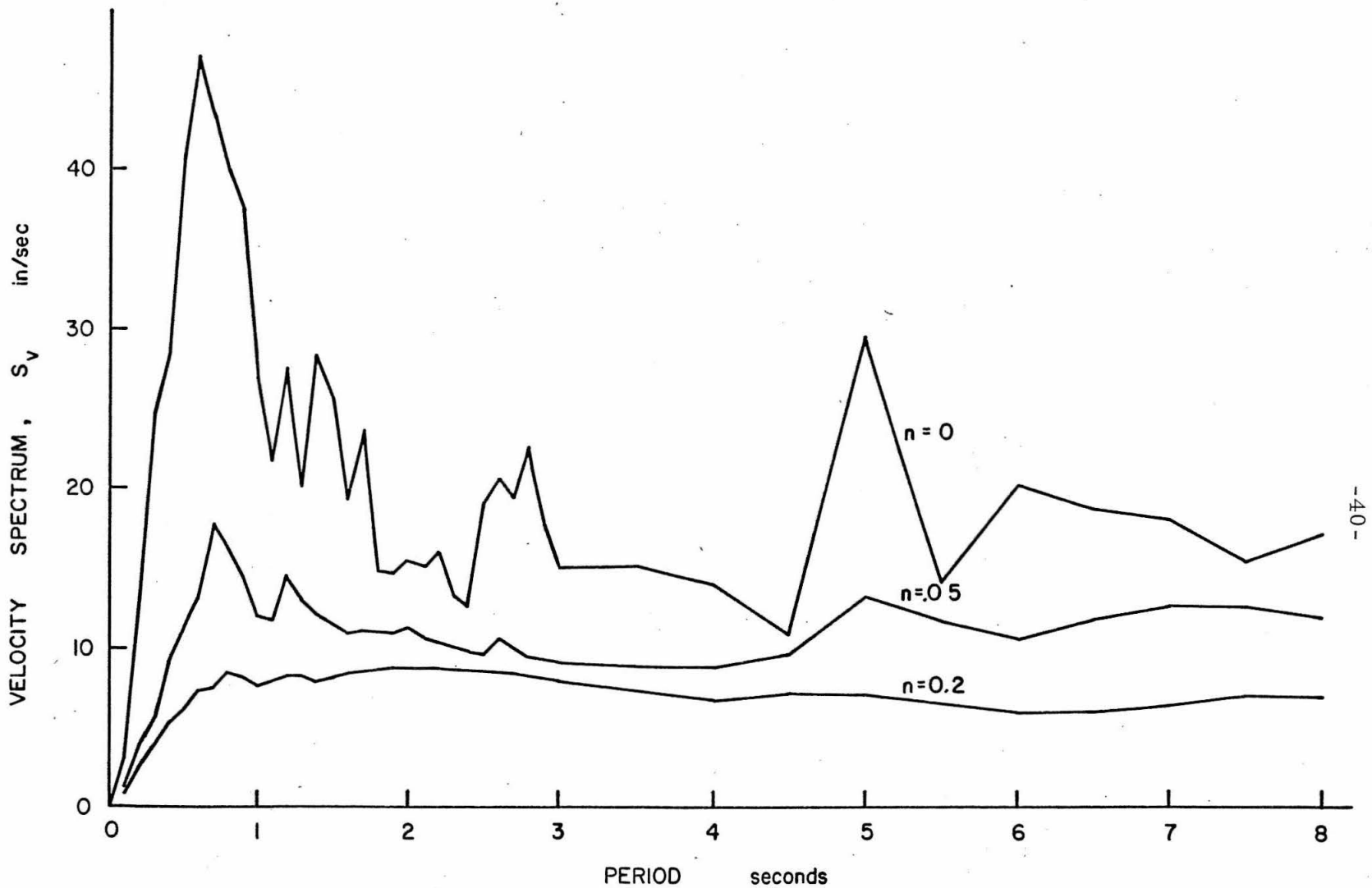

FIG, 1.11 VELOCITY SPECTRA OF BERKELEY DATA, 60.00 SEC.

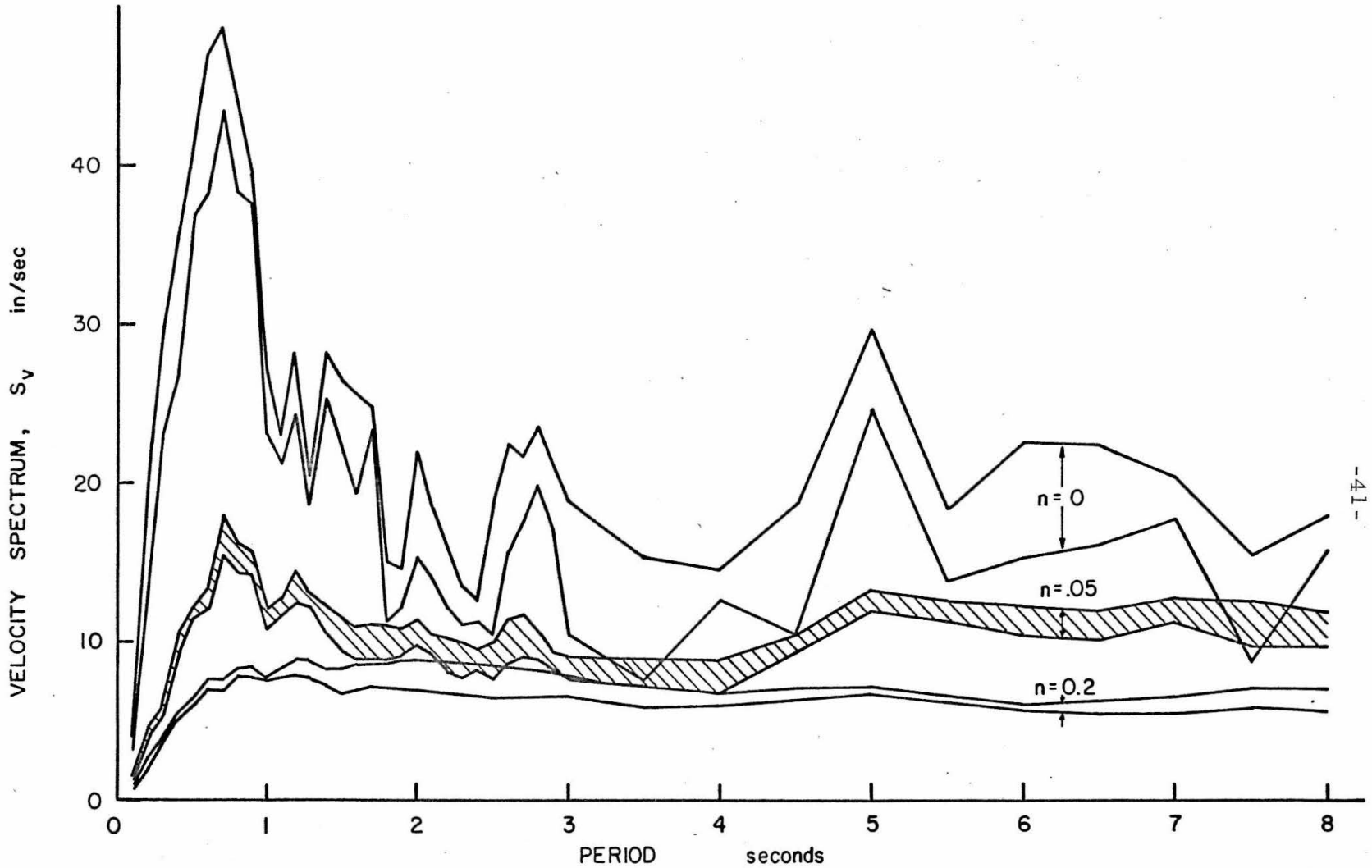

FIG. 1.12 SCATTER OF THE VELOCITY SPECTRA FROM THE FOUR DIFFERENT VERSIONS.

as an equivalent train of velocity impulses, Berg showed that the scatter was attributable to a random error in reading the accelerogram. Furthermore, reducing the scatter would require better resolution in recording the ground motion, and equally dependable ways of preparing the input data.

Apart from the differences mentioned here between the C.I.T. and Michigan results for the same input data, the two calculation procedures have produced identical spectra. The spectra results are not as sensitive to the integration techniques used in solving Eq. 1.16 as were the displacement results to the integration techniques used in the earlier part of this chapter.

Standardization of the calculations will in this case be restricted to fixing the length of the record and deciding how to treat those maximum responses which have a tendency to occur just after the record is completed. These two requirements are related for both become important in the case of undamped spectra and for cases where residual long period ground oscillations (i.e., between five and ten seconds) toward the end of a record, create large spectral values.

Because the earthquake excitation does not actually cease at the point where the record has been rather arbitrarily cut off, an assumption of zero acceleration beyond the specified length introduces an approximation in the spectra. Moreover, the undamped spectral values resulting from C.I.T.'s 60.01 sec. record, shown in Fig. 1.6, occur frequently beyond the end of the record, particularly for periods greater than 2-1/2 sec. Hence some standardizing

procedure needs to be specified.

Two additional methods may be mentioned. The first is simply to go no further than the specified duration, which is the slightly quicker and easier method, but simply evades the difficulty by accepting an uncertain error. The second is to carry on with the actual adjusted record beyond the specified duration until the velocity has changed sign three times. About fifteen extra seconds of data would be required for the ten-second period spectral values.

For a detailed explanation of how the scatter of the spectrum curves of Fig. 1.12 can be attributed to random errors in reading the accelerogram, reference can be made to Berg[17] who has covered this aspect thoroughly in reporting the Michigan results. The narrowing of the scatter with increased damping can also be explained on the basis of random reading errors.

Finally, it may be pointed out that the spread of the spectrum curves resulting from different investigators reading the same original accelerogram is similar to the deviations between digital and analog response spectrum calculations published earlier[5]. This indicates that in effect the analog results of reference 1 can be considered to have the same general engineering accuracy as the more recent digital computations.

I. Summary and Conclusions

A procedure has been outlined for adjusting the records of strong-motion earthquake accelerations once they have been reduced to digital form. A parabolic base line adjustment is made to the acceleration, ensuring that the mean square velocity is a minimum. The ground velocity and displacement are calculated from the adjusted acceleration. Various checks are made to verify that there is no loss of accuracy during the digital computer calculations and a standardized method for carrying out the calculations, as a result of these checks, is recommended. This method is then used to compare the results of four independent reductions to digital form of identical copies of a particular earthquake record. The resulting displacements show a wide scatter that is attributed to random errors in reading the original accelerogram.

Response spectra are also calculated from the adjusted acceleration. Checks are made to ensure that no loss of accuracy can be attributed to the digital calculations and standardized methods of defining the record length are studied. The pseudo-velocity spectra are compared with the velocity spectra and found to agree within tolerable engineering limits except perhaps for the longer periods. The velocity spectra from the four adjusted accelerations compared earlier are calculated and display a scatter that is not as serious as that of the ground displacements. This scatter has also been attributed to random errors in individual reading of the accelerogram.

It is concluded that the full eight-figure accuracy of the modern digital computer is necessary to realize the full capability of the displacement calculations from acceleration records. Without taking care to preserve this numerical accuracy, errors may accumulate which are larger than those coming from the original digitization. Further accuracy of displacement and spectrum results will require more accurate instruments to record the original ground motion acceleration and equally dependable ways of preparing and digitizing the input data. At the present stage of earthquake engineering design much further accuracy is perhaps not yet warranted, for the uncertainties in predicting earthquake locations and magnitudes far outweigh the uncertainties found in this study as depicted by the scatter of the displacement and spectrum curves.

II. PROBABILITY DENSITY DISTRIBUTIONS OF THE MAXIMUM RESPONSE OF SIMPLE OSCILLATORS TO RANDOM EXCITATION

A. Introduction

One of the main problems in earthquake engineering is determining the behavior of a structure subjected to a given strong-motion earthquake excitation. In particular, the engineer is interested in the forces and strains suffered by the structure, and more particularly still, in the maximum values of these quantities as they vary during the motion. There is a number of reasons for choosing to concentrate on the maximum relative velocity of a simple, one degree-of-freedom structure, from among all the possible responses of interest. An important reason is that one class of dynamics problems is readily solved by equating energy inputs with energy dissipations, and expressions for the maximum energy of a structure frequently involve the velocity[3].

It is possible to characterize an earthquake and its effect on a simple, one degree-of-freedom structure by means of the maximum relative velocity response spectrum, commonly called the response spectrum. This is defined as the maximum relative velocity attained by the mass in a linear, viscously damped structure during base excitation. The equation of motion for such a structure can be written

$$m\ddot{x} + c\dot{x} + kx = -m\ddot{y}(t) \qquad (2.1)$$

or

$$\ddot{x} + 2n\omega_o \dot{x} + \omega_o^2 x = -\ddot{y}(t) \qquad (2.2)$$

where m is the mass, c the coefficient of viscous damping, k the stiffness, x is the relative displacement, $\ddot{y}(t)$ is the absolute ground acceleration, $n = c/2\sqrt{(km)}$ is the fraction of critical damping and $\omega_o = \sqrt{(k/m)}$ is the natural frequency. Eq. 2.2 indicates that the maximum value of $\dot{x}$ depends on the two parameters n and ω_o. In the earthquake engineering field the two parameters used are the natural period $T = 2\pi/\omega_o$, and n. Curves of the response spectra, in terms of n and T, are available for all of the recorded strong-motion earthquakes[1]. Nearly all have a similar form. The undamped curve has a wildly oscillating portion at low periods (up to one second), and tends to vary about a reasonably constant level for higher periods; as the damping is increased the curves smooth out and indicate progressively lower maxima.

Although it might be expected that the spectra of future strong-motion earthquakes will be similar to these, the oscillatory portions indicate that there is some doubt as to how close the similarity will be. The eight components of the four strongest ground motions recorded up to 1959 have been used by G. W. Housner to calculate an average spectrum, with which it is possible to estimate the expected maximum response to future earthquakes[4]. However, it is not possible to arrive at any conclusions regarding the spread of such future maximum responses about their mean value from such a small sample. One of the problems answered in this chapter arises directly from this. How can sufficient information be obtained

on maximum responses so that the distribution about the mean can be deduced?

These distributions have been of increasing interest at the present time to those design engineers in a position to take advantage of a prior knowledge of the probability of survival, or of failure, of a structure. The types of questions frequently asked are the following. Suppose that a standard worst earthquake for a particular location had been agreed on, and that an ensemble of such earthquakes with identical statistical properties could be obtained. How do the structural parameters of mass, damping and stiffness affect the average value of the maximum stress suffered at some critical point by a simple structure? What is the probability that the maximum stress is a certain multiple of the ensemble average of the maximum and how do the mass, damping and stiffness affect these probabilities?

In order to answer these questions the problem will be formulated in as simple a manner as possible. Consider a simple, linear, viscously damped oscillator, of one degree-of-freedom, whose base is capable of random excitation. The particular nature of the excitation is not yet specified although it will be such that the base acceleration will ultimately be any one of the following: white noise, as first used by Housner[6] and later by other authors[7,3,16,8,9]; a Gaussian non-white process with a specified power spectral density, as used by Housner and Jennings[16]; and actual records of strong-motion earthquakes[1]. Once the type of excitation is chosen, together with its duration and some measure of its strength or

intensity, a meaningful study can be made of the statistical properties of the structure's response. These three excitations offer progressively more difficulty in obtaining analytical answers to the distribution problem. In fact the third is even difficult to describe satisfactorily in mathematical form due to its non-stationary nature.

In view of this, Monte Carlo techniques were investigated for an experimental solution having a wide range of usefulness as far as different types of excitation were concerned. The technique could be used by setting up a repetitive excitation, i.e., one whose statistical properties could be repeated at will, applied to the base of a structure sufficiently often to experimentally determine the distribution curves for the maximum response. Suitable choices would have to be made for the damping and period of the structure in order to provide a whole spectrum of useful distribution curves.

The general purpose electric analog computer in the Dynamics Laboratory at the California Institute of Technology and its subsidiary equipment proved to be very useful in obtaining results by these methods. The following section gives a brief account of the experimental procedure and the results that were used for comparison with the theoretical analysis of a later section. This analysis follows Rosenblueth and Bustamante's[9] approach in obtaining the probability densitites of maximum response and their dependence on damping, period and length of excitation, for simple excitations. The accurate calculation of these probability densities is described in the main section, where the comparisons with experimental

results are made, and the chapter concludes with a brief summary and an indication of the future usefulness of the Monte Carlo experimental procedures.

The nomenclature for Chapter II, consistent with that for Chapter I, follows in full.

NOMENCLATURE

c, coefficient of viscous damping

$c_3 = R^2 n\omega_o/2k_1$

E(R), expected, or average, or mean value of R

F(R) = F(R,s), the probability of R having not been exceeded during s seconds of excitation

F(R,t), the probability of R having not been exceeded by time t

f(R) = dF(R)/dR, probability density function

G(ω), power spectral density

J_o, J_1, Bessel functions of the first kind

k, stiffness

k_1, intensity of excitation

$M_m(z)$, a confluent hypergeometric function described in the Appendix

m, mass

$n = c/2\sqrt{km}$, fraction of critical damping

R, a particular value of r

$R_1 = e^{n\omega_o t} R$, a particular value of r_1

$\overline{R}_o$ = E(R) in undamped case

$r = \sqrt{[(\omega_o x)^2 + \dot{x}^2]}$, for undamped case

$r = \sqrt{[(\omega x)^2 + (\dot{x} + n\omega_o x)^2]}$, for damped case

$r_1 = e^{n\omega_o t} r$

s, duration of excitation

$T = 2\pi/\omega_o$, natural period

t, time

t_i, a discrete time value

$\Delta t_i = t_{i+1} - t_i$, time increment

u_i, ground velocity increment at time t_i

$u = u(r,t)$, probability function of r at time t

$u_1 = u_1(r_1,t)$, probability function of r_1 at time t

x, relative displacement of oscillator

$\ddot{y}(t)$, absolute ground acceleration

z, integration variable

$a = R/2\sqrt{(ks)}$, dimensionless response

$\delta(t)$, Dirac delta function

λ, average number of impulses per second

λ_m, the m-th eigenvalue described in the Appendix

σ, standard deviation

σ^2, variance

$\omega_o = \sqrt{(k/m)}$, natural frequency

$\omega = \omega_o\sqrt{(1 - n^2)}$

B. Monte Carlo Techniques

The Dynamics Laboratory was able to provide experimental results, that were suitable for later comparison, by using the following methods.

A low frequency noise generator, whose signal could be passed through filters to provide random excitation with any specified power spectral density, was available. This flexibility was one of the advantages of the analog computer in this study. The power spectral density of an earthquake record is related approximately to the square of the undamped response spectrum, and the possibility arose of using an average spectral density curve, in the same way as Housner and Jennings[16], derived from the average response spectrum curve described in the Introduction. However, because there was an opportunity of checking experimental results against theoretical results only if sufficient simplifications were made, white noise excitation was used, with constant spectral density up to 100 cps.

In the computer, electric elements are used to carry out the operations indicated by the differential equation. A block diagram appearing in Fig. 2.1 indicates the way in which Eq. 2.2 is treated.

To obtain different values of damping and period, adjustments were made to the elements governing these coefficients. During each run the voltage corresponding to the relative velocity $\dot{x}$ in one direction was applied through a simple diode circuit to one plate of a capacitor. Frequent visual checks of this voltage indicated that

EQUATION OF MOTION $\ddot{x} + a_1\dot{x} + a_2x = a_3E_o(t)$

EQUATION FOR ANALOG $\dot{x} = \int_o^t \left[a_3E_o(t) - a_1\dot{x} - a_2x\right] dt$

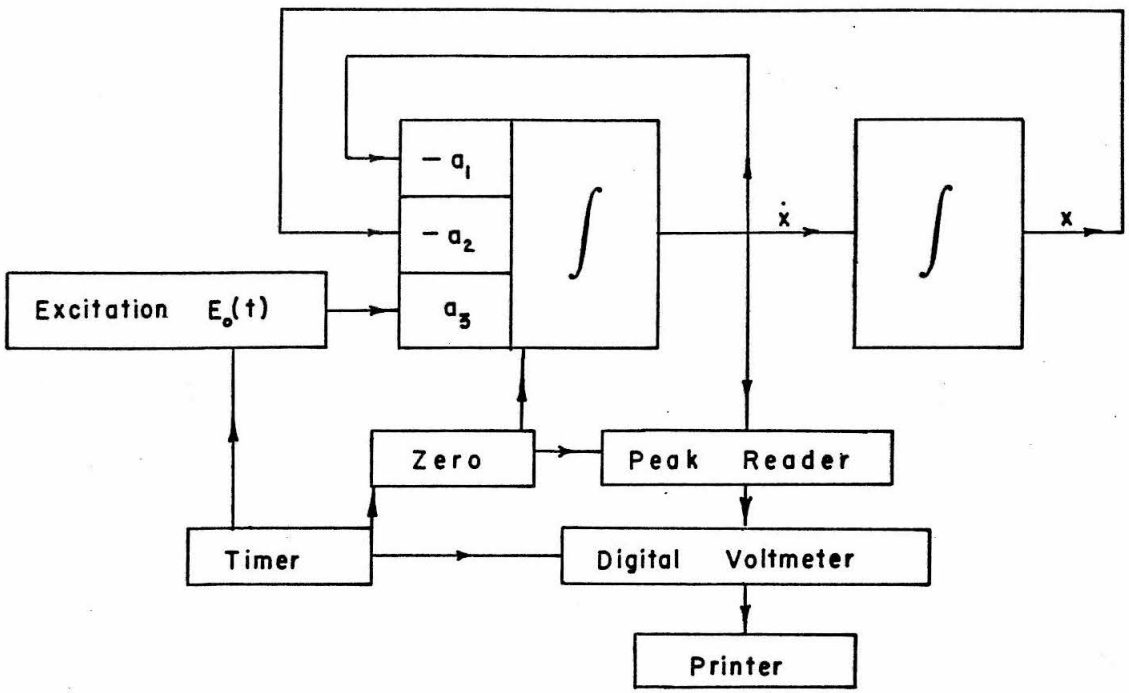

FIG. 2.1 BLOCK DIAGRAM OF ELECTRIC ANALOG FOR MAXIMUM RELATIVE VELOCITY OF OSCILLATOR.

the amplitude was varying sufficiently slowly around the maximum for a check to be kept only in one direction. The capacitor retained the maximum value of the voltage applied to it throughout the excitation. The final value was read by discharging the capacitor through an integrating device and applying the output to a digital voltmeter. This was connected with a digital printer for a permanent record. A thirty-second duration was used throughout with an automatic timing device to start and stop the excitation, measure and record the maximum, reduce the system and the peak reader to zero and repeat the operation. One thousand samples were taken for each of four different periods (0.5, 1.0, 1.5 and 2.0 seconds) and four damping fractions (0, 2, 5 and 10%). The IBM 7094 digital computer at the California Institute of Technology was used to calculate the mean and standard deviation for all sixteen cases, and histograms were plotted showing the frequency of occurrence of the maxima in each case. The output and excitation were suitably proportioned to provide the on-scale readings presented here. In later analyses, the response was brought into dimensionless form by dividing by the undamped mean, so no attempt was made here to record the units of velocity.

Four of the histograms appear in Figs. 2.2 to 2.5 corresponding to $T = 1$ sec. and $n = 0$, 2, 5 and 10%. The mean, μ, and standard deviation, σ, are shown on each histogram and are tabulated together with the remaining twelve results in Table 2.1. It is noticed that the mean and standard deviation both increase with period

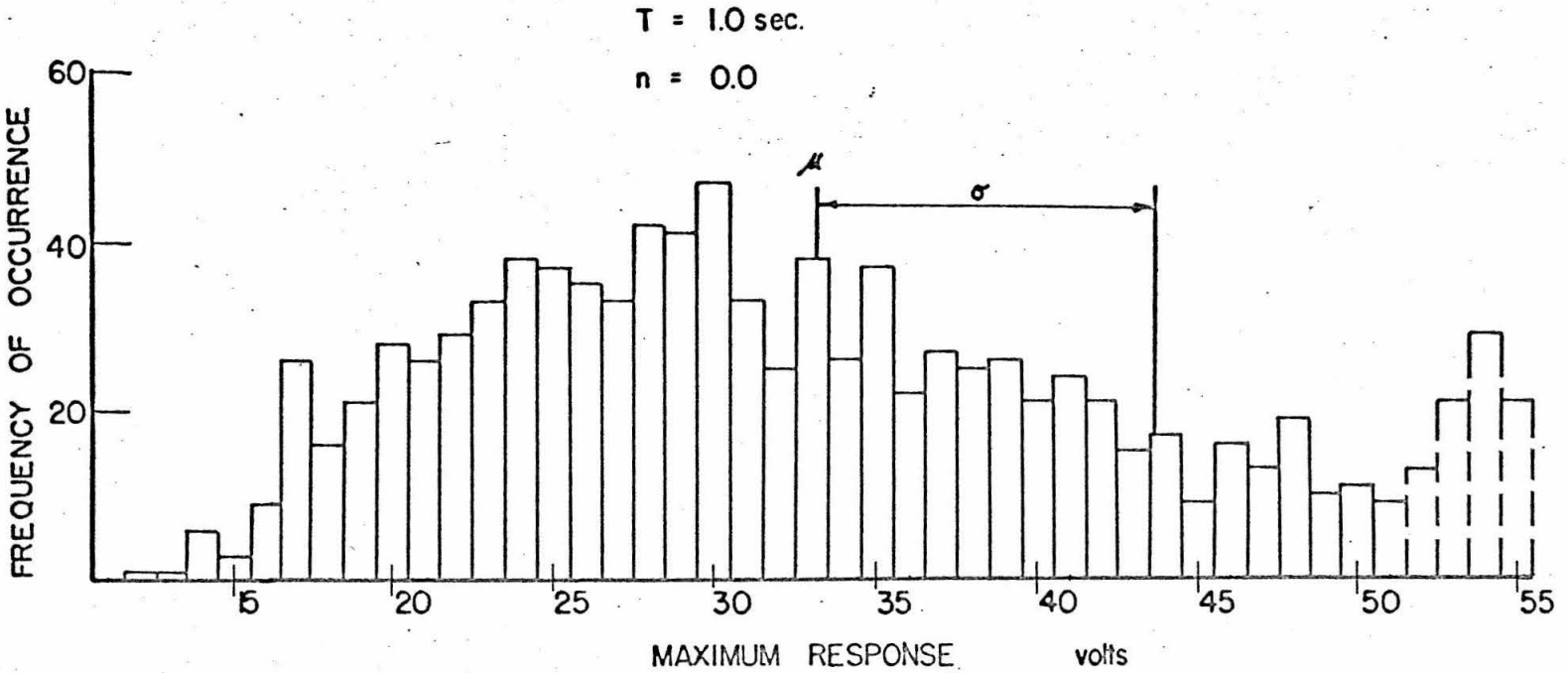

FIG. 2.2 EXPERIMENTAL HISTOGRAM OF MAXIMUM RESPONSE.

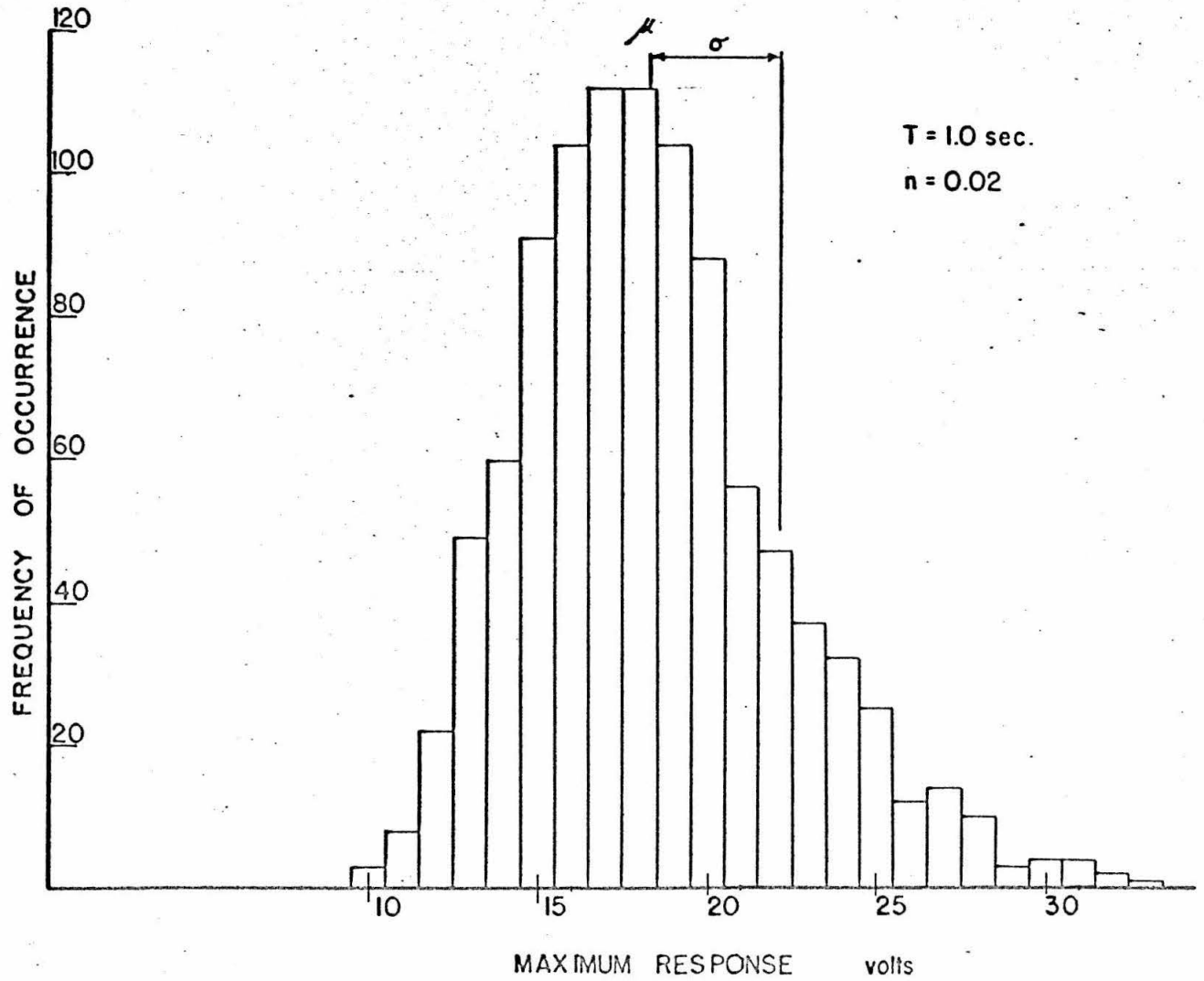

FIG. 2.3 EXPERIMENTAL HISTOGRAM OF MAXIMUM RESPONSE.

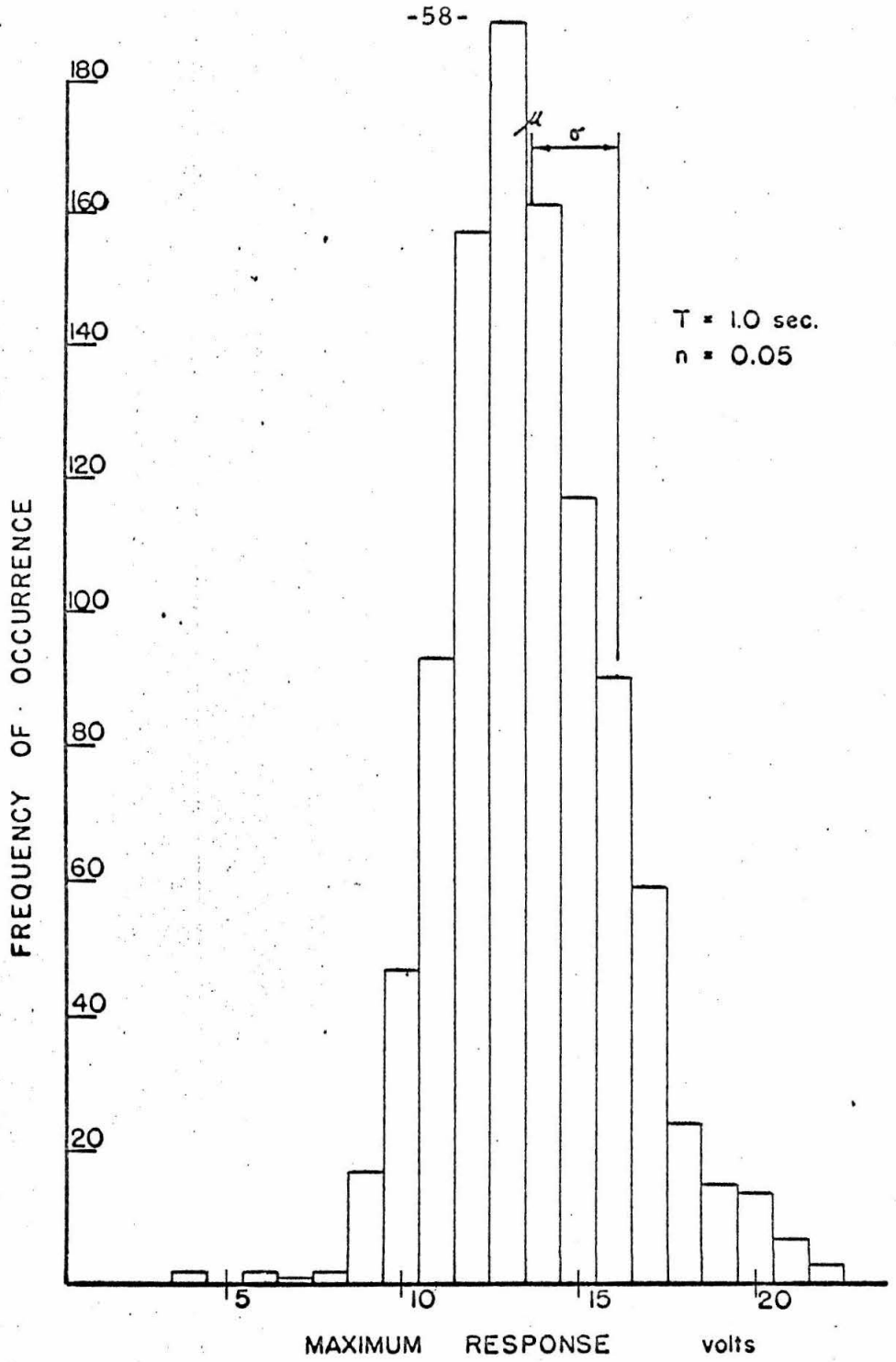

FIG. 2.4 EXPERIMENTAL HISTOGRAM OF MAXIMUM RESPONSE.

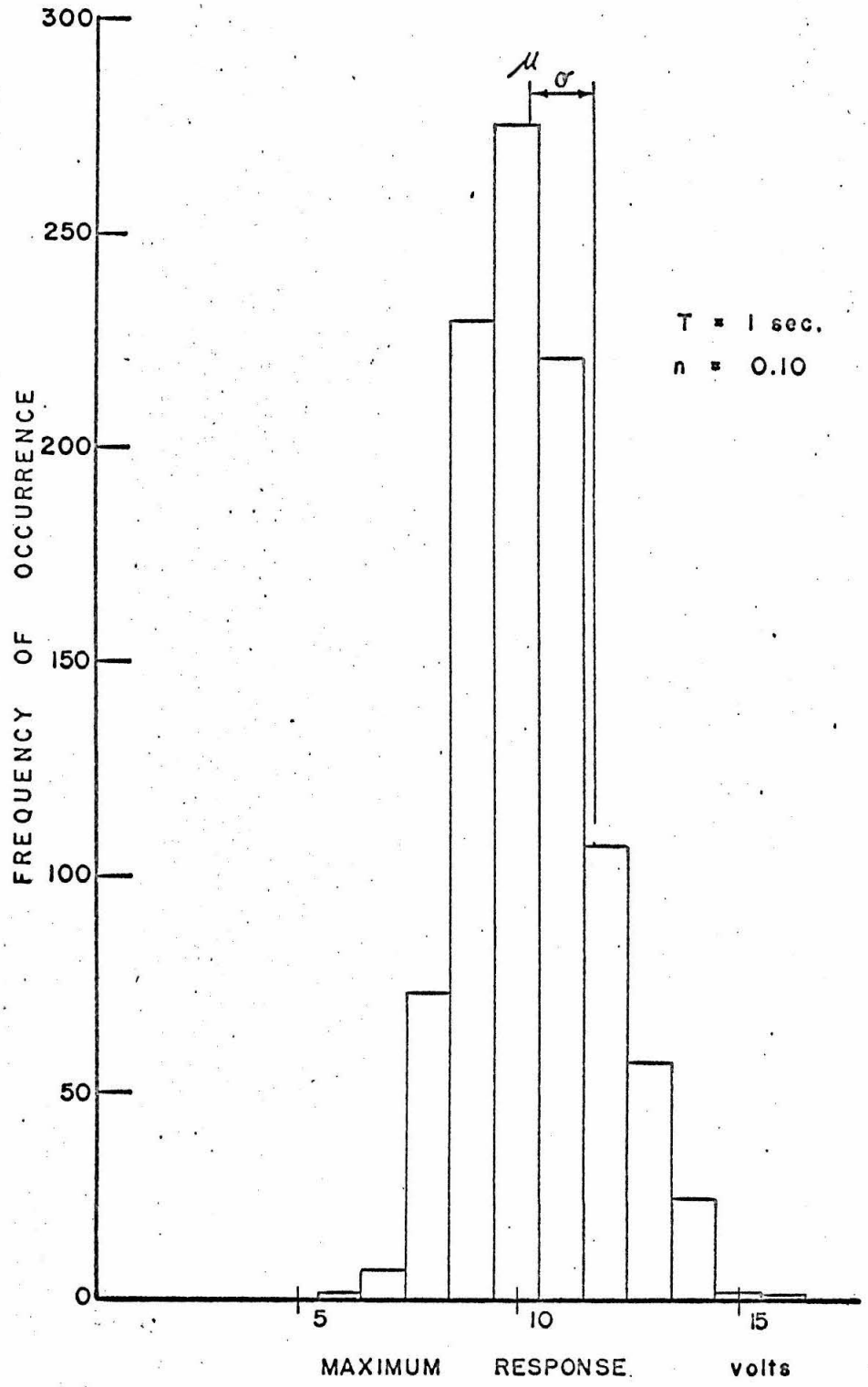

FIG. 2.5 EXPERIMENTAL HISTOGRAM OF MAXIMUM RESPONSE.

for fixed damping. This behavior of the mean is expected from the shape of existing earthquake response spectra.

Table 2.1

Experimental Means and Standard Deviations

Damping%		Period (sec.) 0.5	1.0	1.5	2.0
0	μ	32.0	33.1	32.4	32.3
	σ	10.06	10.63	10.09	10.63
2	μ	14.8	18.3	20.7	22.3
	σ	2.61	3.85	4.97	5.59
5	μ	10.5	13.55	15.4	17.0
	σ	1.60	2.43	2.87	3.53
10	μ	7.8	10.3	11.8	13.1
	σ	1.03	1.45	1.92	2.33

Saturation of the equipment in the undamped cases caused an artificial upper limit at a value of about 50 volts, indicated in Fig. 2.2, where the affected values are shown with dashed lines. The shape of the histograms corresponded closely to the later theoretical curve, except for this portion, and one of the histograms was smoothed out at its upper end to conform to the curve. This resulted in an increase in the mean value of 0.2, or less than 1%, so that the reshaping process was not continued and the error was considered negligible.

A check on the dependence of μ and σ on the sample number indicated that in general the means had settled down after 300 to 500 runs, and the standard deviations after 500 to 600 runs.

C. Analytical Equations for the Distribution

In this section expressions for the probability density are derived following the work of Rosenblueth and Bustamante[9] on probability of survival and extending their results to obtain curves with which to compare those of the previous section. Accurate calculation of the expressions, on the IBM 7094 computer, and an indication of the use to which they can be put, form the main part of section D.

The ground acceleration is assumed to consist of a series of impulses distributed randomly in both magnitude and time, such that the ground velocity changes instantaneously by an amount u_i at time t_i. The acceleration $\ddot{y}(t)$ is thus given by

$$\ddot{y}(t) = \begin{cases} \sum_{i=1}^{j} u_i \delta(t - t_i) , & 0 < t \leq s \\ 0 , & \text{otherwise} \end{cases} \qquad (2.3)$$

where the summation is taken only up to the impulse immediately preceding the time t, i.e. $t_j < t < t_{j+1}$, $\delta(t)$ is the Dirac delta function and s is the duration of the excitation.

Undamped case. The response of a linear undamped oscillator is governed by Eq. 2.2 with $n = 0$. For zero initial conditions, the Duhamel integral representations of x and $\dot{x}$ can be readily substituted into the following expression for a quantity r:

$$r^2 = (\omega_o x)^2 + \dot{x}^2 \qquad (2.4)$$

yielding

$$r^2 = \left[\sum_{i=1}^{j} u_i \sin \omega_o t_i\right]^2 + \left[\sum_{i=1}^{j} u_i \cos \omega_o t_i\right]^2 \qquad (2.5)$$

The quantity r is of prime interest in this analysis because it approximates closely the local maximum absolute values of both $\omega_o x$ and $\dot{x}$ as these maxima vary with time. This can be seen readily from the fact that $\dot{x} = 0$ at maximum x, and that $\dot{x}$ is close to a local maximum as the oscillator passes through $x = 0$. These deductions may be confirmed by observing a record of the response to such an excitation. A record of this type will also indicate that when the oscillator starts from rest, a reasonable length of time, depending on the natural frequency ω_o is required before the oscillatory motion with slowly varying amplitude is built up. Provided that the duration of excitation is much longer than the natural period T, and that the maximum value of r occurs at a time appreciably after the excitation commences, then r serves as a close approximation to the current local maximum value of both $|\omega_o x|$ and $|\dot{x}|$.

Although the two components of the quantity r indicated in Eq. 2.5 are not strictly independent random variables they must be treated, for the purposes of this analysis, as the components of a two-dimensional random walk. The justification of this analysis, and hence of this step, is discussed later in this section. The quantity r in this case is the distance from the origin to the moving point in

the plane. The next part of the analysis is passage to the limiting case of infinitely closely spaced steps of infinitesimal magnitude. In the random walk analogy, Feller[19] has shown that if the step lengths and time increments are respectively held equal, then certain conditions relating them must be fulfilled while passing to the limit in order that the walking speed stays finite, and that there is no predominant drift in the motion. For random variable step lengths and time increments, the conditions may be written for the original ground motion as follows[9]:

$$\lim_{t_2 \to t_1} \frac{E\left(\sum_{t=t_1}^{t_2} u_i^2\right)}{t_2 - t_1} = 2k_1 \text{ , a constant} \qquad (2.6)$$

$$E(u_i) = 0 \qquad (2.7)$$

This intensity, k_1, has been shown[16] to be related to the power spectral density, $G(\omega)$, of the stochastic process of which Eq. 2.3 might be considered a member:

$$2k_1 = \lambda\sigma^2 = \pi G(\omega) \qquad (2.8)$$

where λ is the average number of impulses per second and σ^2 is their variance.

With these conditions (Eqs. 2.6 and 2.7) fulfilled, passage to the limit is possible and the random walk becomes a system governed by the diffusion equation[19]

$$k_1 \nabla^2 u = \frac{\partial u}{\partial t} \tag{2.9}$$

where k_1 is the constant defined in Eq. 2.6 and the probability of finding r between r and $r+dr$ at time t is $2\pi u(r,t)\, r\, dr$, taking into account the radial symmetry in the formulation of the problem. There are two conditions on $u(r,t)$ which enable Eq. 2.9 to be solved.

Firstly, it is required that for all $t \neq 0$ the probability of r having exceeded a chosen radius R be zero. Hence

$$u(R,t) = 0, \quad t > 0 \tag{2.10}$$

This ensures that $u(r,t)$ will have the correct form when substituted into the expression for the probability $F(R,t)$ of R having not been exceeded at all by the time t:

$$F(R,t) = 2\pi \int_0^R u(r,t)\, r\, dr \tag{2.11}$$

Secondly, at $t = 0$, it is certain that $r = 0$. Eq. 2.11 leads to a choice for $u(r,0)$ of

$$u(r,0) = \frac{\delta(r)}{\pi r} \tag{2.12}$$

for then

$$F(R,0) = 2\pi \int_0^R \frac{\delta(r)}{\pi r}\, r\, dr = 1 \tag{2.13}$$

holds for all R, including the value zero.

The boundary condition, Eq. 2.10, affords the possibility of solving the "first passage" problem, because with the initial con-

dition, Eq. 2.12, it is possible to solve Eq. 2.9 and substitute into Eq. 2.11 obtaining the probability, $F(R)$, of R having not been exceeded at all during the s seconds of excitation:

$$F(R) = F(R,s) = 2\pi \int_0^R u(r,s)\, r\, dr \tag{2.14}$$

This is the distribution function[20] for the maximum value of $|\dot{x}|$ during an excitation described by Eqs. 2.3, 2.6 and 2.7. The probability density function $f(R)$ is given by

$$f(R) = \frac{\partial F}{\partial R} \tag{2.15}$$

Only positive values of R are considered so that both $F(R)$ and $f(R)$ are zero for $-\infty < R \leq 0$.

The solutions for $u(r,t)$ and $F(R)$ are given in the Appendix, yielding for the undamped case:

$$F(R) = 2 \sum_m \frac{e^{-k_1 s \lambda_m^2 / R^2}}{\lambda_m J_1(\lambda_m)} \tag{2.16}$$

and

$$f(R) = \frac{4k_1 s}{R^3} \sum_m \frac{\lambda_m}{J_1(\lambda_m)} e^{-k_1 s \lambda_m^2 / R^2} \tag{2.17}$$

where the λ_m's are the zeros of J_o, and J_o and J_1 are Bessel functions of the first kind. In subsequent calculations it is desirable to transform R into a dimensionless quantity by dividing by its expected, or average, value. This is given by

$$E(R) = \int_0^\infty R f(R)\, dR \qquad (2.18)$$

Substituting for f(R) from Eq. 2.17 yields

$$E(R) = 4k_1 s \int_0^\infty \frac{1}{R^2}\left[\sum_m \frac{\lambda_m}{J_1(\lambda_m)}\, e^{-k_1 s \lambda_m^2/R^2}\right] dR \qquad (2.19)$$

The series in Eq. 2.19 does not converge uniformly in R, for at R = ∞ d'Alembert's ratio test indicates that the series diverges as $m \to \infty$. Hence, the series cannot be integrated term by term. Rosenblueth and Bustamante[9] arrive at the same equation (as pointed out by M. L. Juncosa[21]) in terms of a parameter $\alpha = R/2\sqrt{(k_1 s)}$. In terms of this parameter Eq. 2.19 becomes

$$E(R) = 2\sqrt{k_1 s} \int_0^\infty \left[\sum_m \frac{1}{\alpha^2} \frac{\lambda_m}{J_1(\lambda_m)} e^{-\lambda_m^2/4\alpha^2}\right] d\alpha \qquad (2.20)$$

One way of handling the integration of this series is to take the integration up to a sufficiently large finite number, for which the series will still converge uniformly, and interchange the order for this portion of the integral[9]. The top integration limit is so chosen that the asymptotic expansion for the sum of the series provides a negligible contribution to the remainder of the integral. In this way Eq. 2.20 is reduced to

$$E(R) = 2.348\sqrt{k_1 s} \qquad (2.21)$$

Damped Case

The analysis for the damped oscillator follows closely the basic steps for the undamped case and the details are included in the Appendix. The important results are the same as those obtained by Rosenblueth and Bustamante[9] although the methods used follow those of the undamped case and are influenced by the discussion of Caughey and Gray[22]. The main points leading to the probability density function for the damped oscillator follow.

The formulation of the problem does not allow use of the parameter r defined in Eq. 2.4 for the damped case. Instead, the parameter to be used as an approximate local maximum value of both $|\omega_o x|$ and $|\dot{x}|$ is given by

$$r^2 = (\omega x)^2 + (\dot{x} + n\omega_o x)^2 \tag{2.22}$$

where ω is equal to $\omega_o\sqrt{(1-n^2)}$. The analysis is made in terms of a variable r_1 given by

$$r_1 = e^{n\omega_o t} r \tag{2.23}$$

where n is the fraction of critical damping. The probability that $R_1 < r_1 < R_1 + dR_1$ at time t is given by $u_1(R_1,t)2\pi R_1\, dR_1$ and is governed by the equation

$$k_1 e^{2n\omega_o t}\nabla^2 u_1 = \frac{\partial u_1}{\partial t} \tag{2.24}$$

This probability is the same as the probability that $R < r < R + dR$

at time t, where R_1 and R are related by

$$R_1 = e^{n\omega_o t} R \tag{2.25}$$

A further change of variable allows the initial condition and boundary condition corresponding to Eqs. 2.10 and 2.12 to be obtained, and the solution of Eq. 2.24 as an eigenvalue problem is thus possible.

The probability $F(R)$ of r having not exceeded R during the s seconds of excitation is given by

$$F(R) = e^{2n\omega_o s} \sum_{m=1}^{\infty} \frac{\int_0^1 z M_m(z)\, dz}{\int_0^1 z M_m^2(z) e^{c_3 z^2}\, dz} e^{-\nu_m s} \tag{2.26}$$

where z is a dummy integration variable; $M_m(z)$ is an eigenfunction for the problem, a confluent hypergeometric function[23] described in the Appendix, depending on the damping n, natural frequency ω_o, duration s, excitation intensity k_1, the value of the variable R, and the eigenvalue ν_m; and c_3 is a constant given by

$$c_3 = R^2 n\omega_o / 2k_1 \tag{2.27}$$

In the Appendix will be found a description of the eigenvalues ν_m and an account of how Eq. 2.26 for $F(R)$ in the damped case reduces to Eq. 2.16 for $F(R)$ in the undamped case.

The probability density function $f(R)$ is obtained by differentiating Eq. 2.26 partially with respect to R; this is out of the

question except by numerical methods. The curves were obtained numerically for various values of period, damping and duration, as described later in this chapter.

Discussion of the Equations for the Probability Density Functions

Rosenblueth and Bustanmante's calculation[9] of the expected value of the maximum undamped response from Eq. 2.20, although questioned by Juncosa[21], is sound. This is borne out by electronic digital computations of F(R) from Eq. 2.16, f(R) from Eq. 2.17 and E(R) from Eq. 2.18, as described in the next section. Their preference for an asymptotic expansion for F(R) for large R was not followed in the computations. Instead an attempt was made to determine the suitability of Eq. 2.16 as it stood for all values of R of interest, i.e., until F(R) had effectively reached unity. This was carried out for the damped case also, where F(R) is given by Eq. 2.26. The effectiveness of this procedure is set forth in the next section.

The contribution of Caughey and Gray[22] serves to justify the approach of Rosenblueth and Bustamante[9] which forms the basis of this chapter. The assumptions to be satisfied in arriving at Eq. 2.9 and the conditions of Eqs. 2.10 and 2.12 for the undamped case, and the corresponding Eq. 2.24 for the damped case, are as follows.

(a) The white noise ground excitation defined in Eq. 2.3 obeys the specifications of Eqs. 2.6 and 2.7.

(b) The quantity r defined for the undamped case by Eq. 2.5 and for the damped case by Eq. 2.22 is a close estimate of the local

maximum value of both $|\omega_o x|$ and $|\dot{x}|$. This is so provided the damping is small, the duration is much longer than the natural period, and the maximum value of r occurs after an appreciable time from the start of excitation.

These assumptions correspond closely to those required for Caughey and Gray's approach to be comparable. They consider the excitation in Eq. 2.2 to be mathematically white noise, with constant power spectral density for all frequencies between $\pm\infty$. The Fokker-Planck equation is found for the transition probability density concerned with the probability that given the relative displacement and velocity at one instant, they can be found within a differential element of another pair of values a certain time later. Since initially the system starts from rest, this probability reduces to that considered in this section. However, the change of coordinates to polars which is required for introducing the boundary condition of the "first passage" problem does not reduce the Fokker-Planck equation exactly to the diffusion equations, Eqs. 2.9 and 2.24. The difficulty lies in the question of angular dependence of the solutions. This difficulty is removed on assuming that the duration is much longer than the natural period. A different change of coordinates is required to exactly match the radius r of the damped case, but if the damping is kept small, i.e., much less than unity, the diffusion equation, Eq. 2.24, is again obtained. This different mathematical formulation of the problem thus produces the same differential equations as Rosenblueth and Bustamante's approach, under similar assumptions.

D. Digital Computer Extensions to Existing Curves

The distribution function $F(R)$, the probability density $f(R)$ and the expected value of R, $E(R)$, are given for the undamped case by

$$F(R) = 2 \sum_{m=1}^{\infty} \frac{e^{-k_1 s \lambda_m^2 / R^2}}{\lambda_m J_1(\lambda_m)} \tag{2.16}$$

$$f(R) = \frac{4k_1 s}{R^3} \sum_{m=1}^{\infty} \frac{\lambda_m}{J_1(\lambda_m)} e^{-k_1 s \lambda_m^2 / R^2} \tag{2.17}$$

$$E(R) = 4k_1 s \int_0^{\infty} \frac{1}{R^2} \left[\sum_{m=1}^{\infty} \frac{\lambda_m}{J_1(\lambda_m)} e^{-k_1 s \lambda_m^2 / R^2} \right] dR \tag{2.19}$$

A table of the zeros of J_o and of the values of J_1 at these zeros is available [23]. The calculations were made in terms of the dimensionless quantity α given by

$$\alpha = \frac{R}{2\sqrt{k_1 s}} \tag{2.28}$$

so that no specific values were required of R, k_1 or s. The procedure was to calculate each term of the series in Eq. 2.16, 2.17 and 2.19 until a prescribed accuracy had been attained in all three, including the approach of $F(R)$ to unity. It was found that the number of terms required varied between two, for low values of α, up to twelve, for the highest value of α needed for the prescribed accuracy. To four significant figures, the calculation of $E(R)$ from

Eq. 2.19 gave the same result as Eq. 2.21 as was expected. This confirmation indicates that the value obtained by M. L. Juncosa[21] is in error, as suspected by Rosenblueth and Bustamante. Use was made of this value of $E(R)$ for the undamped case in the representation of $F(R)$ and $f(R)$ as well as all the subsequent results for the damped case. The response R was brought into dimensionless form by describing it in terms of the fraction of the expected undamped response $\overline{R}_o$. In terms of the dimensionless variable $R/\overline{R}_o$, Figs. 2.6 and 2.7 show $F(R)$ and $f(R)$, which were calculated to four significant figures. In Fig. 2.6 are also indicated some points obtained from Rosenblueth and Bustamante's plot of $Q = 1 - F(R)$; these agree very closely.

Figure 2.6 can be considered as indicating the probability of survival of undamped structures during excitation of fixed k_1s. If the average maximum response is designed to be a quantity $\overline{R}_o$, then the probability that the maximum response will not have reached any particular multiple of this can be read off the curve.

Figure 2.7 can be readily adapted to compare with the experimental results mentioned in section B of this chapter. The scales on the graph can be adjusted to facilitate the comparison with a histogram, for example, showing the frequency of actual maximum responses to a standard excitation. Such a procedure is described later in this section.

The distribution function $F(R)$ is given for the damped case by Eq. 2.26. It can be seen from the detailed analysis in the

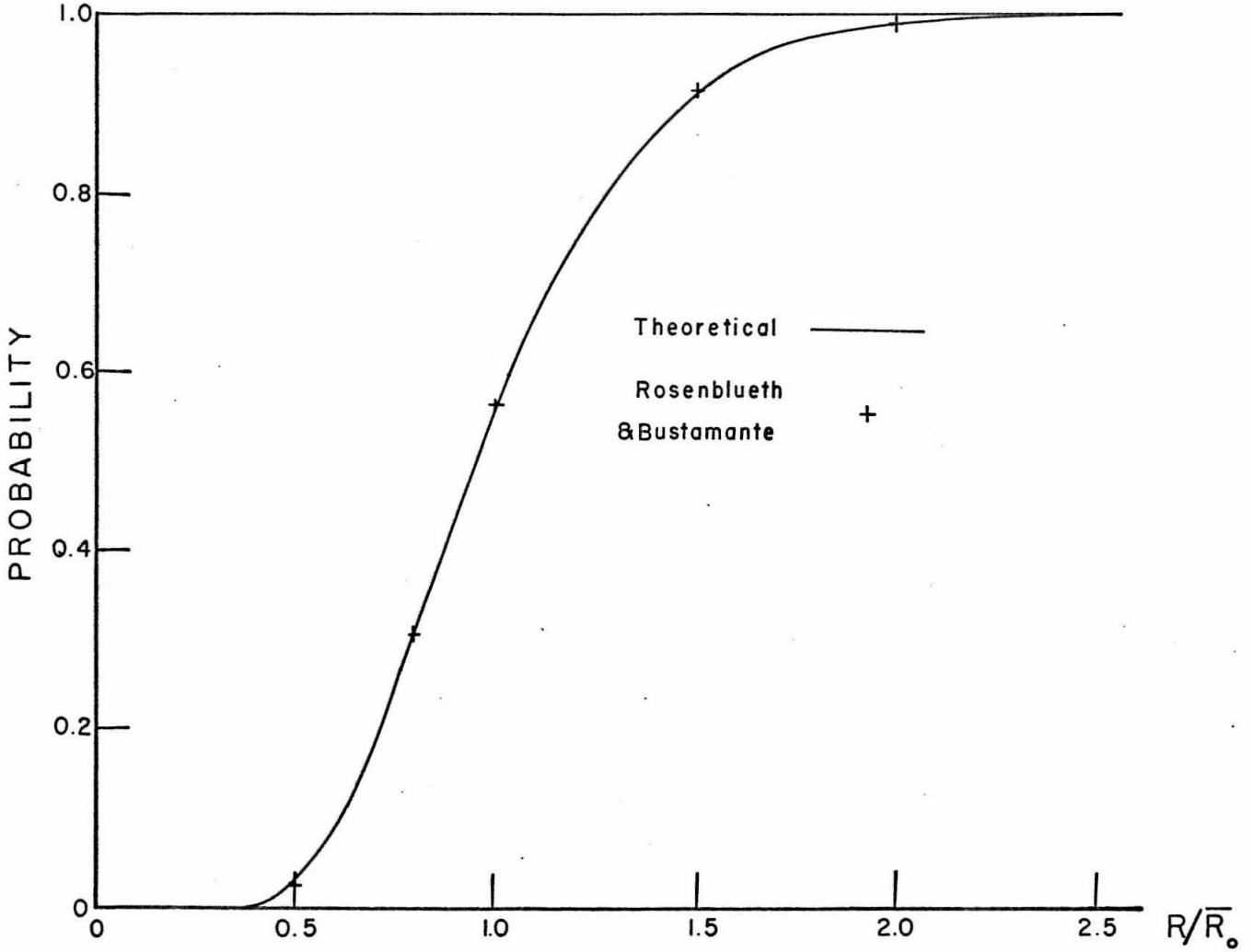

FIG. 2.6 UNDAMPED PROBABILITY DISTRIBUTION OF MAXIMUM RESPONSE.

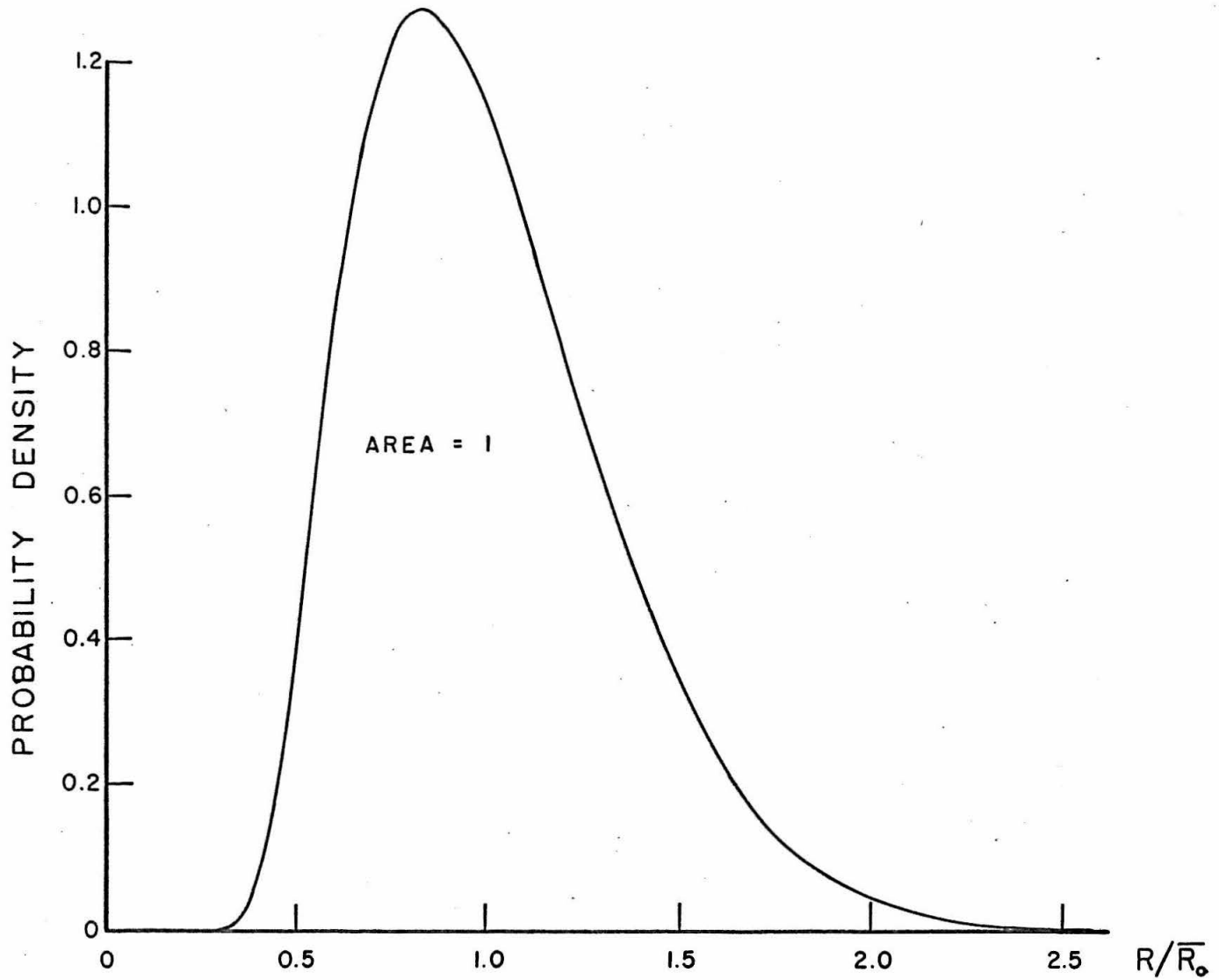

FIG. 2.7 UNDAMPED PROBABILITY DENSITY OF MAXIMUM RESPONSE.

Appendix that the damping n only appears with the natural frequency in the form $n\omega_o$ and hence with the natural period in the form n/T. This is expected from the form of Eq. 2.24, where $n\omega_o$ appears. Furthermore, the duration s only appears with the damping and natural frequency and hence in the form ns/T. When $\overline{R}_o$ is introduced as the expected value of the undamped response, given by Eq. 2.21, F(R) can be expressed solely as a function of $R/\overline{R}_o$ and ns/T. A number of preliminary tests were run to check the accuracy of the computer program and then to check the results against two of the curves of Rosenblueth and Bustamante. These are now briefly described.

Calculation of the eigenvalues ν_m and of the confluent hypergeometric functions $M_m(z)$ were made to both six and eight significant figures. The second value altered F(R) only in the fifth significant figure, and was therefore not used. The integrations were divided into both twenty and forty equal steps, and twenty steps were found to give the same order of accuracy in the results for F(R). All the subsequent calculations of F(R) used six figures in ν_m and $M_m(z)$ and divided the integrations into twenty equal steps. The two curves used as a check had values of $n\omega_o s$ of 1 and 20. These appear in Fig. 2.8, together with some points plotted from Rosenblueth and Bustamante's results. The comparison is very good, except perhaps for the highest values of $R/\overline{R}_o$, where presumably they used the asymptotic expression described in their paper[9]. Computing to four significant figures in F(R) required a maximum

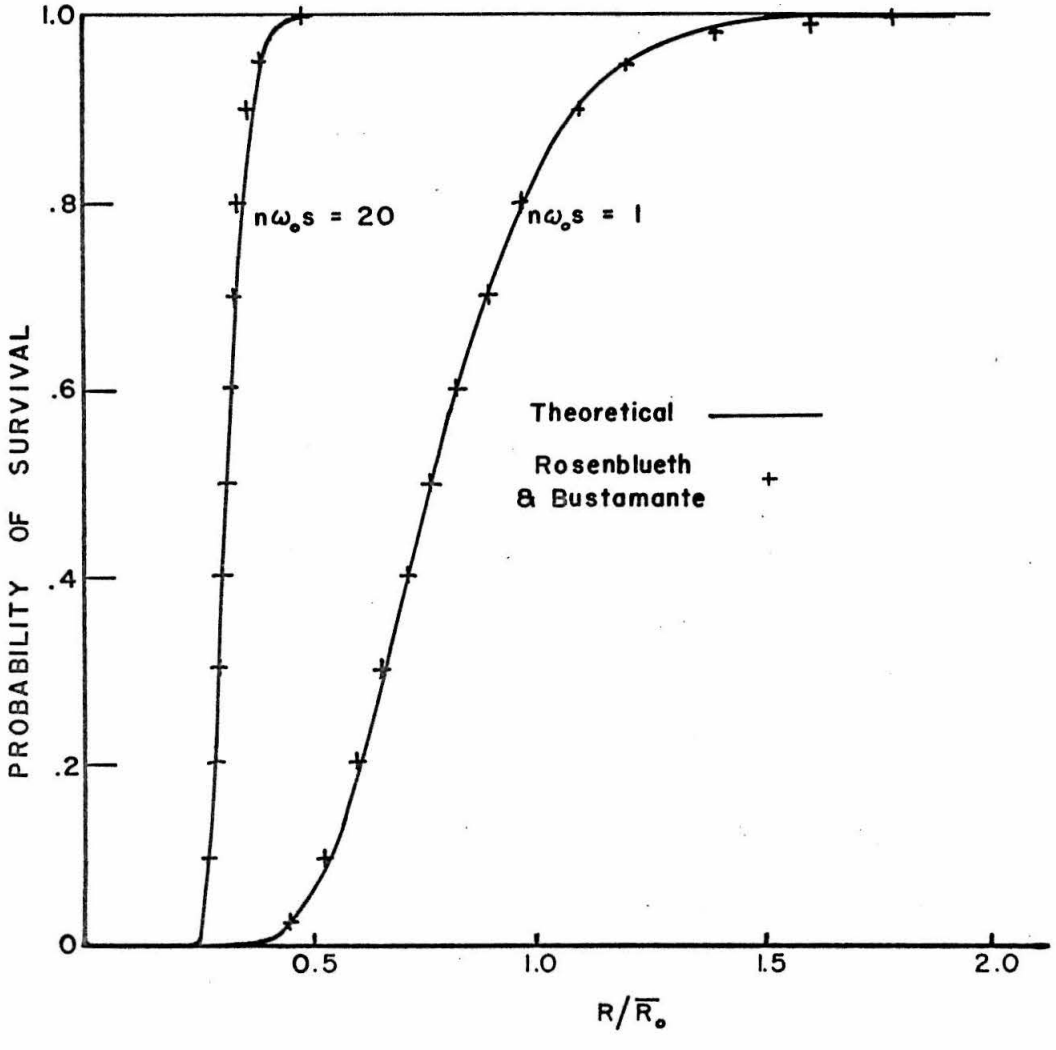

FIG. 2.8 COMPARISON OF TWO PROBABILITY DISTRIBUTIONS.

number of terms in the summation of Eq. 2.26 of five. This indicates that probably no asymptotic expression was in fact necessary.

Theoretical curves for comparison with the earlier experimental histograms were then computed using the corresponding values of ns/T. In order to obtain sufficient accuracy in the numerical differentiation that followed the calculation of $F(R)$, between 34 and 70 points were taken for each curve. The derivative at each point used the three ordinates on each side of the point, and for this reason the "distributions" or probability density functions appearing in Figs. 2.9 to 2.12, where comparisons are made with the four previous histograms, do not appear complete in some cases at the upper ends. The scales of the theoretical curves were adjusted to compare with the histograms in the following manner. The abscissa scales were multiplied by the corresponding experimental undamped means and the ordinate scales were multiplied by factors to give an area of 1000. This approach in effect fixed the experimental and theoretical means to be identical in the undamped case. Table 2.2 contains all these adjusted means and standard deviations. Figures 2.10 to 2.12 show that for the damped case the experimental results are consistently lower than the theoretical curves. The tendency is greater for the 10% damping cases where the difference between the experimental and theoretical mean is up to 4%. This discrepancy is to be expected for the damped cases, since the experimental results give the probability density of the maximum relative velocity $\dot{x}$ whereas referring to Eq. 2.22 indicates that the analysis deals with the quantity r which may be appreciably greater than the maximum $\dot{x}$. In particular, if

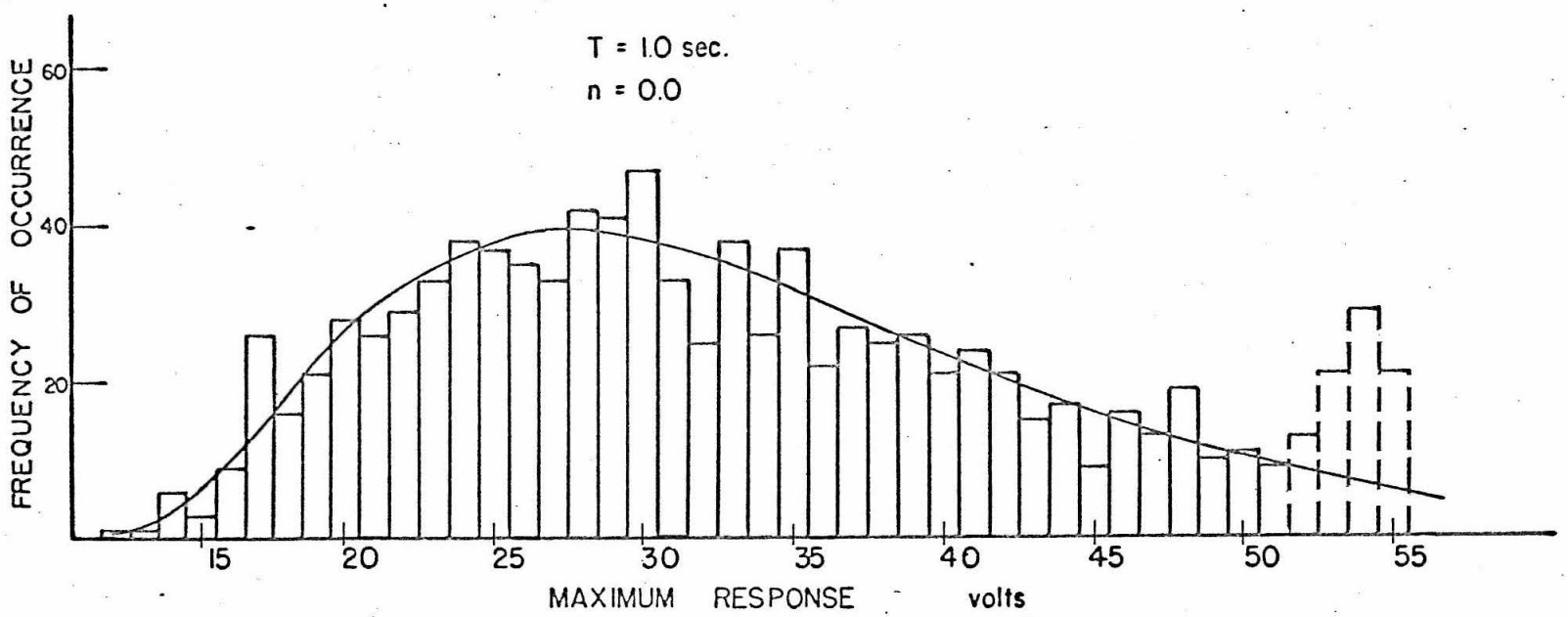

FIG. 2.9 THEORETICAL AND EXPERIMENTAL DISTRIBUTIONS OF MAXIMUM RESPONSE.

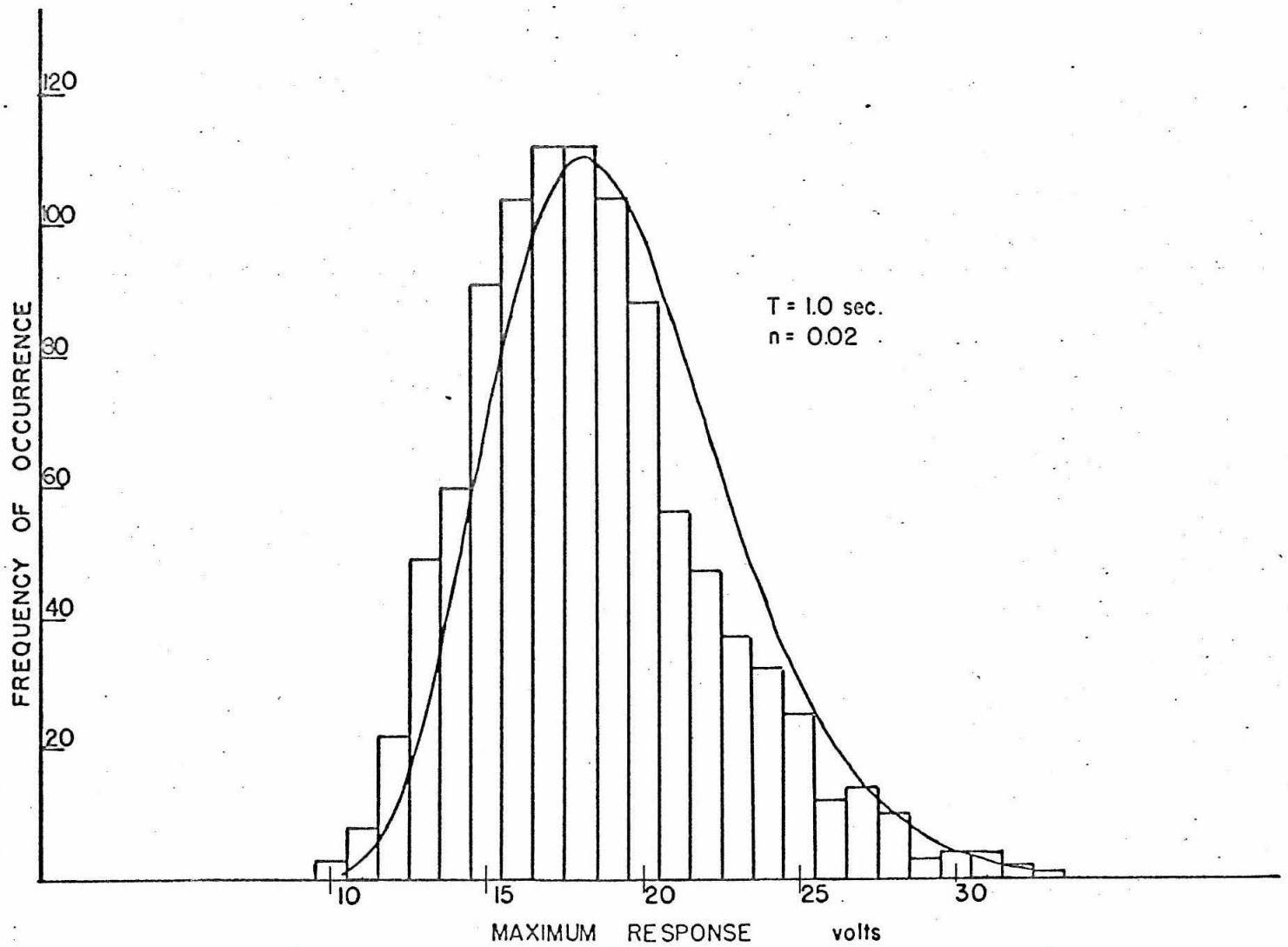

FIG. 2.10 THEORETICAL AND EXPERIMENTAL DISTRIBUTIONS OF MAXIMUM RESPONSE.

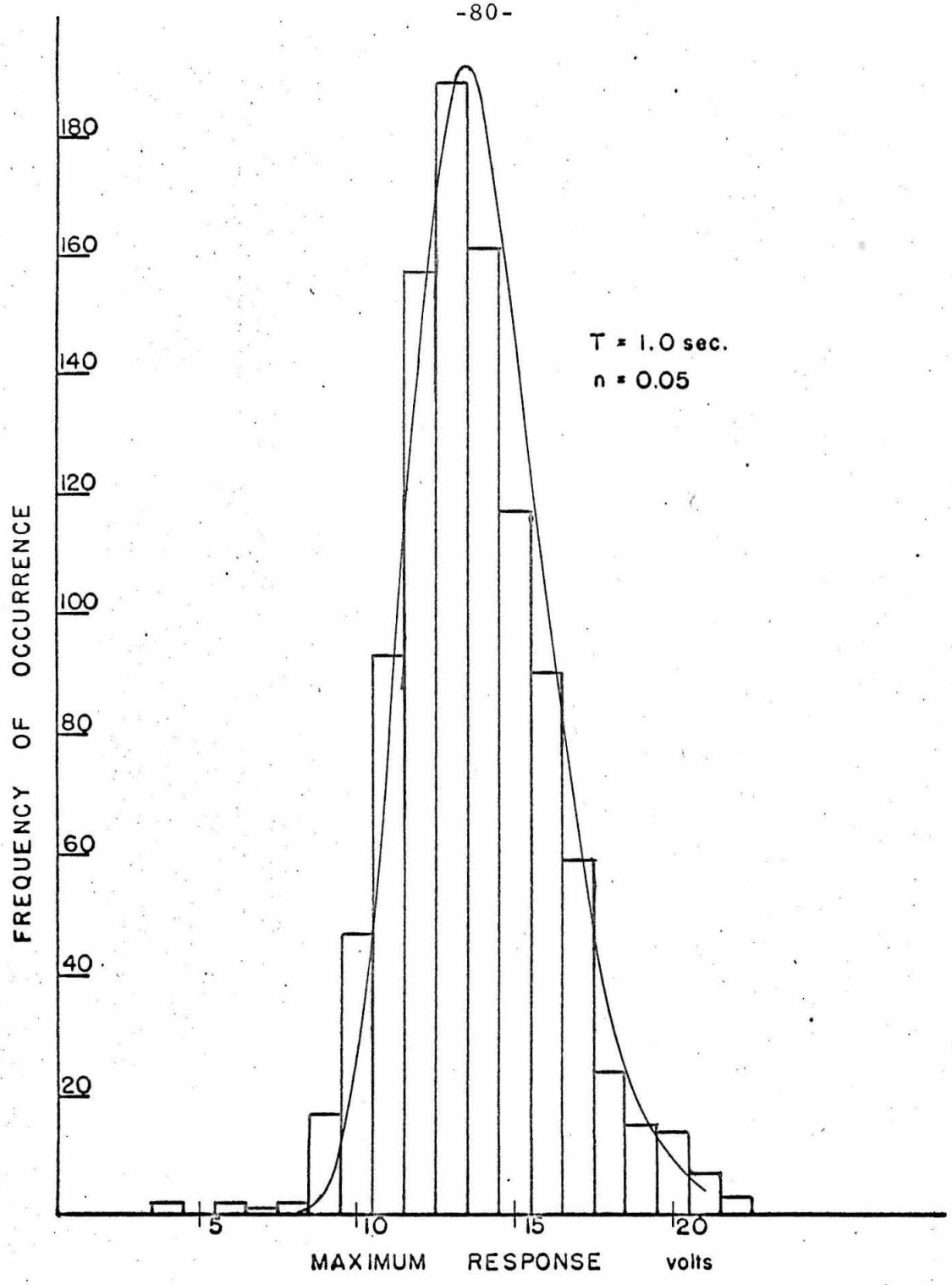

FIG. 2.11 THEORETICAL AND EXPERIMENTAL DISTRIBUTIONS OF MAXIMUM RESPONSE.

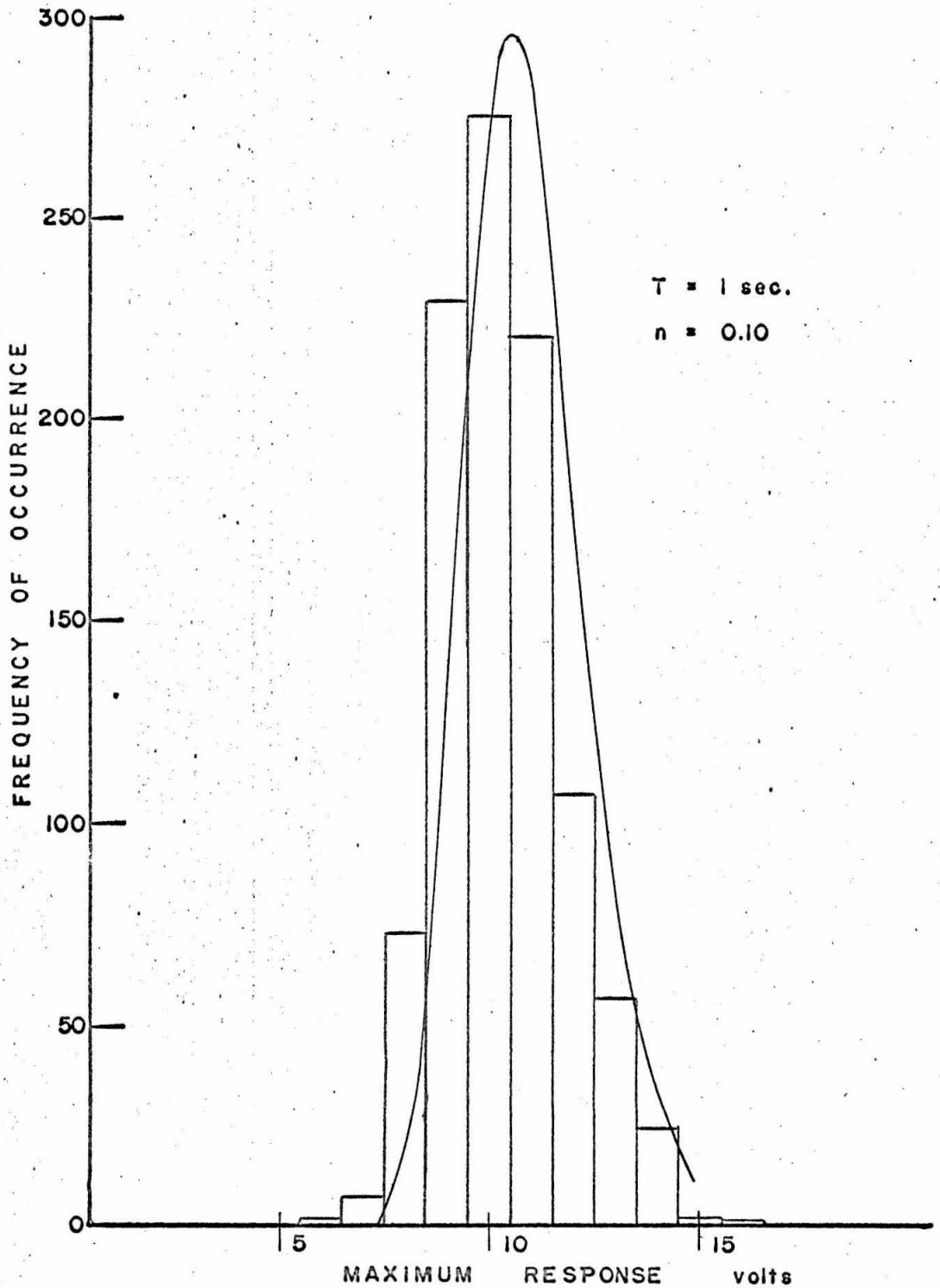

FIG. 2.12 THEORETICAL AND EXPERIMENTAL DISTRIBUTIONS OF MAXIMUM RESPONSE.

the maximum velocity is not reached at the equilibrium position $x = 0$, but at an instant when $\omega_o x$ is of the order of, say, one-tenth of the maximum $\dot{x}$, then for 10% damping r will be 4% larger than $\dot{x}$. This calculation indicates that for high damping ratios, the quantity r is not a close approximation to the maximum $\dot{x}$.

Table 2.2

Theoretical Means and Standard Deviations
Using Undamped Means from Table 2.1

Damping %		Period (sec.) 0.5	1.0	1.5	2.0
0	μ	32.0	33.1	32.4	32.3
	σ	10.42	10.8	10.6	10.5
2	μ	14.5	19.0	20.8	22.5
	σ	2.31	3.68	4.48	5.23
5	μ	10.4	13.9	15.6	17.3
	σ	1.29	2.10	2.63	3.14
10	μ	7.8	10.7	12.3	13.6
	σ	0.825	1.33	1.72	2.06

In general, though, Tables 2.1 and 2.2 and the four representative comparisons of Figs. 2.9 to 2.12 indicate that the theoretical distributions obtained here, under the assumptions that have been made, agree well with the Monte Carlo experimental distributions.

A further suitable set of values of the parameter ns/T were then chosen to provide a particular family of curves for $F(R)$. The selection was based on a value for s of thirty seconds and values for n/T of 0.00125, 0.0025, 0.005, etc., up to 0.16. These values are suitable for damping values of 1, 2, 4 and 8%, and periods of

1/4, 1/2, 1, 2, 4, and 8 seconds. The distribution functions are plotted in Fig. 2.13 and the density functions in Fig. 2.14, obtained by differentiating as before. Included are the undamped curves from Figs. 2.6 and 2.7. Table 2.3 contains the mean values and standard deviations for the nine curves. The distributions are labelled A to I by decreasing ns/T. It is easy to see how the distributions are altered when one of these three variables n, s and T are allowed to vary, keeping the other two constant.

Table 2.3

Theoretical Normalized Average Response and Standard Deviations

Curve	$\frac{ns}{T}$	$\frac{n}{T}$ when s = 30	$\mu = E(R/\overline{R}_o)$	σ
A	4.8	0.16	0.268	0.030
B	2.4	0.08	0.353	0.047
C	1.2	0.04	0.455	0.074
D	0.6	0.02	0.573	0.113
E	0.3	0.01	0.685	0.164
F	0.15	0.005	0.803	0.219
G	0.075	0.0025	0.885	0.263
H	0.0375	0.00125	0.938	0.294
I	0.0	0.0	1.0	0.331

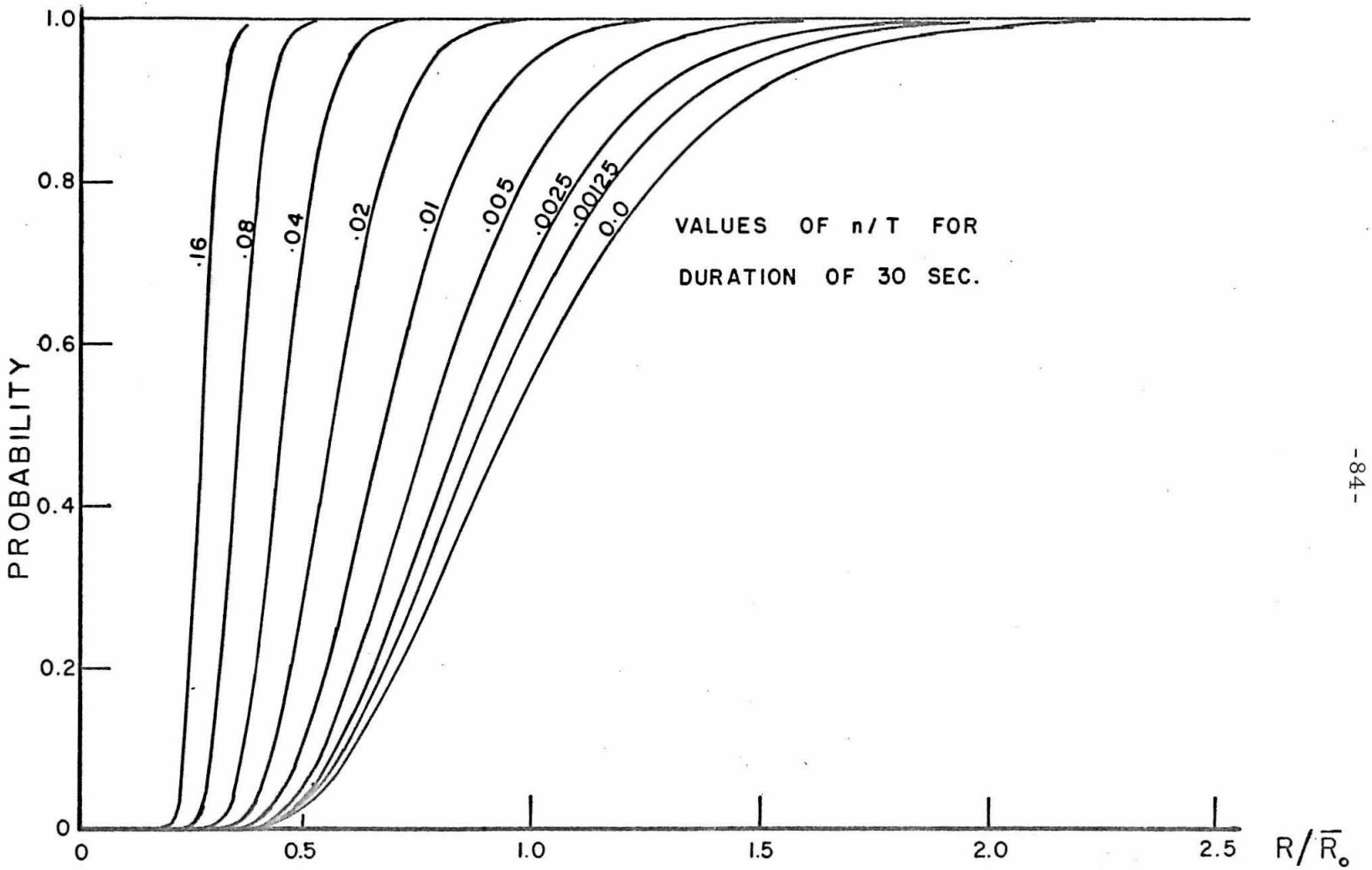

FIG. 2.13 THEORETICAL PROBABILITY DISTRIBUTIONS FOR DURATION OF 30 SEC.

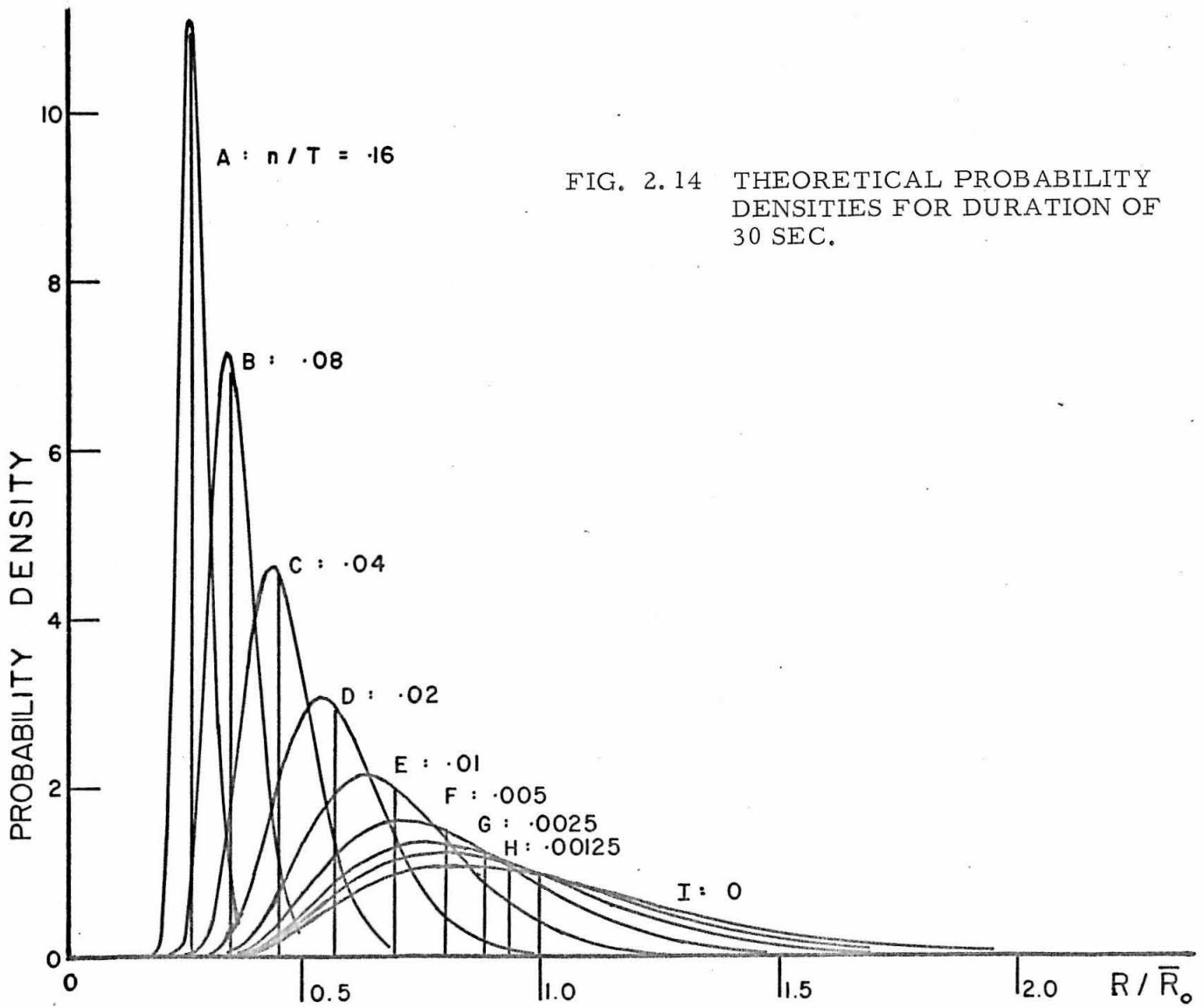

FIG. 2.14 THEORETICAL PROBABILITY DENSITIES FOR DURATION OF 30 SEC.

These curves may be presented in a different style comparable with the usual way of presenting response spectra. This is shown in Fig. 2.15. The horizontal scale is in terms of both T/s, reverting to the general case, as well as T when s is taken as 30 sec. At any particular damping given by the six curves, the average maximum, as a fraction of the undamped average, is given by the vertical scale. Associated with each of nine average maxima is its own corresponding distribution obtained from Fig. 2.14, of which four have been transferred. As was pointed out earlier, any particular value of the parameter ns/T defines its own average maximum response and distribution about this average.

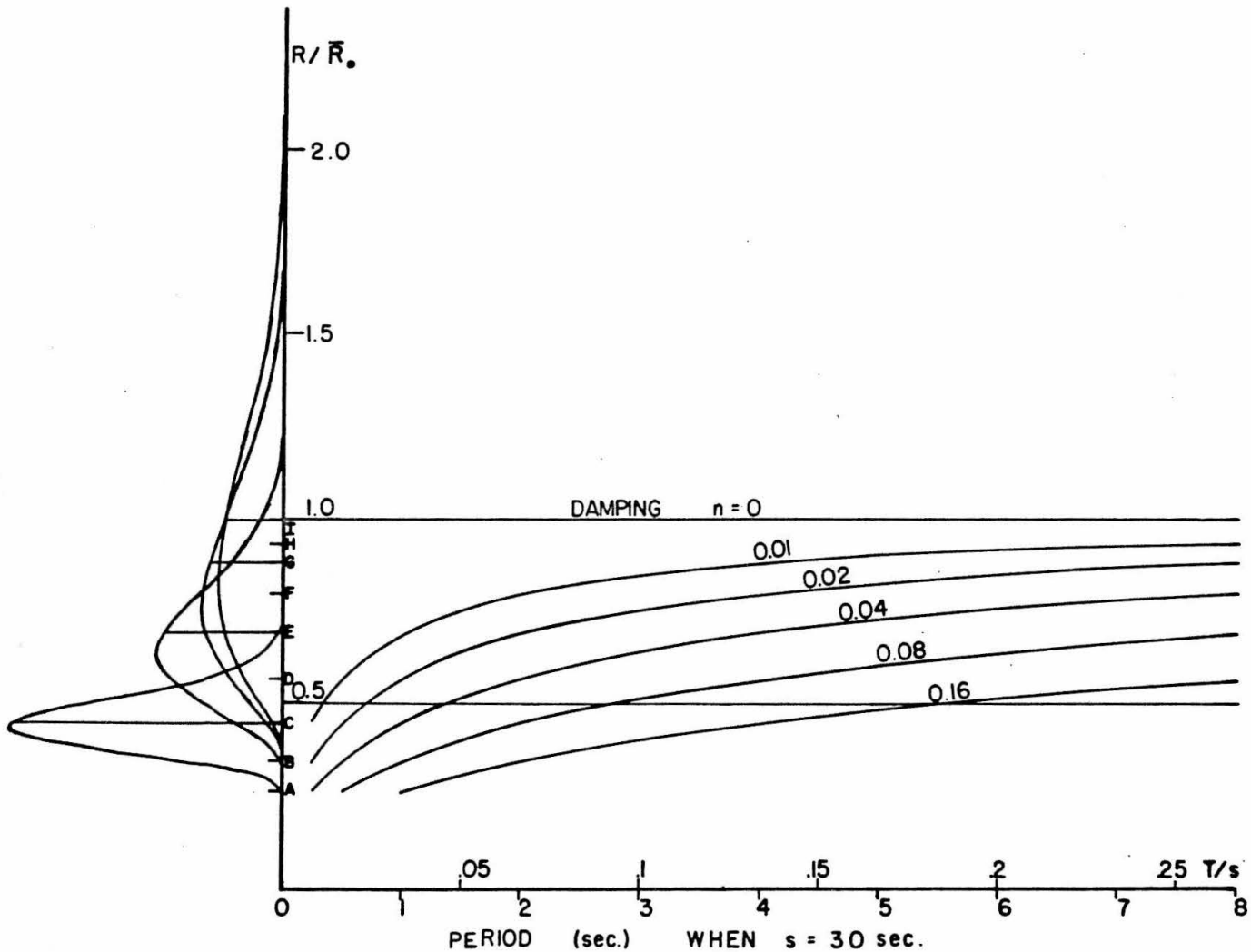

FIG. 2.15 AVERAGE RELATIVE VELOCITY SPECTRA AND DISTRIBUTION ABOUT THE MEAN.

E. Summary and Conclusions

The confidence with which average response spectra can be regarded depends on the spread or distribution of individual spectral values about this average. The distribution of the maximum relative velocity response has been investigated experimentally by Monte Carlo techniques using an electrical analog of white noise excitation with constant duration. Tabulated results of the mean and standard deviation for several values of damping and period, and the histograms presented, indicate how the distributions depend on these two structural parameters.

Confirmation of the distributions is sought by analytical methods. An extension of Rosenblueth and Bustamante's results allows analytical expressions to be found for the distributions of a quantity differing little from the relative velocity, again using white noise excitation. Careful electronic digital computation confirms that Rosenblueth's approximate numerical techniques produce accurate probabilities of survival. Further computations have been made to produce a family of distributions of approximate maximum response, normalized with respect to the undamped maximum response. Each member of the family, with its mean and standard deviation, depends on the parameter ns/T.

Comparison with the experimental histograms using the appropriate values of ns/T indicate that both approaches to the question of determining the distributions yield similar results. The differences are readily explained by the fact that the theoretical

approach uses a parameter depending on both the relative velocity and relative displacement instead of the relative velocity alone.

From the results of this chapter it is concluded that Monte Carlo techniques offer a promising approach to the statistical problems of earthquake engineering. The flexibility of the electric analog computer is very suitable for obtaining different types of statistical samples. For example, the power spectral density of the excitation is simple to change from white to that of an average earthquake's. The convenience and speed of the digital computer when used to analyze the results have a distinct superiority over other methods. This hybrid computation, utilizing both analog and digital computers where each can be used to best advantage, has proved invaluable in aiding these Monte Carlo studies.

It is also concluded that the approximations of Rosenblueth and Bustamante's analysis, confirmed as satisfactory by Caughey and Gray on theoretical grounds, and the approximations of their numerical calculations have combined to give reasonably accurate probabilities of survival, confirmed by the digital computation described herein. Provided the damping is small, the distributions are close to the experimental ones. This limitation does not apply to the experimental procedure which has the added advantage of versatility. It seems likely that the general results would not be much altered by small changes in the shape of the power spectral density[22]; this can be checked easily by Monte Carlo methods. It is concluded that experimental Monte Carlo techniques will play an important role in further work in this field.

III. FOURIER SPECTRA OF GROUND MOTION RECORDS

A. Introduction

Earthquake engineers have always been interested in the relative safety, in regions of strong seismic activity, of structures built on hard bedrock and those on softer overlying sedimentary deposits. Many studies have been carried out in recent years of the role of the surface material's physical characteristics in regard to the amplification or otherwise of ground motion arriving at a deep rock-soil interface and travelling to the surface. According to the summary of the then current knowledge by Duke[24], soil conditions and local geology govern to a marked degree the damage to engineering structures during strong-motion earthquakes. Based to a large extent on the work of the Japanese seismologists Sezawa, Kanai, and Takahasi, the report of Matthiesen et al.[10] describes studies made of the theoretical amplification of sinusoidal plane waves in bedrock during passage through an overlying stratified soil system. These studies of particular sites, using appropriate soil properties where available, such as layer thicknesses, densities, and velocities of propagation of compressional waves (P waves), indicate that sinusoidal wave forms of various periods might be amplified up to sixteen times for the lower periods and up to six times for longer periods. Such magnifications may occur when a train of waves sets up essentially a resonance condition.

It might be expected, however, that during an actual earthquake,

nonlinear deviations from the assumed characteristics of the soil, and the transient nature of the excitation, would result in a considerable modification of the solution. Thus the theoretical amplification of a train of sinusoidal waves might considerably overestimate the motion at the ground surface.

A good deal of theoretical work and some experimental investigations have been carried out recently at the National University of Mexico on the problem of expected spectral responses for earthquakes in the vicinity of Mexico City. The paper by Herrera et al.[11], which refers to much of the published work in this area, attempts to predict the velocity response spectra at the ground surface of the Valley of Mexico. Use is made of the expected spectra at the rock-soil interface, the dynamic properties of the overlying clay, and calculations of sinusoidal wave amplification factors. Provided certain simplifying assumptions regarding the physical properties and dynamic behavior of the soil layers are met, the results indicate that magnification factors for the undamped velocity response spectra can be in excess of ten. Various adjustments to the data are required if there are slight deviations from the assumed properties.

Before going any further with theoretical studies of the amplification of sinusoidal waves and the magnification of undamped spectra of earthquakes during passage through soil layers overlying bedrock, it would seem that direct measurement of actual ground motions at suitable sites to provide a check on the applicability of some of the assumptions would be valuable. Simultaneous records of ground

motion at adjacent sites with different soil properties would be required, and a comparison should be made of the frequency components, using the Fourier amplitude spectrum technique[5].

Some results have been reported for simultaneous strong-motion records in Mexico City by Zeevaert[26] who has compared the response spectra at two sites and discussed their characteristics making use of local soil conditions.

The State of California Division of Water Resources is currently interested in this problem. This organization is concerned with the different types of earthquake motion occurring in the various foundation materials on which their engineering structures are built. They have asked the U. S. Coast and Geodetic Survey to complete the instrumentation necessary for such an investigation and the California Institute of Technology has been asked to work out suitable methods for analyzing the results. This chapter summarizes the progress made up to this time and indicates the procedure which might eventually be standardized for similar analyses. The study involves simultaneous recording at two different but reasonably close sites of the ground motion caused by earthquakes sufficiently far removed to be effectively equidistant from each site. Suitable earthquakes should have a magnitude greater than four and should occur within one to two hundred miles from two sites not more than ten miles apart. A meaningful comparison of the frequency components present in the vibration of bedrock granite and overlying soil layers can then be made.

Earthquakes with suitable records for this investigation are expected to occur an average of two or three times each month. The ground motion of earthquakes occurring this frequently will be very small, with displacements having a maximum value of about 1/100 mm. It is to be emphasized that these ground motions are much smaller than those which interest earthquake engineers, and it is to be hoped that opportunities for similar comparisons for destructive earthquake ground motions will be forthcoming. Until such destructive ground motion can be experimentally studied, it will be dangerous to attempt generalizations or extrapolations from the type of small motion studies reported in the present work. The final results will thus have to wait until sufficient data has been collected from large earthquakes.

The first part of this chapter describes the data recording and digitizing techniques of the USCGS with particular reference to the seismometer and digital reader. The next section contains the derivation of the expression for the Fourier spectrum of the ground acceleration in terms of the Fourier spectrum of the digitized record. The reasons for choosing Fourier analysis of the records are related to the response characteristics of the instrumentation and to the required knowledge of the predominant frequencies in the records. This is explained further after the Fourier spectra relationship is derived. Three methods are described for the calculation of the Fourier spectrum of the record and reasons are given for the ultimate selection of one.

A number of tests is then described in which the digital computer program was checked by calculating the Fourier spectrum and undamped relative velocity spectrum of a particular record. Tests were also carried out to check the accuracy of the digitizing procedure and to find the dependence of the Fourier spectra on the duration of the record used. To facilitate the comparison between the Fourier spectra resulting from the records at different sites, the spectra were smoothed by a process described by Blackman and Tukey[25]. Finally a standardized method for the calculation of Fourier spectra from records such as are being collected by the USCGS is recommended.

The nomenclature for Chapter III, consistent with that for the previous two chapters, follows in full.

NOMENCLATURE

$A_1 = A_1(t) = \int_0^t a(t) \cos \omega_o t \, dt$

$A_2 = A_2(t) = \int_0^t a(t) \sin \omega_o t \, dt$

$a(t)$, ground acceleration input

$E_1(t)$, envelope of the $\dot{x}(t)$ curve

$F_a(T), F_g(T)$, Fourier spectra of $a(t)$, $g(t)$, in terms of T

$F_a(\omega), F_g(\omega)$, Fourier spectra of $a(t)$, $g(t)$, in terms of ω

$FT[a(t)]$, $FT[g(t)]$, Fourier transforms of $a(t)$, $g(t)$

$g(t)$, instrument trace displacement output

$h(\tau)$, weighting function, or the displacement response to a unit velocity impulse at $\tau = 0$

$M = M(T)$, system magnification, equal to the ratio $g(t)_{max.}/y(t)_{max.}$ when $y(t)$ is sinusoidal

N, total number of points in a digitized record

s, duration of earthquake record

T, period

t_i, g_i, coordinates of the i-th point of the record, $1 \leq i \leq N$

$x = x(t)$, relative displacement response

$\dot{x} = \dot{x}(t) = x_1(t)$, relative velocity response

$Y(\omega) = FT[h(t)]$, frequency response function

$y(t)$, ground displacement input

$\theta(t) = \tan^{-1}(A_2/A_1)$

ξ, τ, dummy integration variables

$\phi(\omega)$, phase response

ω, frequency

ω_o, natural frequency of a single degree-of-freedom system

B. Data Recording

The USCGS has at this stage set up instruments at three sites indicated in Fig. 3.1. The first two were seven miles apart, one on outcropping bedrock granite at Ft. Tejon and one at Wheeler Ridge on alluvial deposits overlying the bedrock. Ten suitable earthquakes were recorded at these two sites, although only two of the records were available for the present analysis. The instruments at the alluvium site were then removed and a third site was established on outcropping Tehachapi granitics at a similar distance from the first. With these two sites on bedrock granite an opportunity was afforded to check the similarity of the bedrock ground motions.

At each site three similar instruments in the N-S, E-W, and vertical directions were set up on concrete foundations. The instruments are Benioff portable seismometers physically and electrically identical for both the horizontal and vertical models. The transducer is a balanced, variable-reluctance type designed to produce a voltage proportional to the ground velocity. The undamped natural period is one second which places the instrument between strong-motion accelerometers with natural frequency up to 15 or 20 cps and the long period seismometers with natural periods up to thirty seconds.

The response is recorded by light beam galvanometers (one meter light path) on photographic paper, giving a magnification of up to six thousand for sinusoidal ground motion. Under sinusoidal excitation this magnification figure is the ratio of the trace amplitude to the ground motion amplitude. The records, traced out at

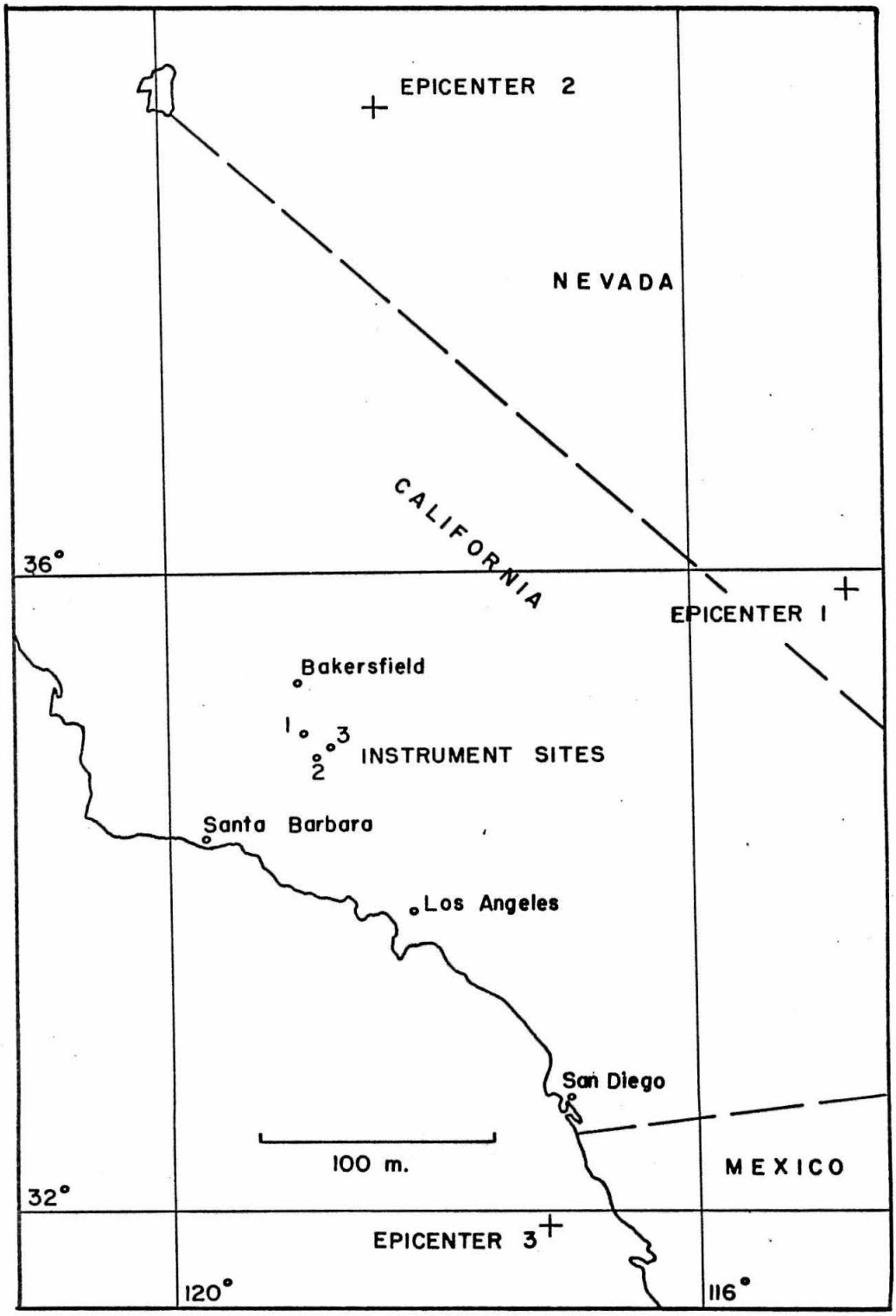

FIG. 3.1 INSTRUMENT SITES AND EARTHQUAKE EPICENTERS.

0.4 cm./sec., are synchronized with each other and with standard time by signals from a radio transmitter. The recording drum holds twelve hours of record, automatically replaced from an internal spool, and needing servicing and resetting two or three times a week.

Records from suitable earthquakes were chosen, and 60 cm., corresponding to 150 sec., were reduced to digital form using a reading machine. The Benson-Leyner reader in use by the USCGS accommodates the 60 cm. of record in three settings. Every 20 cm. can be divided into 1000 equal divisions, i.e., the electronics of the machine will digitize any particular setting of the cross-hairs to 1/5 mm. Greater accuracy in the actual digitizing of the cross-hair setting is indeed possible, in fact a resolution of one thousandth of an inch is claimed, but is not warranted when the thickness of the trace is considered. Although the record was not magnified it appeared very easy to read within a range of 1/2 mm. The record was aligned manually on the back-lighted screen using adjacent non-oscillating traces as an aid in lining the record up. The beginning and end of each setting were recorded in the machine, i.e., the origin and range were defined, and the record was subsequently read by setting the cross-hairs successively on the points at which the slope changed. The result was 150 sec. of record defined by four hundred to nine hundred pairs of coordinates, not equi-spaced, with an average time increment of 0.2 to 0.4 sec. It may be noticed that this average time increment is not as fine as would be required to define accurately the diagrams of ground velocity for California strong-motion earthquakes[2].

A digitizing check would be desirable but has not yet been made, primarily because of the unavailability, for the duration of the study, of a digital reader similar to the one in use by the USCGS. Such a check of the spectra arising from different individuals reading the same record would be expected to show a similar scatter that that indicated for the undamped response spectra shown in Fig. 1.12.

Calibration tests for each instrument and its accompanying galvanometer included a determination of the system magnification, M, for a series of frequencies ranging from 0.1 to 1.5 cps. by tenths, and up to 10 cps. by larger increments. These tests consisted of laboratory calibrations for the seismometer constants, and field calibrations of the system magnification. The field tests simulated the ground motion with a sine wave generator feeding an oscillating current into an electromagnetic calibration coil. The instrumentation was adjusted so that the resulting frequency response curves all had a value of five thousand at 1 cps. as indicated in Fig. 3.2. The peak magnification is shifted towards the high frequency or low period side of the natural frequency of 1 cps. This is typical of response curves for damped systems with an exciting force amplitude proportional to the square of the exciting frequency.

The system magnification is down by a factor of more than 100 at periods longer than three seconds, and the accuracy of any spectrum calculation might be considered impaired. But the actual sinusoidal responses from which the curve is derived can be read to 1% or better in this region, the accuracy falling off rapidly for the low periods of less than 0.4 seconds. This point is mentioned when the predominant features of the calculated spectra are discussed.

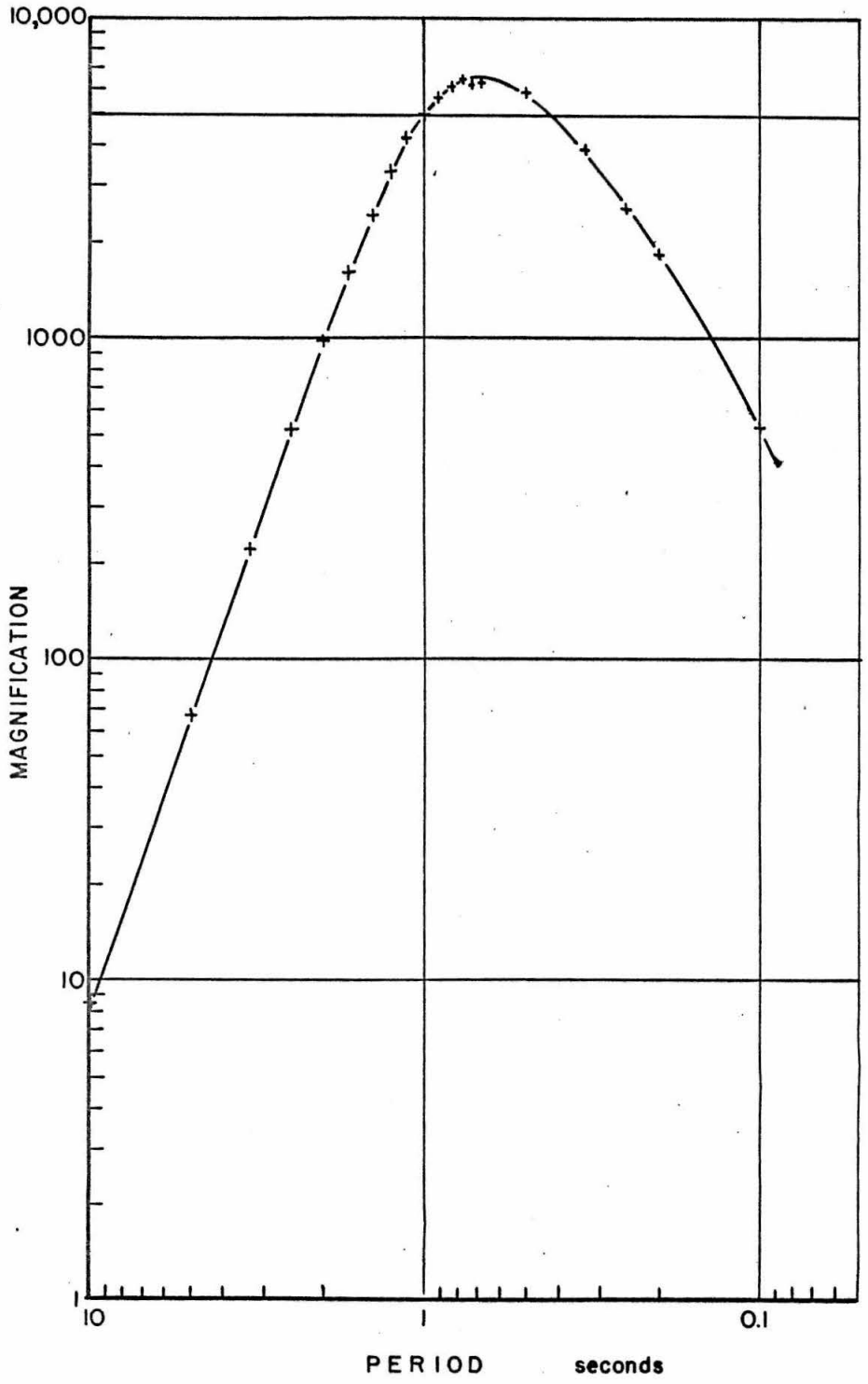

FIG. 3.2 TYPICAL SYSTEM MAGNIFICATION CURVE.

C. Fourier Amplitude Spectra

The frequency components in the ground acceleration were obtained from the instrument record by making use of Fourier transform theory as follows.

Figure 3.3 shows in diagrammatic form an input ground acceleration, $a(t)$, applied to a constant parameter linear system with "weighting function" $h(\tau)$, such that the output function $g(t)$ is given by

$$g(t) = \int_{-\infty}^{t} a(\xi)h(t-\xi)\, d\xi \tag{3.1}$$

By changing variables to $\tau = t-\xi$, this transforms to

$$g(t) = \int_{0}^{\infty} a(t-\tau)h(\tau)\, d\tau \tag{3.2}$$

Now consider the system to represent the sensing and recording instruments described earlier with an output trace ordinate $g(t)$. The response of the system to a unit velocity impulse τ time units earlier is $h(\tau)$.

In order to obtain the desired relationship for the Fourier spectrum, the response to a complex input is investigated. Suppose $a(t)$ is derived from the complex displacement input $y(t)$ given by

$$y(t) = e^{i\omega t} \tag{3.3}$$

where ω is the frequency, given by $\omega = 2\pi/T$. Hence

$$a(t) = -\omega^2 e^{i\omega t} \tag{3.4}$$

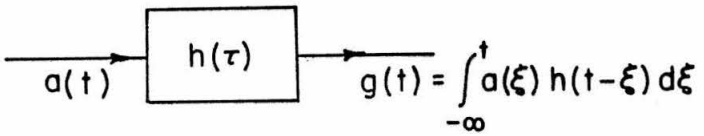

FIG. 3.3 CONSTANT PARAMETER LINEAR SYSTEM

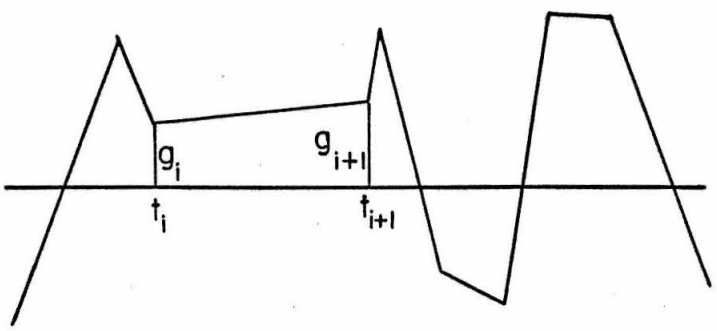

FIG. 3.4 LINEARIZED RECORD.

Substituting this expression for $a(t)$ into Eq. 3.2 yields the complex response

$$g(t) = -\omega^2 \int_0^\infty e^{i\omega(t-\tau)} h(\tau)\, d\tau \tag{3.5}$$

$$= -\omega^2 Y(\omega)\, e^{i\omega t} \tag{3.6}$$

where

$$Y(\omega) = \int_0^\infty h(\tau) e^{-i\omega\tau}\, d\tau \tag{3.7}$$

For a physically realizable system, $h(\tau)$ is zero for negative τ, i.e., the system responds only to inputs which have already occurred. For this reason the integration in Eq. 3.7 can be taken from $-\infty$ to $+\infty$, in which case $Y(\omega)$ can alternatively be defined as the Fourier transform of the weighting function.

By writing $Y(\omega)$ in the form

$$Y(\omega) = |Y(\omega)|\, e^{i\varphi(\omega)} \tag{3.8}$$

where $|Y(\omega)|$ is the absolute value of $Y(\omega)$ and $\varphi(\omega)$ represents the phase response, Eq. 3.6 yields

$$|g(t)| = \omega^2 |Y(\omega)| \tag{3.9}$$

This expression for $|g(t)|$ is thus a measure of the amplitude of the displacement response of the system to a sinusoidal displacement input of unit amplitude and frequency ω, and is thus identical to the system magnification, M, mentioned in the last section. Hence the following

equation holds for $|Y(\omega)|$.

$$|Y(\omega)| = M/\omega^2 \tag{3.10}$$

Taking the Fourier transform of Eq. 3.2, and noting the convolution integral on the right-hand side, yields

$$FT[\,g(t)\,] = FT[\,a(t)\,]\cdot FT[\,h(t)\,] \tag{3.11}$$

$$= FT[\,a(t)\,]\; Y(\omega) \tag{3.12}$$

The Fourier amplitude spectrum is given by the amplitude of the Fourier transform. Writing $F_a(\omega)$, $F_g(\omega)$ as the Fourier amplitude spectra of a(t), g(t), resp., in terms of ω, it is seen that the spectra of g(t) and a(t) are related by

$$F_g(\omega) = F_a(\omega)\cdot |Y(\omega)| \tag{3.13}$$

Substituting for $|Y(\omega)|$ from Eq. 3.10, yields the following expression for $F_a(\omega)$:

$$F_a(\omega) = F_g(\omega)\cdot \omega^2/M \tag{3.14}$$

Rewriting this in terms of the period, T, yields

$$F_a(T) = F_g(T)\cdot 4\pi^2/T^2M \tag{3.15}$$

Two points may be noticed here.

(i) In general, the Fourier transform of a function g(t) need not exist, in which case Eq. 3.11 would be meaningless. In the develop-

ment of the subject of Fourier transforms and their relationship with power spectral density functions this difficulty is avoided by considering "truncated" functions, which are defined to be zero outside a certain range[20]. A similar situation holds in this investigation, where the trace of interest has a finite length so that its Fourier transform does exist.

(ii) The relationship between the Fourier spectra of the ground acceleration and that of the record, given by Eq. 3.15, does not have an analogy in response spectra analysis. It is necessary, for response spectra, that the record be that of the ground acceleration to be used in Eq. 2.2. However, Eq. 3.15 indicates that provided a magnification curve is obtainable of the type in Fig. 3.2, the instrument used for Fourier spectra of ground acceleration need not have the characteristics of an accelerometer with a flat response up to frequencies of 15 or 20 cps. Lower undamped natural frequencies are associated with less stiff restoring forces and hence more sensitivity. The sensitive instruments used in this study have made it possible to take readings of the ground motion of small distant earthquakes. These occur with sufficient regularity to make the study possible in a reasonable length of time, which would not be the case otherwise.

The predominant frequencies of strong-motion earthquake records are also of some interest and Fourier analysis would amply supply this information. But much more important to earthquake engineers are the expected maximum responses of structures to

such ground motion and for this reason response spectra analysis of acceleration records is used most often.

D. Methods of Calculating Fourier Spectra

Eq. 3.15 indicates that the Fourier amplitude spectrum, $F_a(T)$, of the ground acceleration in terms of period can be obtained from the magnification curve of the instruments in the sensing and recording system and the Fourier spectrum of the output trace. This spectrum, in turn, is obtained from the Fourier transform of the trace.

Three methods were considered for the numerical calculation of the Fourier transform of the digitized record. The important characteristics of the digitized data which governed the final choice of the first method were:

(a) the fact that the coordinates were not equi-spaced but joined points of change of slope, and

(b) the non-stationary nature of the phenomenon under investigation.

A brief description of the methods follows, still using the frequency ω rather than the period T for convenience.

1. Direct from the integral definition.

The Fourier transform of a record of length s is given by

$$FT[\, g(t)\,] = \int_0^s g(t)e^{-i\omega t}\, dt \qquad (3.16)$$

Fig. 3.4 shows how the record $g(t)$ is split up into steps in all of which $g(t)$ is linear. The integral in Eq. 3.16 can therefore be re-written in the form of a sum of integrals:

$$FT[\, g(t) \,] = \sum_{i=1}^{N-1} \int_{t_i}^{t_{i+1}} g(t) e^{-i\omega t}\, dt \qquad (3.17)$$

where N is the total number of points in the digitized record. After separating the exponential into its real and imaginary parts, the integrations can be performed so that every term in the summation is a function of t_i, g_i, t_{i+1}, g_{i+1} and ω where t_i and g_i are the coordinates of the i-th point. The IBM 7094 digital computer at the California Institute of Technology was used to calculate the individual terms of the summation, obtain the real and imaginary parts of $FT[\, g(t) \,]$, and hence arrive at the Fourier amplitude spectrum.

2. Indirect method arising from the similarity to the undamped relative velocity response spectrum.

Suppose, temporarily, that the record g(t) represents a ground acceleration, a(t), $0 \leq t \leq s$. The relative displacement response, x(t), of an undamped single degree-of-freedom system to this excitation is governed by the equation

$$\ddot{x}(t) + \omega_o^2 x(t) = -a(t) \qquad (3.18)$$

where ω_o is the natural frequency of the system. The relative velocity is thus

$$\dot{x}(t) = \int_0^t a(\tau) \cos \omega_o (t - \tau)\, d\tau \qquad (3.19)$$

which can be written as

$$\dot{x}(t) = \cos \omega_o t \int_0^t a(\tau) \cos \omega_o \tau \, d\tau + \sin \omega_o t \int_0^t a(\tau) \sin \omega_o \tau \, d\tau \qquad (3.20)$$

Writing $A_1(t)$, $A_2(t)$, for the two integrals appearing here, the relative velocity becomes

$$\dot{x}(t) = \cos \omega_o t \cdot A_1(t) + \sin \omega_o t \cdot A_2(t) \qquad (3.21)$$

$$= \sqrt{(A_1^2 + A_2^2)} \cos [\omega_o t - \theta(t)] \qquad (3.22)$$

where $\theta(t) = \tan^{-1}(A_2/A_1)$. Now the velocity response to excitation of this type actually exhibits an oscillatory nature with a varying amplitude, as described in Chapter II. This indicates that the functions $\sqrt{A_1^2 + A_2^2}$ and θ vary reasonably slowly with time. Hence the envelope, $E_1(t)$, of the relative velocity curve is given to a close approximation by

$$E_1(t) = \sqrt{[A_1^2(t) + A_2^2(t)]} \qquad (3.23)$$

The value of $E_1(t)$ at the end of the record is therefore obtained by substituting for A_1 and A_2:

$$E_1(s) = \sqrt{\left[\left\{ \int_0^s a(\tau) \cos \omega_o \tau \, d\tau \right\}^2 + \left\{ \int_0^s a(\tau) \sin \omega_o \tau \, d\tau \right\}^2 \right]} \qquad (3.24)$$

For a given record $a(t)$ of duration s, this expression depends only on ω_o and takes on different values as ω_o is varied over the values corresponding to the desired values of T. But from Eq. 3.16 the

Fourier amplitude spectrum of a record $a(t)$ of duration s is given by exactly the same expression with ω_o replaced by ω. This indicates that the Fourier amplitude spectrum of the record $g(t)$ is given approximately by the final value of the envelope of the undamped relative velocity response to a base acceleration $a(t)$ equal numerically to $g(t)$. It is noticed that the essence of the above approximate method is the treatment of the ground motion record as though it were an acceleration. It of course does not in fact have to be an acceleration record, since the mathematical formulation will in any event produce the proper Fourier spectrum of the original curve. This affords another method of calculating the Fourier amplitude spectrum. Writing $\dot{x}(t) = x_1(t)$, Eq. 3.18 is transformed into a pair of first order equations:

$$\begin{aligned} \dot{x}(t) &= x_1(t) \\ \dot{x}_1(t) &= -a(t) - \omega_o^2 x(t) \end{aligned} \tag{3.25}$$

It is relatively easy to adapt a digital computer program to handle such equations numerically when $a(t)$ is composed of unequal linear segments. Provided sufficiently close watch is kept on the velocity $\dot{x}(t)$, so that the value of its envelope can be obtained at the end of the record, this indirect approach affords an interesting way of obtaining an approximate Fourier amplitude spectrum. However, it is much more suited to analog computer techniques using the electric analog response spectrum analyzer[5] in which amplitudes can be read on the screen of a cathode ray tube. When compared

with the simplicity and inherent accuracy of the first method, this indirect approach loses some of its appeal.

3. Indirect method making use of the autocorrelation function and the power spectral density.

The increased availability of digital computers and their convenience for repetitive numerical analysis has been accompanied by much improved methods of power spectral analysis of random processes with discrete data points[25]. Because existing techniques used in correlation studies rely on equally spaced data and, furthermore, are more adapted to handling stochastic processes, they are somewhat inappropriate for the basically simple analysis required in the current work, but the approach is different from both previous methods and is mentioned for that reason.

E. Results of Calculations

Three earthquakes, whose epicenters are indicated in Fig. 3.1, were used in this study. Table 3.1 contains their magnitudes and detailed locations, while Table 3.2 lists the sites. The two instrument sites for the first two earthquakes were located at Wheeler Ridge on alluvium and at Ft. Tejon on granite. The third earthquake was recorded at Ft. Tejon and at another granitic location at Tehachapi, indicated in Fig. 3.1.

Table 3.1
Earthquake Data

No.	Magnitude	Epicenter	Origin data and time
1	4.4	35°54'N, 114°48'W	9/23/64 18:10:44 GCT
2	4.9	38°55'N, 118°25'W	10/23/64 13:57:09 GCT
3	5.6	31°55'N, 117°09'W	12/22/64 20:54:35 GCT

Table 3.2
Site Locations

Site	Rock Type	Location	Earthquakes
1. Wheeler Ridge	Alluvium	35° 1'32"N, 118°59'55"W	1,2
2. Ft. Tejon	Granite	34°52'19"N, 118°54' W	1,2,3
3. Tehachapi Granitics	Granite	34°56'11"N, 118°49'14"W	3

The first two earthquakes were digitized in full by the USCGS at San Francisco, while only one component of the third was digitized by the author at the Seismological Laboratory of the California Institute of Technology. The first earthquake was not digitized as carefully as the remaining two, and only one test was run using this data, apart from the frequent preliminary test runs to check the computer program.

This one test using earthquake No. 1 was a check of the explanation of method (2) in Section D of this Chapter for the calculation of Fourier spectra. Firstly, the Fourier amplitude spectrum of the digitized instrument trace was calculated. Secondly, the digitized trace was considered mathematically to contain the numerical values of a ground acceleration and the computer program developed in Chapter I for response spectra was applied. Method (2) explained how the envelope of such a response at the end of the excitation was related to the Fourier spectral value. Furthermore, if the maximum response occurs at the end of the excitation its value will be close to that of the envelope there. This second treatment of the trace should thus correspond to the first only when the maximum response is reached near the end of the record.

The results for the E-W component of earthquake No. 1 are plotted in Fig. 3.5 where the vertical unit is mm. sec., in effect the result of integrating a trace in mm. against time in seconds. It may be noted that at six periods the two values are very similar. The calculation for the second curve indicated that at these six

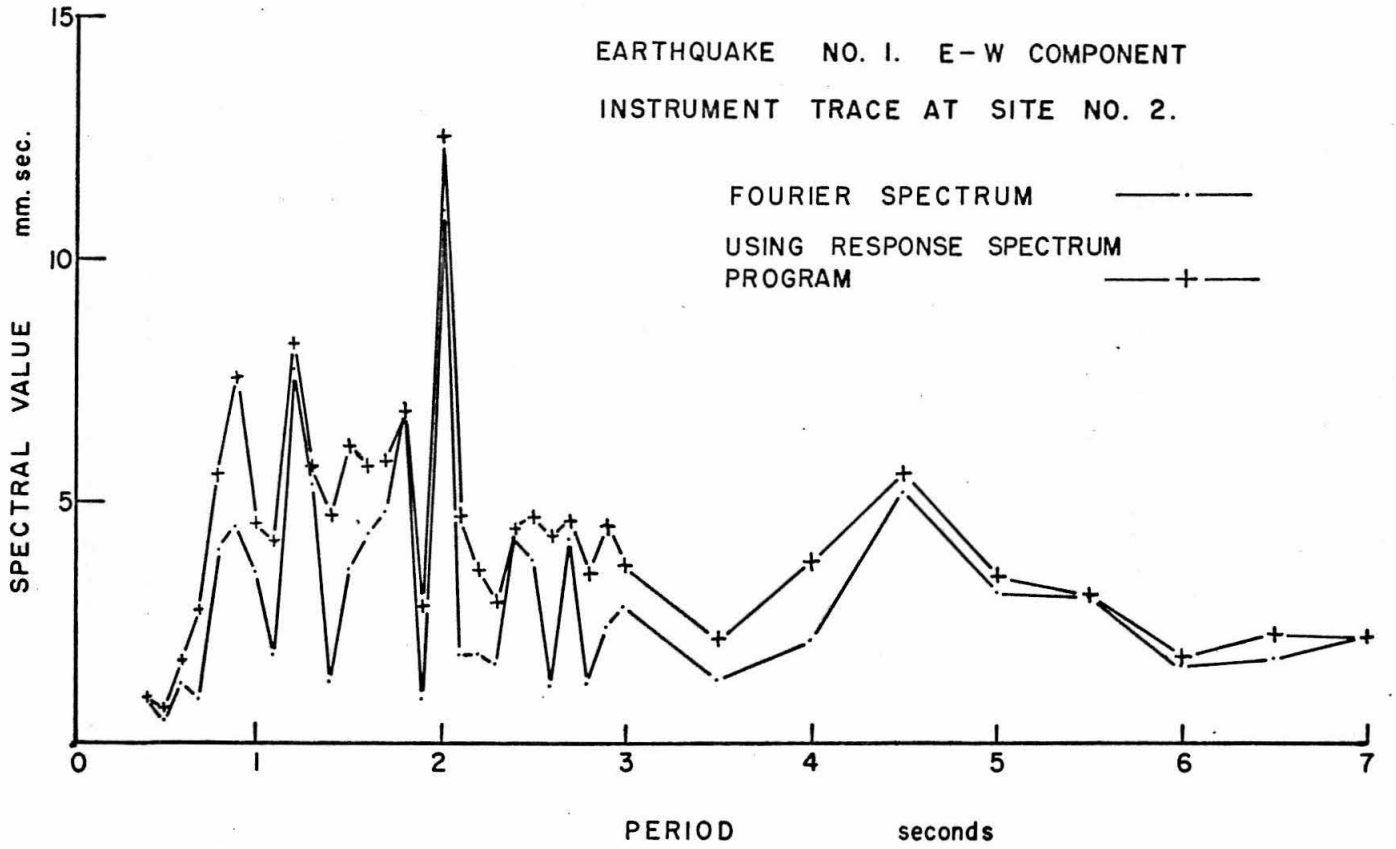

FIG. 3.5 CHECK OF METHOD (2) OF SECTION D.

points the maximum value did occur towards the end, thus providing an approximate check of method (2).

The digitized earthquake No. 2 was then used to calculate a set of Fourier spectra, appearing in Figs. 3.6 to 3.8. Since these curves are the spectra of the ground acceleration, the vertical unit is that of a velocity, mm./sec. The predominant features of these spectra are listed below.

(i) The spectra for the alluvium site lie with few exceptions above those for the granite site. This indicates that for the most part, the ground motion is magnified on passage through the alluvium layers.

(ii) The spectra for the horizontal motions, in Figs. 3.6 and 3.7 are greater than that for the vertical motion in general, particularly for the alluvium site. This agrees with the results that are usually observed for strong-motion earthquakes.

(iii) All the spectra have an extremely oscillatory behavior, more apparent at the lower periods where the spectral values are closely spaced. It is immediately apparent that this sensitivity to changes of period renders any ratio calculation completely out of the question. Such a magnification curve would be even more oscillatory and slight changes in the periods at which the values are calculated would be likely to give a very different picture. It is easy to see how a slight horizontal shift of either of the two curves in each figure would affect the ratio calculation. Any direct calculation of magnification factors for passage through alluvium layers should be avoided for these reasons.

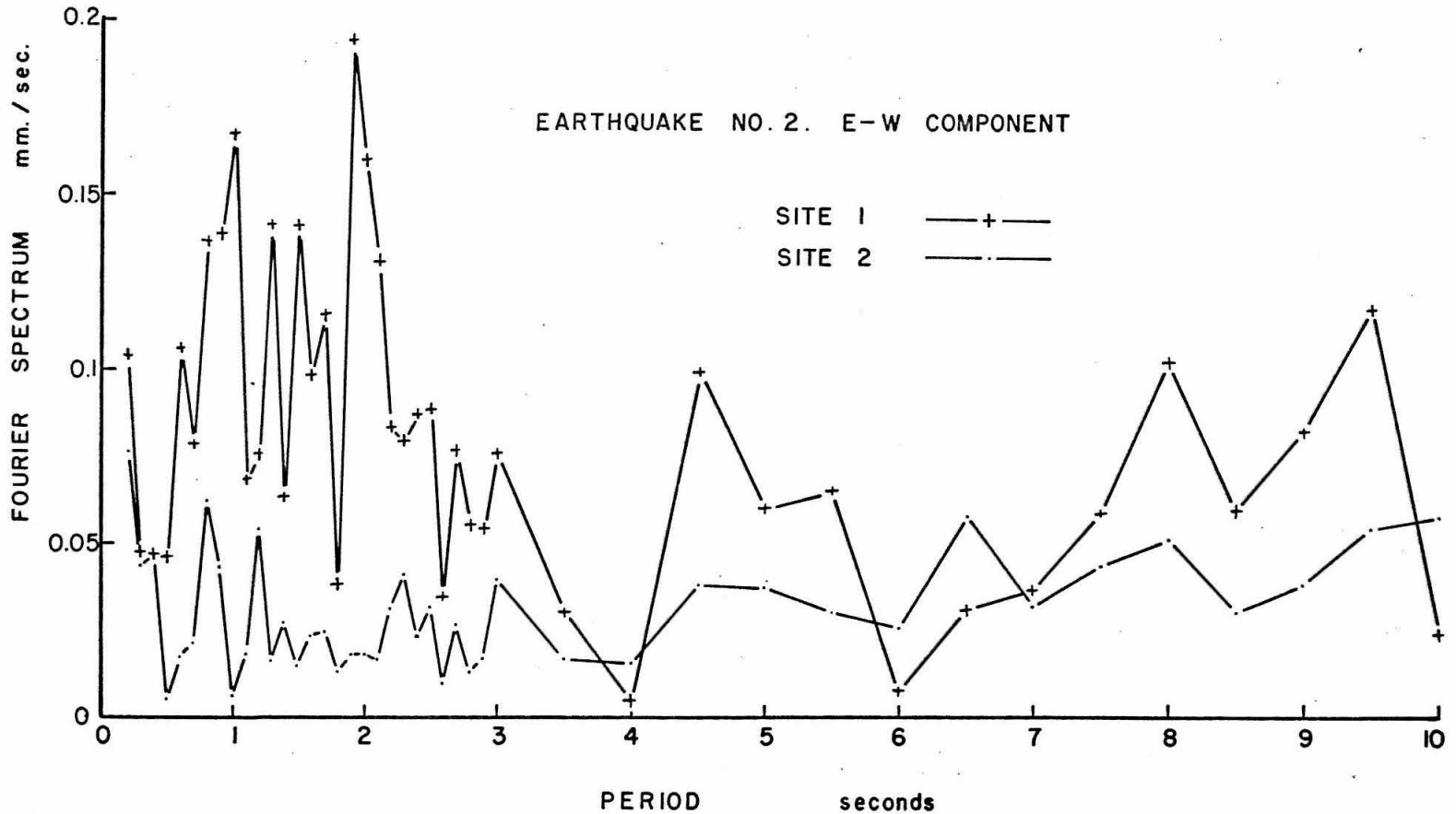

FIG. 3.6 FOURIER AMPLITUDE SPECTRA OF GROUND ACCELERATION.

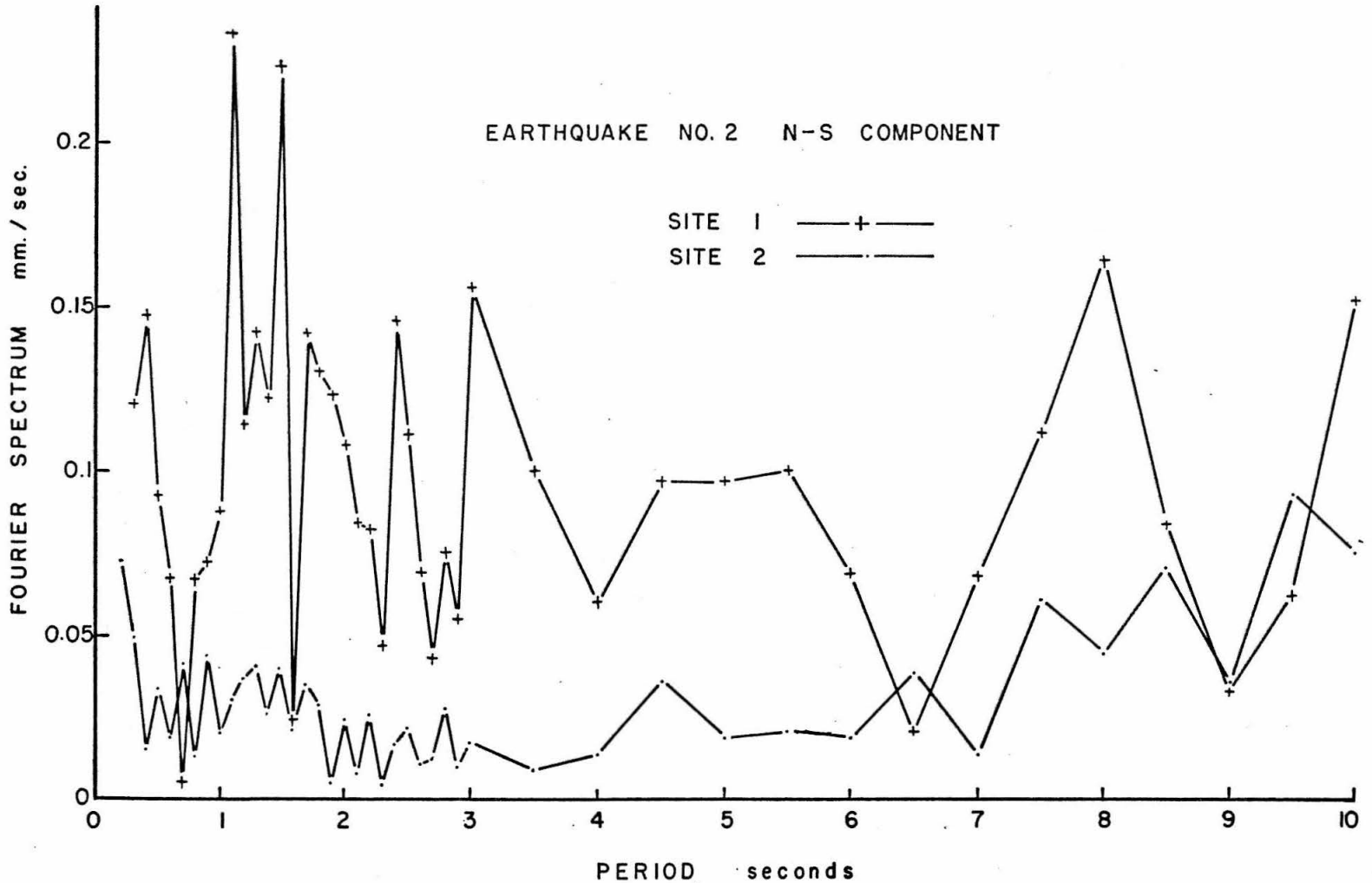

FIG. 3.7 FOURIER AMPLITUDE SPECTRA OF GROUND ACCELERATION.

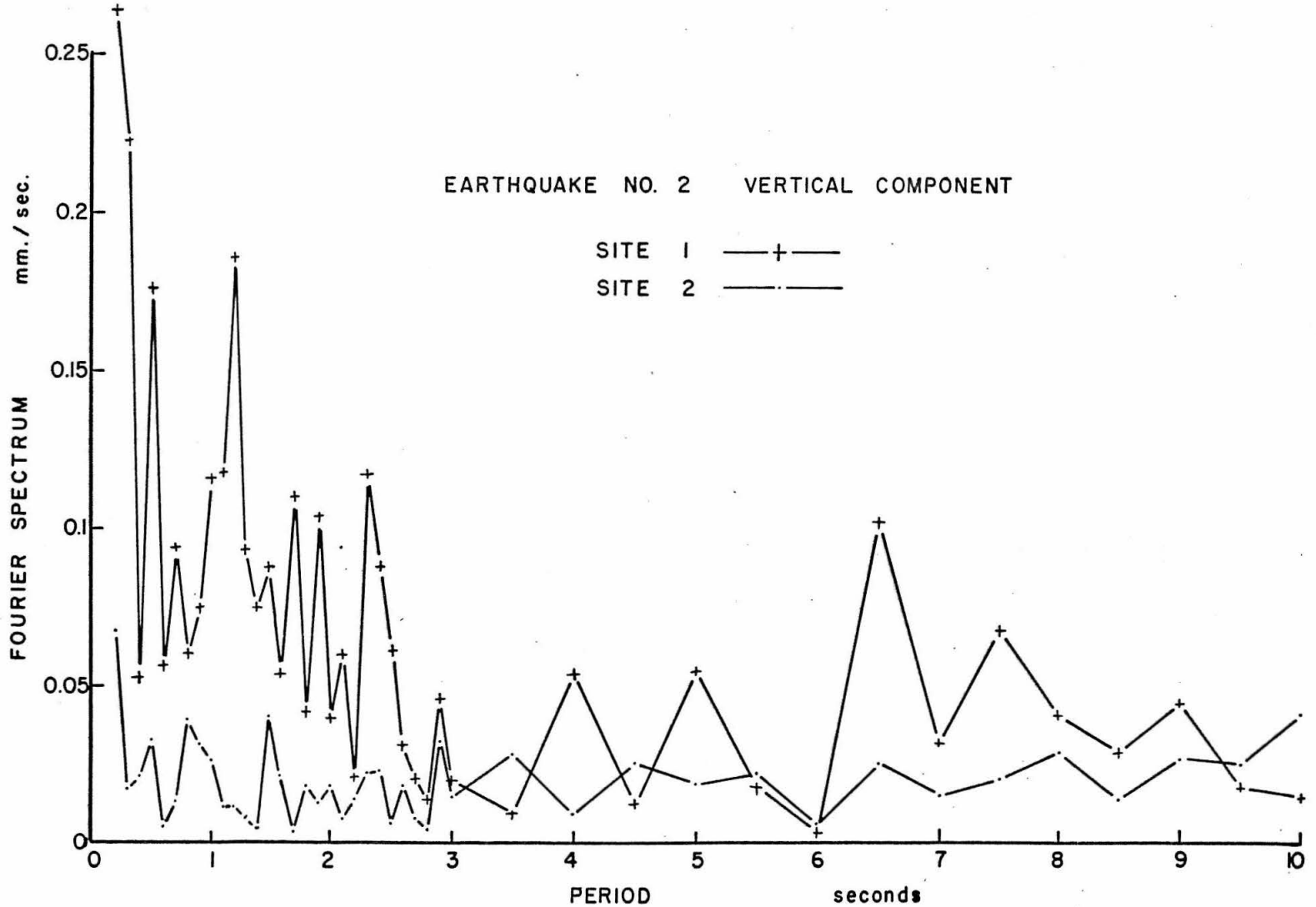

FIG. 3.8 FOURIER AMPLITUDE SPECTRA OF GROUND ACCELERATION.

(iv) The high spectral values for the 0.2 sec. period, (in fact, Fig. 3.7 read off scale at that point) caused some suspicion to fall on the instrument magnification curves at these low periods. In fact, these curves are obtained from the sinusoidal response curves, which in turn cannot be read to the usual accuracy of 1% for all periods less than 0.4 sec. Hence the resulting Fourier spectra are only approximate for these periods.

The question that arose next was that of the accuracy of setting up the traces in the reading machine prior to digitizing. On attempting to do this, it was apparent that the width of the trace was of the same order or even greater than the accuracy to which the machine digitized the cross-hair position. This meant that in lining up the cross-hairs on an adjacent non-oscillating trace, errors of up to two or three units (2/5 to 3/5 mm.) might be expected, and this lining up occurred for every 20 cm. length.

The E-W component of earthquake No. 2 was altered with specified shifts to the base line in the computer, simulating these lining up errors, with the resulting spectra shown in Fig. 3.9. As was to be expected, the long period values were altered most -- by up to 100%. There was negligible effect for periods less than four seconds.

In order to verify that the above tilting and shifting errors were in fact present, the base line for every 20 cm. length was adjusted with a linear correction so that the mean square of the record was minimized. The record is already an approximate relative velocity, so this step corresponds to the conditions on the

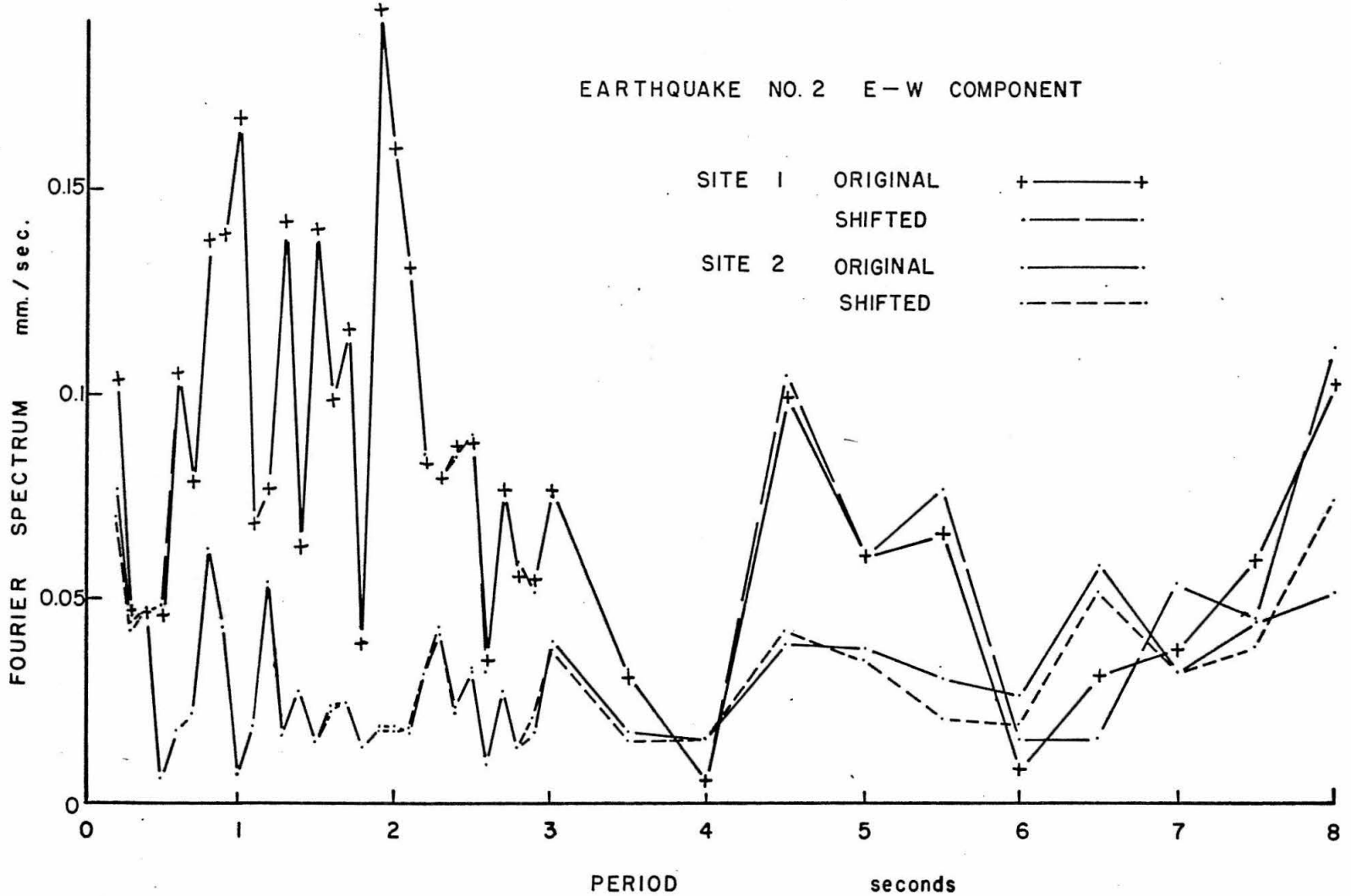

FIG. 3.9 EFFECT OF SPECIFIED SHIFT OF BASELINE.

correction applied to the ground acceleration in Chapter I. The result of this correction for the whole 60 cm. record length is shown in Fig. 3.10 which indicates a negligible effect up to a period of three seconds and only a 30% change for a few higher periods. In these two figures, the original spectral values are plotted throughout and any changed value is indicated only if it plots further than about 1/20 in. away, for clarity.

One other source of possible error in the digitizing procedure lies in failing to choose suitable points between which the record is assumed to be linear. Frequently choosing just the peaks is not sufficient, particularly for slowly oscillating traces. Some analyses have been performed in which half-period cosine waves are inserted between successive points, requiring that only the peaks be chosen. For the records used in this study it was apparent that the many frequencies present would not allow this second system to give accurate results. The analysis chosen for these records relies on the records being linear between data points.

The dependence of the Fourier spectra of ground acceleration on duration was investigated using the same E-W component of earthquake No. 2. Fig. 3.11 shows the effect of using 150, 125 and 100 sec. durations. It is apparent that the general shape is followed reasonably closely by the 125 sec. result and not as well by the 100 sec. result. No definite tendency is shown towards higher or lower values. These conclusions agree with the results of some Fourier spectrum calculations of strong-motion earthquakes[5].

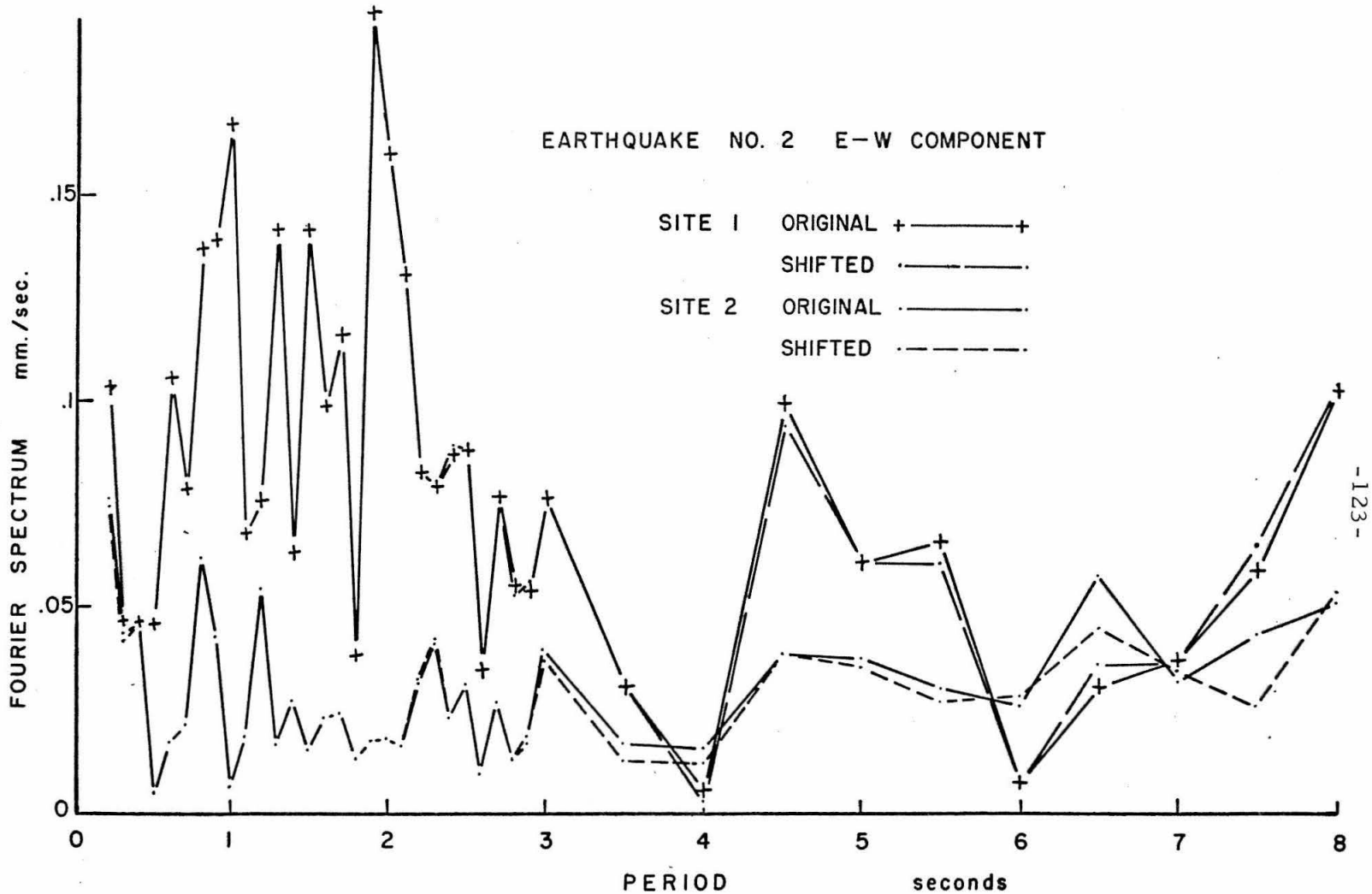

FIG. 3.10 LEAST SQUARES FIT TO SHIFTED BASELINE.

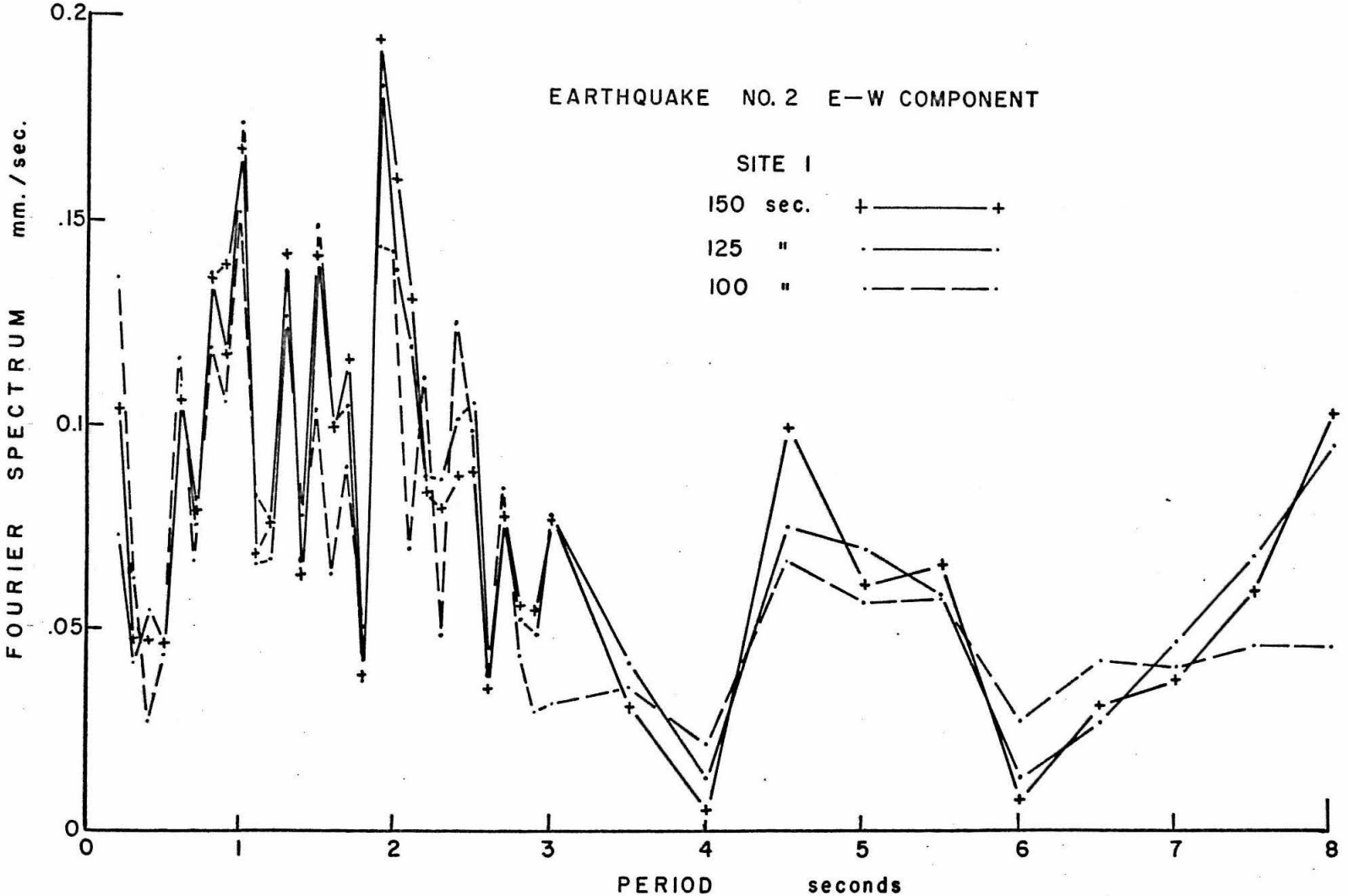

FIG. 3.11 DEPENDENCE ON DURATION OF RECORD.

An attempt was then made to render the spectra more suitable for comparing the two sites. To reduce the oscillatory behavior required some means of smoothing the curves by an averaging process. The Seismology Laboratory have been using for some time a weighted average smoothing process called "hanning" described in detail by Blackman and Tukey[25]. This smoothing process is applied to power spectra when calculated from equally spaced records and attempts to make an allowance for the fact that the original record is a smooth function between these discrete points. Although the current investigation was yielding Fourier spectra which were not calculated from the same type of data, the hanning process was applied to some of the spectra in order to facilitate the comparison of the spectra at the two sites. The process replaces each interior ordinate y_i by $y_{i-1}/4 + y_i/2 + y_{i+1}/4$ and each end ordinate by half the sum of the end ordinate and its neighbor. This substitution leaves the area under the curve unaltered which means that the energy of the ground motion at a particular frequency is redistributed among adjacent frequencies without altering the value of the total energy.

The results of this smoothing are illustrated in Figs. 3.12 to 3.14, obtained from Figs. 3.6 to 3.8, showing the spectra for earthquake No. 2 at the two sites, Wheeler Ridge and Ft. Tejon. From these smoothed curves it is possible to deduce a little about the magnification of the ground motion through the alluvium layers at the Wheeler Ridge site. For low periods, up to two or three seconds, the magnification fluctuates about the value of five, while

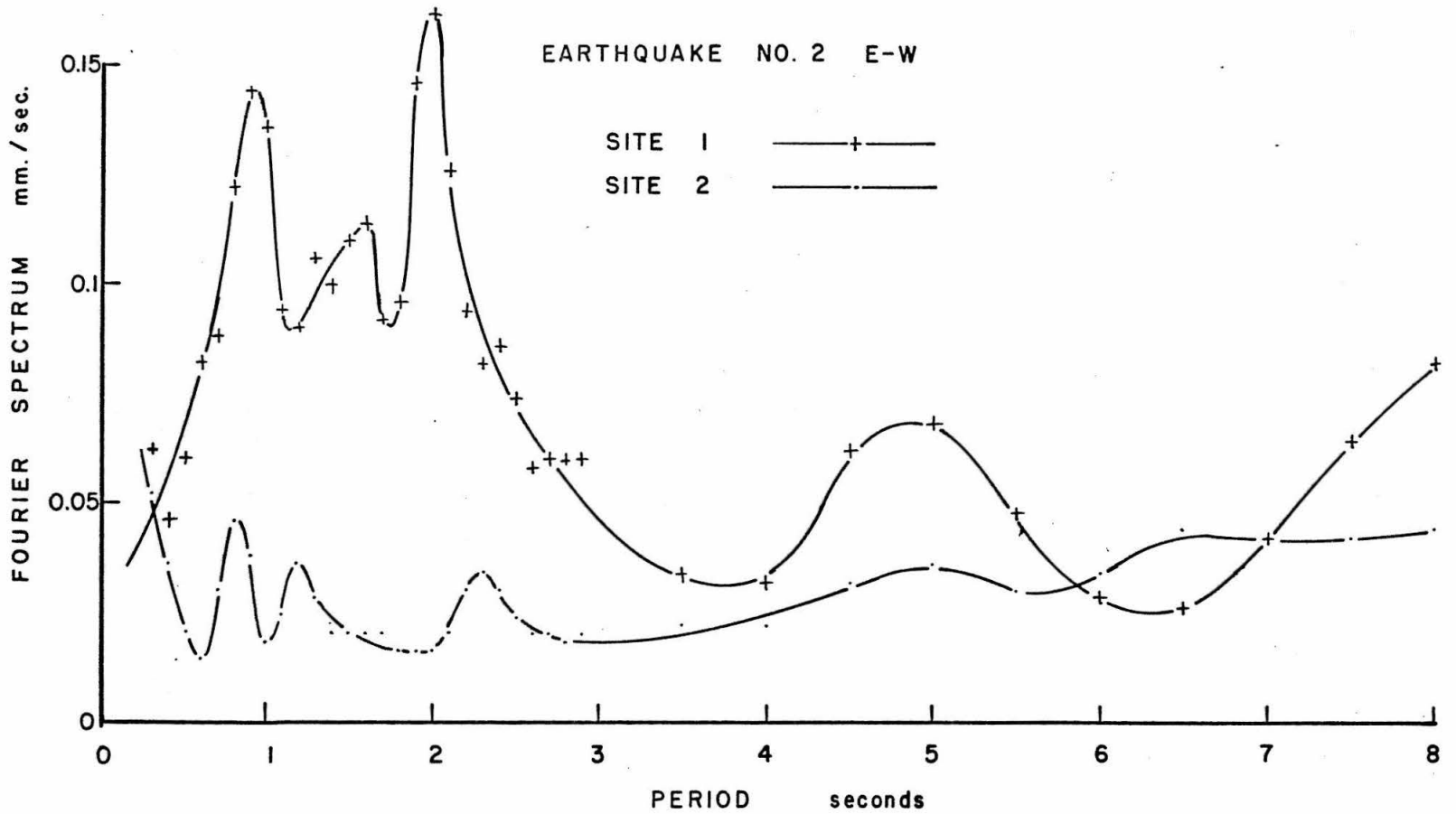

FIG. 3.12 SMOOTHED FOURIER SPECTRA OF GROUND ACCELERATION.

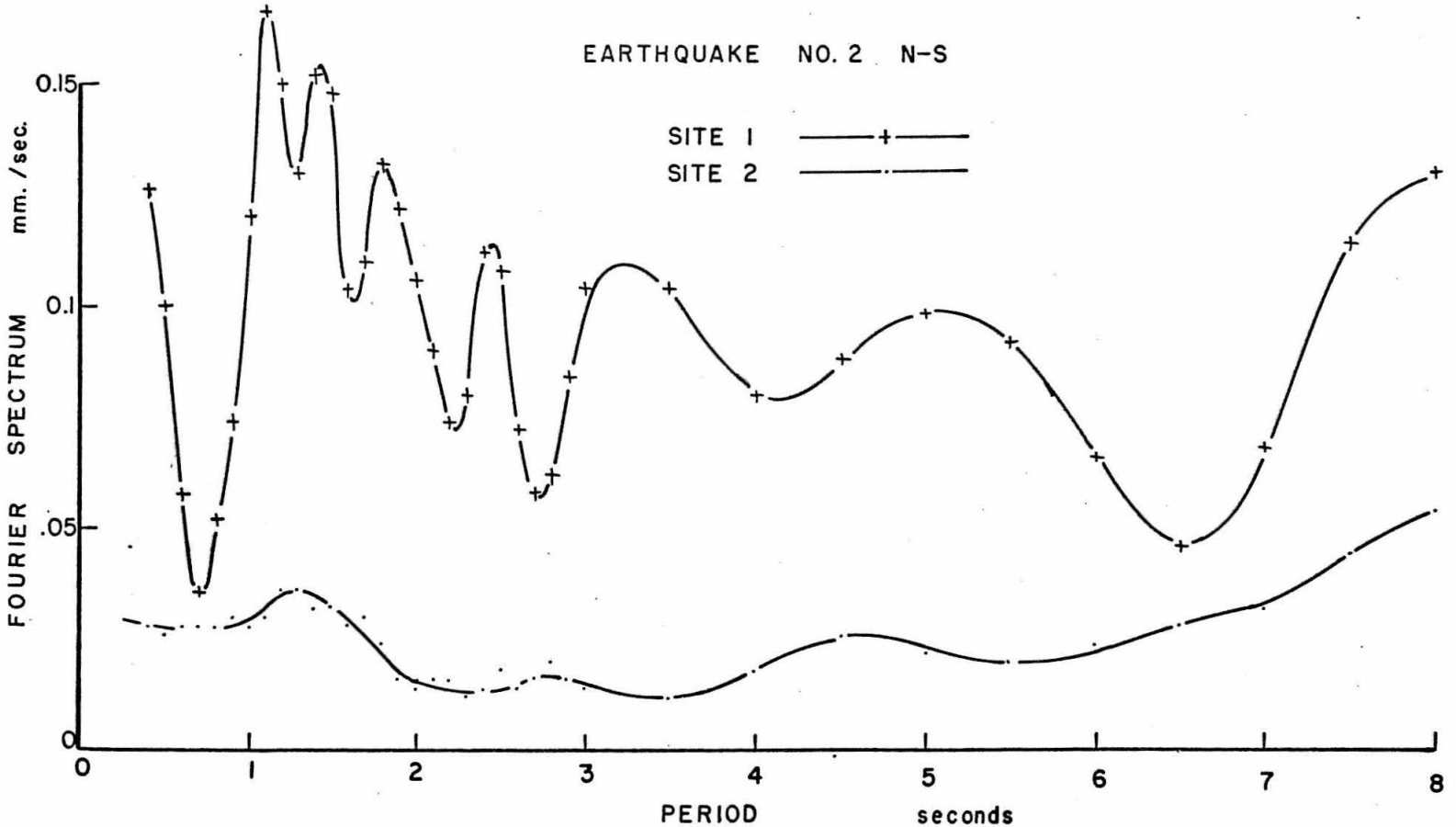

FIG. 3.13 SMOOTHED FOURIER SPECTRA OF GROUND ACCELERATION.

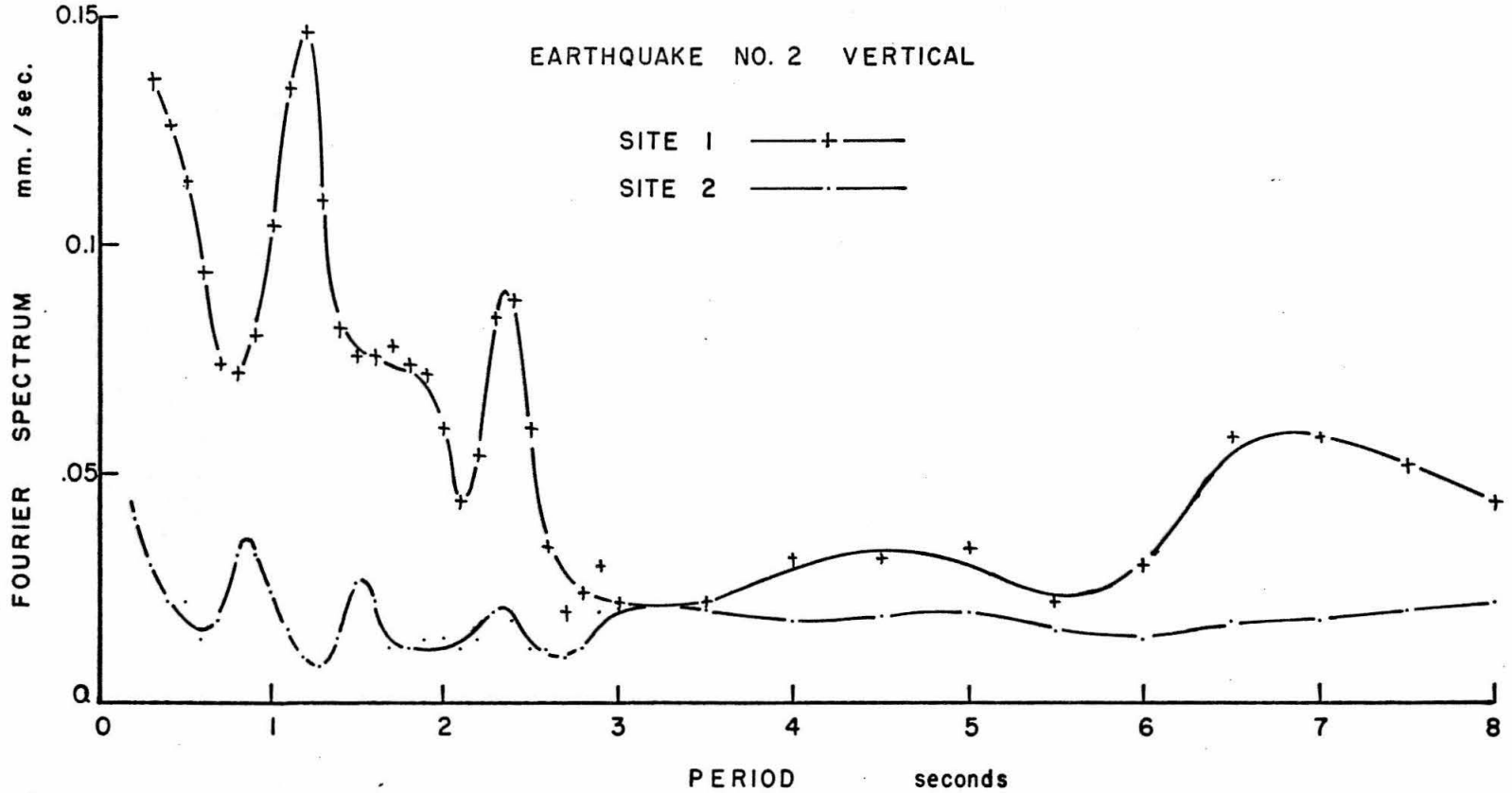

FIG. 3.14 SMOOTHED FOURIER SPECTRA OF GROUND ACCELERATION.

for the longer periods the magnification in general is much less, dropping to unity and lower in some places.

Two sites on granite were included as a last step in this study and one component of earthquake No. 3 was analyzed. The Fourier spectra are shown in Fig. 3.15 and are smoothed in Fig. 3.16 where the general similarities are evident. The two sites were six miles apart and the epicenter of this earthquake was two hundred and fifty miles away. It would appear that the spectra are not as similar as might be expected. The point to be recognized from this dissimilarity is that the spectra of earthquake No. 2 in the granite at Ft. Tejon will differ, by a similar amount, from that in the granite below the Wheeler Ridge alluvium site. This means that the ground motion in the bedrock granite at the alluvium site is not known any more accurately than is indicated by Fig. 3.16, and the comparisons of the spectra in Figs. 3.12 to 3.14 must be made with this in mind.

Standard analysis procedure

In view of the results described in this section, a standard method of calculating Fourier amplitude spectra of records of this type might be recommended.

(i) Use a constant duration for all earthquakes. The length used in this investigation was 150 sec., and is suitable for reading in three sections of 50 sec. each, this corresponding to 20 cm. of record.

(ii) Set up each section in the reader, lining up against the adjacent traces, and read off the points of change of slope.

FIG. 3.15 FOURIER AMPLITUDE SPECTRA OF GROUND ACCELERATION.

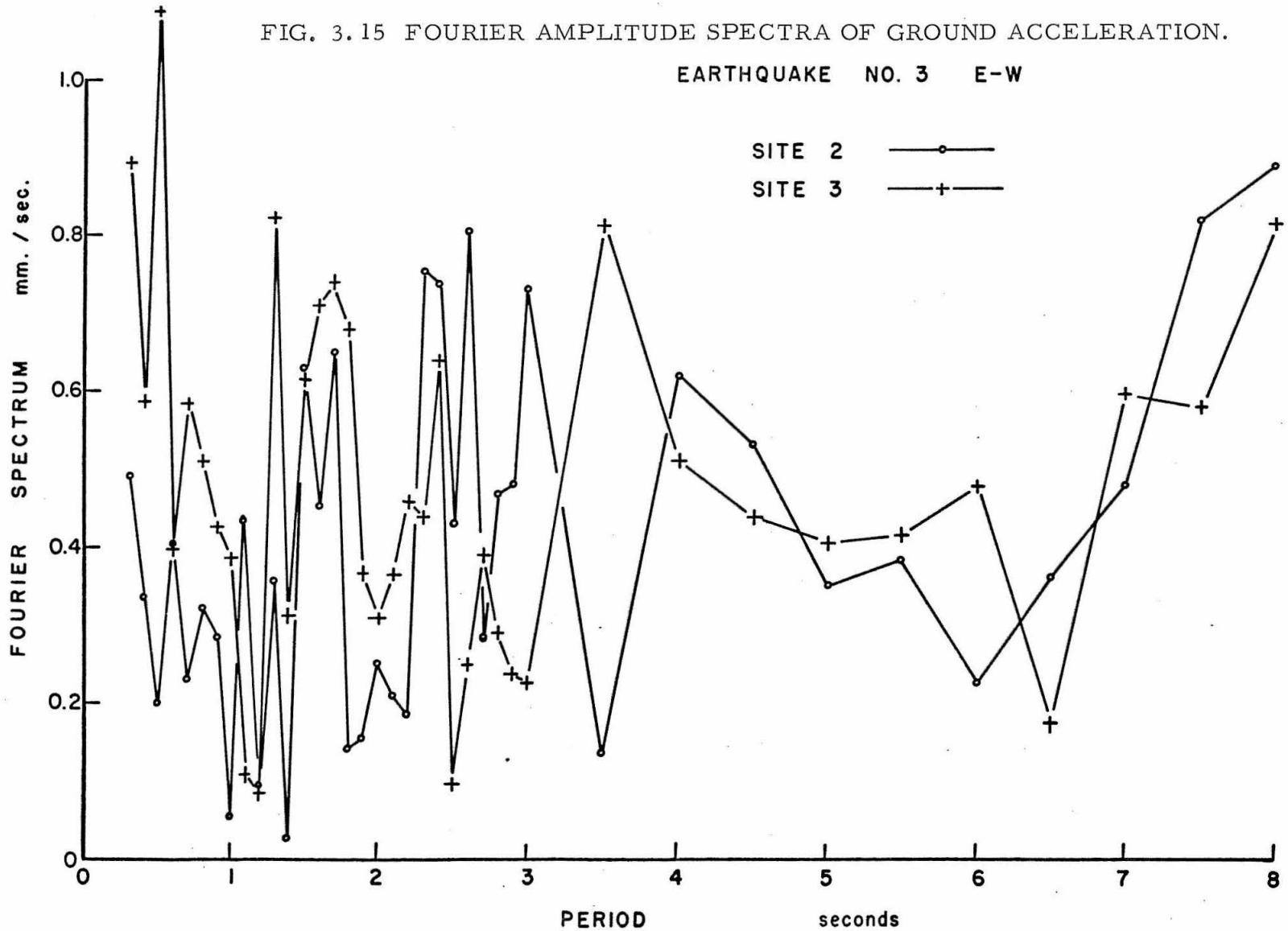

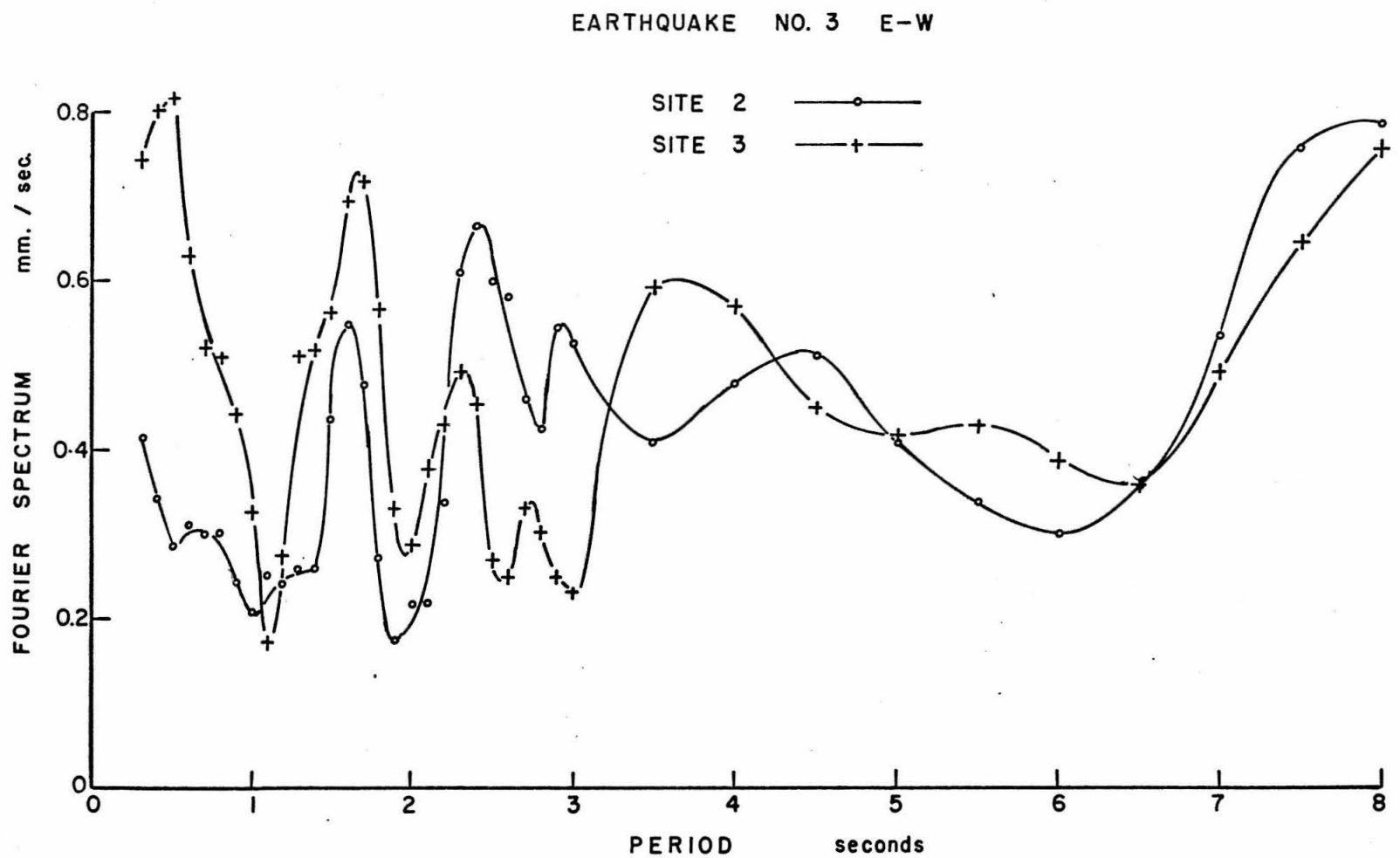

FIG. 3.16 SMOOTHED FOURIER SPECTRA OF GROUND ACCELERATION.

Digitizing to the nearest 1/5 mm. was found to be satisfactory, using a minimum point spacing of about 1/2 mm.

(iii) Compute the Fourier spectra of the ground acceleration as described in method (1) of Section D, making use of the instrument magnification curves.

(iv) Smooth the spectra by the method described in this section, and if required, estimate the predominant ratios.

F. Summary and Conclusions

The USCGS is carrying out an investigation of the ground motion at adjacent dissimilar sites due to distant earthquakes and this chapter has described the method of analysis of the records developed at the California Institute of Technology, and suggested for future adoption.

The instrumentation is described in some detail and the system magnification curves, corresponding to frequency response curves for the instruments, are described.

The equation connecting the Fourier spectrum of the ground acceleration with that of the instrument trace is derived, making use of the system magnification curve. It is concluded that the Fourier spectrum analysis is well suited to the records obtained by the USCGS in this study. Response spectrum analysis described in Chapter I is suitable only for acceleration records that would have been much more difficult to obtain.

Three methods for calculating the Fourier spectrum of a record trace are discussed and several reasons are given for the choice of a simple method, directly from the definition. Using this method, a number of tests are made on data from three small distant earthquakes measured at three neighboring sites--one on alluvium overlying bedrock granite and the other two on outcropping granite. Only the third earthquake was recorded at the two granite sites.

The general appearance of the Fourier spectra is discussed particularly as regards their oscillatory nature. The effect of irregu-

larities in setting up the records for digitizing is studied and it is concluded that visual lining up, coupled with careful choosing of points, produces spectra of satisfactory accuracy. The dependence of the spectra on the chosen duration is also discussed. Before any comparison can be made of the spectra at two different sites, a smoothing process is used on the spectral ordinates. It is concluded that the resulting curves are more suitable than the originals for comparison.

The earthquake recorded at the two granite sites gives results that are more different than might have been expected. An important conclusion is that any comparison of spectra at different sites must take into account the possibility of both spectra being in error by as much as that indicated in Fig. 3.16. The best that might be said at this point is that amplifications need not be considered important unless they indicate a factor of about four.

It is concluded that many more records at the sites mentioned here will have to be analyzed before more definite statements can be made regarding the amplification of ground motion. In particular, before extending the results to strong-motion earthquakes, much greater ground motions are needed. Meanwhile, a standard method of analysis based on the results of tests in this investigation is recommended.

REFERENCES

1. Alford, J. L., Housner, G. W. and Martel, R. R., Spectrum Analyses of Strong-Motion Earthquakes, Pasadena: California Institute of Technology Earthquake Research Laboratory, (revised edition, 1964).

2. Berg, G. V. and Housner, G. W., "Integrated Velocity and Displacement of Strong Earthquake Ground Motion," Bulletin of the Seismological Society of America, Vol. 51, No. 2, (April, 1961), pp. 175-189.

3. Hudson, D. E., "Response Spectrum Techniques in Engineering Seismology," World Conference on Earthquake Engineering, Berkeley, California (June, 1956).

4. Housner, G. W., "Behavior of Structures During Earthquakes," Proceedings ASCE, Vol. 85, No. EM4 (Oct. 1959), pp.109-129.

5. Hudson, D. E., "Some Problems in the Application of Spectrum Techniques to Strong-Motion Earthquake Analysis," Bulletin of the Seismological Society of America, Vol. 52, No. 2 (April, 1962), pp. 417-430.

6. Housner, G. W., "Characteristics of Strong-Motion Earthquakes," Bulletin of the Seismological Society of America, Vol. 37, No. 1, (Jan. 1947), pp. 19-31.

7. Housner, G. W., "Properties of Strong Ground Motion Earthquakes," Bulletin of the Seismological Society of America, Vol. 45, No. 3 (July, 1955), pp. 197-218.

8. Bycroft, G. N., "White Noise Representation of Earthquakes," Proceedings ASCE, Vol. 86, No. EM2, (April 1960), pp. 1-16.

9. Rosenblueth, E. and Bustamante, J. I., "Distribution of Structural Response to Earthquakes," Proceedings ASCE, Vol. 88, No. EM3, (June 1962), pp. 75-106.

10. Matthiesen, R. B., Duke, C. M., Leeds, D. J., and Fraser, J. C., Site Characteristics of Southern California Strong-Motion Earthquake Stations, Los Angeles: University of California, Department of Engineering, Report No. 64-15 (Feb., 1964).

11. Herrera, I., Rosenblueth, E , and Rascon, O. A., "Earthquake Spectrum Prediction for the Valley of Mexico," Third World Conference on Earthquake Engineering, New Zealand (1965).

12. Neumann, F., United States Earthquakes, 1940, (Serial No. 647), U. S. Department of Commerce, (1942).

13. Housner, G. W., "Ground Displacement Computed from Strong-Motion Accelerograms," Bulletin of the Seismological Society of America, Vol. 37 (1947), pp. 299-305.

14. Veletsos, A. S., Newmark, N. M., and Chelapati, C. V., "Deformation Spectra for Elastic and Elastoplastic Systems Subjected to Ground Shock and Earthquake Motions," Third World Conference on Earthquake Engineering, New Zealand, (1965).

15. Jenschke, V. A., Clough, R. W., and Penzien, J., "Characteristics of Strong Ground Motions," Third World Conference on Earthquake Engineering, New Zealand, (1965).

16. Housner, G. W., and Jennings, P. C., "Generation of Artificial Earthquakes," Proceedings ASCE, Vol. 90, No. EM1, (Feb., 1964), pp. 113-150.

17. Berg, G. V., "A Study of Error in Response Spectrum Analyses," First Chilean Conference on Seismology and Earthquake Engineering, Santiago, Chile (July, 1963).

18. Rosenblueth, E., "Some Applications of Probability Theory in Aseismic Design," World Conference on Earthquake Engineering, Berkeley, California (June, 1956).

19. Feller, W., An Introduction to Probability Theory and its Applications, Second Edition, New York: John Wiley and Sons, Inc., (1957).

20. Bendat, J. S., Principles and Applications of Random Noise Theory, New York: John Wiley and Sons, Inc., (1958).

21. Juncosa, M. L., Discussion of "Distribution of Structural Response to Earthquakes," by E. Rosenblueth and J. I. Bustamante, Proceedings ASCE, Vol. 89, No. EM1, (Feb., 1963).

22. Caughey, T. K., and Gray, A. H., Discussion of "Distribution of Structural Response to Earthquakes," by E. Rosenblueth and J. I. Bustamante, Proceedings ASCE, Vol. 89, No. EM2, (April, 1963).

23. Handbook of Mathematical Functions, M. Abramowitz and I. A. Stegun, Editors, New York: Dover Publications, Inc. (1965).

24. Duke, C. M., "Effects of Ground on Destructiveness of Large Earthquakes," Proceedings ASCE, Vol. 84, No. SM3, (August, 1958).

25. Blackman, R. B., and Tukey, J. W., The Measurement of Power Spectra, New York: Dover Publications, Inc., (1959).

26. Zeevaert, L., "Strong Ground Motions Recorded During Earthquakes of May the 11th and 19th, 1962, in Mexico City," Bulletin of the Seismological Society of America, Vol. 54, No. 1, pp. 209-231, (Feb., 1964).

APPENDIX

A. Solution of the diffusion equation in the undamped case.

In polar coordinates, ignoring any θ-variation, Eq. 2.9 becomes

$$k_1\left(\frac{\partial^2 u}{\partial r^2} + \frac{1}{r}\frac{\partial u}{\partial r}\right) = \frac{\partial u}{\partial t} \tag{A.1}$$

Eigenfunctions $\psi_m(r)$ are sought satisfying

$$k_1(\psi_m'' + \frac{1}{r}\psi_m') = -\nu_m\psi_m \tag{A.2}$$

with eigenvalues ν_m, and a solution for $u(r,t)$ is then formed from a series of these eigenfunctions:

$$u(r,t) = \sum_m a_m(t)\psi_m(r) \tag{A.3}$$

where the coefficients $a_m(t)$ depend on t. Solving Eq. A.2, with the requirement that no ψ_m is to go to infinity at $r = 0$ and $t > 0$ when subsequently used in Eq. A.3, yields

$$\psi_m = J_o\left(\sqrt{\frac{\nu_m}{k_1}}\, r\right) \tag{A.4}$$

The boundary condition, Eq. 2.10, applied to these eigenfunctions, yields the equation:

$$J_o\left(\sqrt{\frac{\nu_m}{k_1}}\, R\right) = 0 \tag{A.5}$$

from which the eigenvalues ν_m can be calculated. Substitution of Eqs. A.2 and A.3 into Eq. A.1 yields

$$\sum_m (a_m \nu_m + \dot{a}_m)\psi_m = 0 \tag{A.6}$$

and this is satisfied by

$$a_m(t) = A_m e^{-\nu_m t}, \quad A_m \text{ a constant} \tag{A.7}$$

Substitution back into Eq. A.3 yields

$$u(r,t) = \sum_m A_m J_o\left(\sqrt{\frac{\nu_m}{k_1}}\, r\right) e^{-\nu_m t} \tag{A.8}$$

The constants A_m are found using the initial condition, Eq. 2.12, which leads to

$$u(r,0) = \sum_m A_m J_o\left(\sqrt{\frac{\nu_m}{k_1}}\, r\right) = \frac{\delta(r)}{\pi r} \tag{A.9}$$

Multiplying both sides by $rJ_o\left(\sqrt{\frac{\nu_m}{k_1}}\, r\right)$, integrating from 0 to R, and using the orthogonality of the Bessel functions, yields

$$A_m \frac{R^2}{2}\left[J_1\left(\sqrt{\frac{\nu_m}{k_1}}\, R\right)\right]^2 = \int_0^R \frac{\delta(r)}{\pi} J_o\left(\sqrt{\frac{\nu_m}{k_1}}\, r\right) dr \tag{A.10}$$

Hence

$$\frac{1}{A_m} = \pi R^2 \left[J_1\left(\sqrt{\frac{\nu_m}{k_1}}\, R \right) \right]^2 \qquad (A.11)$$

Substitution into Eq. A.9 yields

$$u(r,t) = \sum_m \frac{1}{\pi R^2} \cdot \frac{1}{J_1^2\left(\sqrt{\frac{\nu_m}{k_1}}\, R \right)} \cdot J_o\left(\sqrt{\frac{\nu_m}{k_1}}\, r \right) e^{-\nu_m t} \qquad (A.12)$$

Returning to Rosenblueth and Bustamante's notation for the zeros of J_o, λ_m is substituted for $\sqrt{(\nu_m/k_1)}R$ so that

$$\nu_m = \frac{\lambda_m^2 k_1}{R^2} \qquad (A.13)$$

and the λ_m's are defined by

$$J_o(\lambda_m) = 0 \qquad (A.14)$$

Putting this into Eq. A.12 and substituting in Eq. 2.14 yields

$$F(R) = 2\pi \int_0^R \left[\sum_m \frac{1}{\pi R^2} \cdot \frac{J_o(\lambda_m \frac{r}{R})}{J_1^2(\lambda_m)} e^{-k_1 s \lambda_m^2 / R^2} \right] r\, dr \qquad (A.15)$$

The series can be integrated term by term, i.e., the order of integration and summation can be interchanged, only if the series converges uniformly in r. This is evidently the case as can readily be shown. Firstly, it may be noticed that $J_1(\lambda_m)$ is never zero for the zeros of J_o and J_1 interlace. By writing the limiting forms of the Bessel

functions for large arguments:

$$J_\nu(x)_{max.} \sim \sqrt{\frac{2}{\pi x}} \tag{A.16}$$

and the approximation for λ_m:

$$\lambda_m \sim \pi(m - \tfrac{1}{4}) \tag{A.17}$$

it is seen that the m-th term of the series is of the form

$$c_4 \sqrt{\frac{m}{r}}\, e^{-c_5 m^2} \tag{A.18}$$

for large m, where c_4 and c_5 are positive constants. Cauchy's test using the m-th root of the m-th term can be used to prove convergence provided $r \neq 0$. But $r = 0$ is ruled out because in that case every term is zero. Hence the series is uniformly convergent and can be integrated term by term yielding

$$F(R) = 2 \sum_m \frac{e^{-k_1 s \lambda_m^2 / R^2}}{\lambda_m J_1(\lambda_m)} \tag{2.16}$$

Differentiation is permissible inside the summation sign so that substitution of Eq. 2.15 gives the probability density function f(R):

$$f(R) = \frac{4k_1 s}{R^3} \sum_m \frac{\lambda_m}{J_1(\lambda_m)} e^{-k_1 s \lambda_m^2 / R^2} \tag{2.17}$$

B. Derivation of the probability distribution $F(R)$ for the damped case.

The response of a damped oscillator to base excitation is governed by Eq. 2.2. The Duhamel integral representations of x and of the quantity $\dot{x} + n\omega_o x$ (obtained on differentiating the expression for x) are similar in appearance and can be readily substituted into the following expression for r:

$$r^2 = (\omega x)^2 + (\dot{x} + n\omega_o x)^2 \tag{2.22}$$

yielding

$$r^2 = e^{-2n\omega_o t}\left[\left(\sum_{i=1}^{j} u_i e^{n\omega_o t_i} \sin \omega_o t_i\right)^2 + \left(\sum_{i=1}^{j} u_i e^{n\omega_o t_i} \cos \omega_o t_i\right)^2\right] \tag{A.19}$$

Introducing the variable r_1 given by

$$r_1 = e^{n\omega_o t} r \tag{2.23}$$

yields

$$r_1^2 = \left(\sum_i u_i e^{n\omega_o t_i} \sin \omega_o t_i\right)^2 + \left(\sum_i u_i e^{n\omega_o t_i} \cos \omega_o t_i\right)^2 \tag{A.20}$$

These components of r_1 are similar to those of r given by Eq. 2.5. However in this damped case the random variable $u_1 e^{n\omega_o t_i}$ replaces u_i and hence the intensity k_1 defined by Eq. 2.6 must be replaced by $k_1 e^{2n\omega_o t}$, the factor of two in the exponent arising because the velocity is squared in the intensity calculation.

Passage to the limit in this case leads to a random walk governed by the equation

$$k_1 e^{2n\omega_o t} \nabla^2 u_1 = \frac{\partial u_1}{\partial t} \tag{2.24}$$

where the probability of finding r_1 between R_1 and $R_1 + dR_1$ at time t is $2\pi u_1(R_1,t)R_1\, dR_1$. This is the same as the probability that r lies between R and $R + dR$ where R_1 and R are related by

$$R_1 = Re^{n\omega_o t} \tag{2.25}$$

The conditions on $u_1(r_1,t)$ allow Eq. 2.24 to be solved, similarly to the undamped case. For all $t > 0$, the probability of r_1 having exceeded a chosen R_1 is to be zero. Hence

$$u_1(R_1,t) = 0, \quad t > 0 \tag{A.21}$$

This allows the probability, $F(R_1,t)$, of R_1 having not been exceeded at all by the time t to be written:

$$F(R,t) = 2\pi \int_0^{R_1} u_1(r_1,t) r_1\, dr_1 \tag{A.22}$$

The initial condition on $u_1(r_1,t)$ is obtained from the knowledge that

$$F(R_1,0) = 1 \tag{A.23}$$

in which case a suitable value of $u_1(r_1,0)$ is

$$u_1(r_1,0) = \frac{\delta(r_1)}{\pi r_1} \tag{A.24}$$

As in the undamped case, solving Eq. 2.24 under the conditions of Eqs. A.21 and A.24 leads to the solution of the "first passage" problem, allowing an expression to be written for the probability, F(R), of R having not been exceeded by r (since it is the same as the probability of R_1 having not been exceeded by r_1):

$$F(R) = F(R_1,s) = 2\pi \int_0^{Re^{n\omega_o s}} u_1(r_1,s) r_1 \, dr_1 \tag{A.25}$$

To solve Eq. 2.24 it is transformed by the change of coordinates:

$$r_1 = zRe^{n\omega_o t} \tag{A.26}$$

The probability density u_1 thus becomes a function of z and t governed by the equation

$$n\omega_o z \frac{\partial u_1}{\partial z} + \frac{k_1}{R^2}\left(\frac{\partial^2 u_1}{\partial z^2} + \frac{1}{z}\frac{\partial u_1}{\partial z}\right) = \frac{\partial u_1}{\partial t} \tag{A.27}$$

The boundary condition, Eq. A.21, becomes

$$u_1(1,t) = 0 , \qquad t > 0 \tag{A.28}$$

and the initial condition, Eq. A.24, becomes

$$u_1(z,0) = \frac{1}{\pi R^2}\,\frac{\delta(z)}{z} \tag{A.29}$$

Eigenfunctions $\psi_m(z)$ are sought satisfying

$$n\omega_o z\psi_m' + \frac{k_1}{R^2}(\psi_m'' + \frac{1}{z}\psi_m') = -\nu_m\psi_m \tag{A.30}$$

where ν_m is an eigenvalue. Under the transformation

$$\xi = -\frac{R^2 n\omega_o}{2k_1} z^2 = -c_3 z^2 \tag{A.31}$$

Eq. A.30 becomes

$$\xi\psi_m''(\xi) + (1-\xi)\psi_m'(\xi) - \frac{\nu_m}{2n\omega_o}\psi_m(\xi) = 0 \tag{A.32}$$

which is a confluent hypergeometric equation with solution[23]

$$\psi_m(\xi) = M\left(\frac{\nu_m}{2n\omega_o}, 1, \xi\right) \tag{A.33}$$

or

$$\psi_m(z) = M\left(\frac{\nu_m}{2n\omega_o}, 1, -c_3 z^2\right) = M_m(z) \tag{A.34}$$

A second independent solution, although defined in this case where the second parameter is unity, is discarded because it goes to infinity at $z = 0$. This cannot be permitted in an equation of the form of the following Eq. A.35. A solution to Eq. 2.24 is now sought in the form:

$$u_1(z,t) = \sum_m a_m(t)\psi_m(z) \tag{A.35}$$

where the coefficients $a_m(t)$ depend on t.

The boundary condition, Eq. A.28, applied to this series, yields the following condition on the eigenfunctions $\psi_m(z)$:

$$M\left(\frac{\nu_m}{2n\omega_o}, 1, -c_3\right) = 0 \tag{A.36}$$

It is more convenient if the third parameter of this function, usually the variable, is positive, so use is made of a transformation[23] yielding

$$M\left(1 - \frac{\nu_m}{2n\omega_o}, 1, c_3\right) = 0 \tag{A.37}$$

Typical shapes of this function for two values of c_3 are shown in Figs. A.1 and A.2. The eigenvalues ν_m were obtained from those values of the first paratemer at which M had the value zero. These zeros were determined in order by careful computer calculations whenever they were required.

Substitution of Eqs. A.30 and A.35 into Eq. A.27 yields

$$\sum_m (a_m \nu_m + \dot{a}_m)\psi_m(z) = 0 \tag{A.38}$$

which is satisfied by

$$a_m(t) = A_m e^{-\nu_m t}, \quad A_m \text{ a constant} \tag{A.39}$$

Substitution back into Eq. A.35 yields

$$u_1(z,t) = \sum_m A_m e^{-\nu_m t} M_m(z) \tag{A.40}$$

The constants A_m are found as in the undamped case by using the initial condition Eq. A.29, leading to:

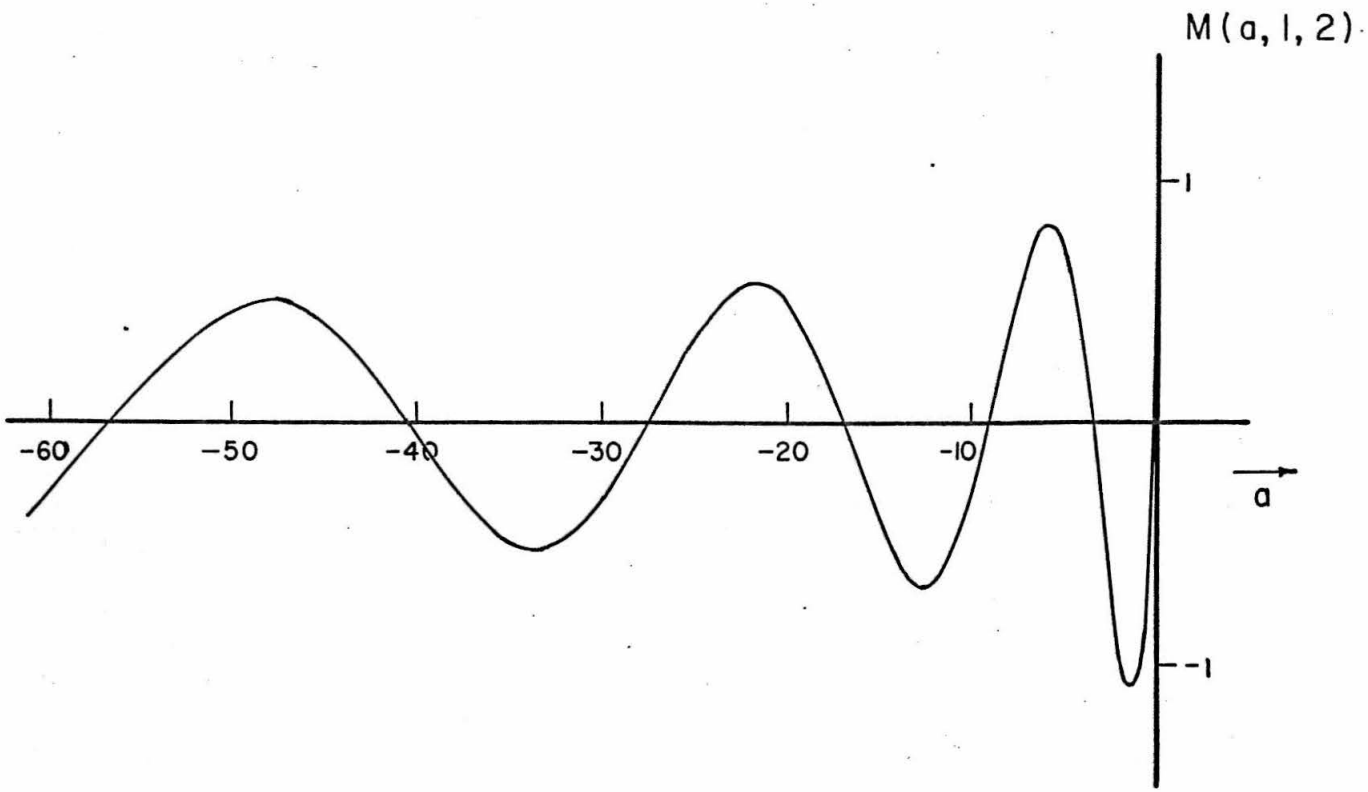

FIG. A.1 VARIATION OF THE CONFLUENT HYPERGEOMETRIC FUNCTION M(a, 1, 2) WITH THE PARAMETER, a.

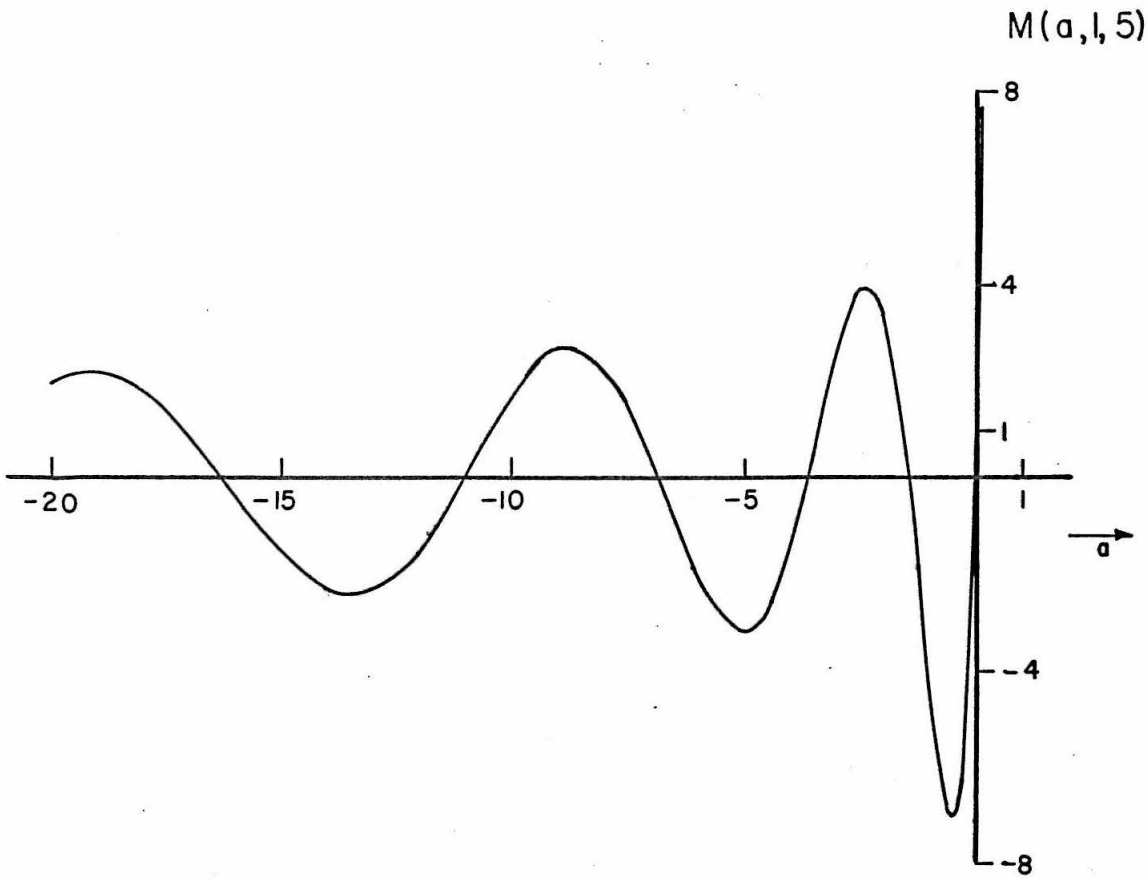

FIG. A.2 VARIATION OF THE CONFLUENT HYPERGEOMETRIC FUNCTION M(a, 1, 5) WITH THE PARAMETER, a.

$$u_1(z,0) = \sum_m A_m M_m(z) = \frac{1}{\pi R^2} \cdot \frac{\delta(z)}{z} \qquad (A.41)$$

The functions $M_m(z)$ are orthogonal with respect to the weighting factor $ze^{c_3 z^2}$. Multiplying through by $M_i(z)$ and this weighting factor, and integrating from 0 to 1 thus yields A_m[9]

$$\frac{1}{A_m} = 2\pi R^2 \int_0^1 z M_m^2(z) e^{c_3 z^2} dz \qquad (A.42)$$

Substitution of this expression for A_m into Eq. A.40 yields

$$u_1(z,t) = \sum_m \frac{M_m(z) e^{-\nu_m t}}{2\pi R^2 \int_0^1 z M_m^2(z) e^{c_3 z^2} dz} \qquad (A.43)$$

The probability, F(R), of R having not been exceeded by r is now obtained by substituting Eqs. A.43 and A.26 into Eq. A.25):

$$F(R) = 2\pi \int_0^1 \left[\sum_m \frac{M_m(z) e^{-\nu_m s}}{2\pi R^2 \int_0^1 z_1 M_m^2(z_1) e^{c_3 z_1^2} dz_1} \right] z R^2 e^{2n\omega_o s} dz \qquad (A.44)$$

The definite integral in the denominator does not participate in the outside integration--the dummy variable is written z_1 to indicate this. The expression for F(R) simplifies to

$$F(R) = e^{2n\omega_o s} \sum_m \frac{\int_0^1 zM_m(z)\,dz}{\int_0^1 zM_m^2(z)e^{c_3 z^2}\,dz} e^{-\nu_m s} \qquad (2.26)$$

on changing the order of integration and summation in Eq. A.44. The justification for this step rests on the validity of the corresponding step for the undamped case and the description in the next section of the reduction of Eqs. A.26 and A.36 to the undamped Eqs. 2.16 and A.5, on letting the damping fraction, n, tend to zero.

C. Reduction to the undamped equations.

The eigenvalues, ν_m, in the damped case are given by the roots of Eq. A.37, as the first parameter, $1 - \nu_m/2n\omega_o$, is varied. These roots are negative as indicated in Fig. A.1. Hence the eigenvalues can be obtained from the positive roots of Eq. A.36:

$$M\left(\frac{\nu_m}{2n\omega_o}, 1, -c_3\right) = 0 \tag{A.36}$$

Defining

$$a = \frac{\nu_m}{2n\omega_o} \tag{A.45}$$

it is possible to write the constant c_3 as

$$c_3 = \frac{R^2 n\omega_o}{2k_1} = \frac{R^2 \nu_m}{4k_1 a} \tag{A.46}$$

Hence the eigenvalue equation for the undamped case is given from Eq. A.36 by

$$\lim_{n \to 0} M\left(\frac{\nu_m}{2n\omega_o}, 1, -c_3\right) = 0 \tag{A.47}$$

i.e.

$$\lim_{a \to \infty} M\left(a, 1, -\frac{R^2 \nu_m}{4k_1 a}\right) = 0 \tag{A.48}$$

i.e.[23]

$$J_o\left(\sqrt{\frac{\nu_m}{k_1}}\, R\right) = 0 \tag{A.49}$$

i.e.

$$J_o(\lambda_m) = 0 \tag{A.50}$$

Therefore the zeros of the confluent hypergeometric function reduce correctly to the zeros of J_o as $n \to 0$.

In a similar fashion the eigenfunctions $\psi_m(z)$ in the damped case, given by

$$\psi_m(z) = M\left(\frac{\nu_m}{2n\omega_o}, 1, -c_3 z^2\right) = M_m(z) \tag{A.34}$$

reduce to

$$\psi_m(z) = J_o\left(\sqrt{\frac{\nu_m}{k_1}}\, Rz\right) = J_o(\lambda_m z) \tag{A.51}$$

i.e.

$$\psi_m(r) = J_o\left(\sqrt{\frac{\nu_m}{k_1}}\, r\right) \tag{A.4}$$

which are the undamped eigenvectors.

The probability distribution $F(R)$ in the damped case, given by Eq. 2.26, can be reduced using these results for the eigenvalues and eigenvectors to yield:

$$\lim_{n \to 0} F(R) = \sum_m \frac{\int_0^1 z J_o(\lambda_m z)\, dz}{\int_0^1 z J_o^2(\lambda_m z)\, dz} e^{-\nu_m s} \tag{A.52}$$

Evaluating these integrals is a simple matter, reducing the equation to

$$F(R) = \sum_m \frac{J_1(\lambda_m)/\lambda_m}{\frac{1}{2} J_1^2(\lambda_m)} e^{-k_1 s \lambda_m^2 / R^2}$$

$$= 2 \sum_m \frac{e^{-k_1 s \lambda_m^2 / R^2}}{\lambda_m J_1(\lambda_m)} \tag{2.16}$$

which is the undamped distribution.

D. Correction applied to the ground acceleration.

Suppose that the digitized acceleration record a(t) is different from the true ground acceleration $\hat{a}(t)$ by an amount $\varepsilon(t)$, caused by inaccuracies in the recording system and errors in the digitizing. Hence

$$a(t) = \hat{a}(t) + \varepsilon(t) \tag{A.53}$$

Successful separation of $\varepsilon(t)$ from a(t) will be possible only if some characteristic of a(t) is affected differently by $\hat{a}(t)$ and $\varepsilon(t)$, that is, if the spectra of $\hat{a}(t)$ and $\varepsilon(t)$ are distinguishable. The integral of a(t) is one such property because the error term $\varepsilon(t)$ causes this integral, the unadjusted velocity v(t), to drift away from the base line in an apparently systematic way. Integrating Eq. A.53 yields

$$v(t) = \int_0^t a(t)\,dt = \hat{v}(t) + e(t) \tag{A.54}$$

where $\hat{v}(t)$ is the true ground velocity and e(t) is the error, given by

$$e(t) = \int_0^t \varepsilon(t)\,dt \tag{A.55}$$

The effect of the error in the velocity, or the difference between $\hat{v}(t)$ and e(t), is much more evident than the difference between $\hat{a}(t)$ and $\varepsilon(t)$. For this reason, the error is best reduced by operating on the velocity rather than the acceleration. Similarly, the error might be reduced by operating on the integrated displacement.

However, since in some cases there is a permanent displacement of the ground, the use of the velocity is indicated rather than the displacement.

The form of the drift in the computed velocity indicates that the most objectionable part of $e(t)$ might reasonably be expressed by the initial terms of a power series in t, with zero constant term because $e(0) = 0$, that is,

$$e(t) = c_o t + \frac{1}{2} c_1 t^2 + \frac{1}{3} c_2 t^3 \qquad (A.56)$$

Terminating the series at the cubic term ensures that the main period components of the correction term will remain considerably longer than the longest periods of importance in the ground motion. The component of $e(t)$ having the form of Eq. A.56 can be removed from the ground velocity by minimizing the mean squared value of the expression

$$\hat{v}(t) + e(t) - \left[c_o t + \frac{1}{2} c_1 t^2 + \frac{1}{3} c_2 t^3\right] \qquad (A.57)$$

This leads directly to Eq. 1.6 which permits the calculation of the constants.

When a complete record is available, use can be made of the fact that the final ground velocity must be zero. However, when studies are made of strong-motion earthquakes the records are usually terminated long before the ground motion has finally ceased. In this case it would be expected that any adjustment procedure must result in the ground velocity, towards the end of the record, behaving

in an oscillatory manner about the base line with slowly decaying amplitude. Provided this condition is satisfied, it may be assumed that the adjustment procedure may ignore the precise value of the velocity at the record end.

A different physical argument that might be used in adjusting the acceleration record is the following. If a force is applied to a mass, proportional to the recorded acceleration, the displacement of the mass will exhibit the same drift as mentioned in the preceding paragraphs. This drift can be reduced by attaching the mass to a fixed base with a spring. The spring must be soft enough for the natural period of the resulting oscillator to be longer than the longest important periods present in the ground motion. A suitable period to choose would be the duration of the record, for the record can contain no frequency component with a longer period than this. This choice is equivalent to fitting a correction, different from the above parabolic correction, to the original ground acceleration base line.

The ground velocity is assured of exhibiting a decaying oscillatory behavior towards the end of the record by introducing some viscous damping. Having made a suitable choice of the damping, the system may be considered as a simple filtering element effectively reducing the long period error components.

It may be pointed out that these different procedures are attempts to standardize the adjustment of the recorded ground acceleration and bear little relationship with the actual cause

of instrument and reading inaccuracies. The results obtained by the parabolic method indicate that although the displacements are very sensitive to the corrections, the magnitude of the corrections is of the same order of smallness as the trace thickness and reading error. Neither method can be said to hold appreciable computational advantages over the other.